ASSESSMENT AND COMPARISON OF EXISTING PROCEDURES TO EVALUATE PERFORMANCE OF ARRESTERS IN A WET-POLLUTED ENVIRONMENT

By

Marek Kornowski

A thesis

presented to the University of Manitoba

in partial fulfillment of the

requirements for the degree of

Master of Science

in

Department of Electrical Engineering

Winnipeg, Manitoba

National Library
of Canada

Acquisitions and
Bibliographic Services Branch

395 Wellington Street
Ottawa, Ontario
K1A 0N4

Bibliothèque nationale
du Canada

Direction des acquisitions et
des services bibliographiques

395, rue Wellington
Ottawa (Ontario)
K1A 0N4

Your file *Votre référence*

Our file *Notre référence*

ISBN 0-315-81724-0

Canada

Name _____

Dissertation Abstracts International is arranged by broad, general subject categories. Please select the one subject which most nearly describes the content of your dissertation. Enter the corresponding four-digit code in the spaces provided.

ELECTRONICS AND ELECTRICAL
SUBJECT TERM

0544
SUBJECT CODE

UMI

Subject Categories

THE HUMANITIES AND SOCIAL SCIENCES

COMMUNICATIONS AND THE ARTS
Architecture 0729
Art History 0377
Cinema 0900
Dance 0378
Fine Arts 0357
Information Science 0723
Journalism 0391
Library Science 0399
Mass Communications 0708
Music 0413
Speech Communication 0459
Theater 0465

EDUCATION
General 0515
Administration 0514
Adult and Continuing 0516
Agricultural 0517
Art 0273
Bilingual and Multicultural 0282
Business 0688
Community College 0275
Curriculum and Instruction 0727
Early Childhood 0518
Elementary 0524
Finance 0277
Guidance and Counseling 0519
Health 0680
Higher 0745
History of 0520
Home Economics 0278
Industrial 0521
Language and Literature 0279
Mathematics 0280
Music 0522
Philosophy of 0998
Physical 0523
Psychology 0525
Reading 0535
Religious 0527
Sciences 0714
Secondary 0533
Social Sciences 0534
Sociology of 0340
Special 0529
Teacher Training 0530
Technology 0710
Tests and Measurements 0288
Vocational 0747

LANGUAGE, LITERATURE AND LINGUISTICS
Language
- General 0679
- Ancient 0289
- Linguistics 0290
- Modern 0291

Literature
- General 0401
- Classical 0294
- Comparative 0295
- Medieval 0297
- Modern 0298
- African 0316
- American 0591
- Asian 0305
- Canadian (English) 0352
- Canadian (French) 0355
- English 0593
- Germanic 0311
- Latin American 0312
- Middle Eastern 0315
- Romance 0313
- Slavic and East European 0314

PHILOSOPHY, RELIGION AND THEOLOGY
Philosophy 0422
Religion
- General 0318
- Biblical Studies 0321
- Clergy 0319
- History of 0320
- Philosophy of 0322

Theology 0469

SOCIAL SCIENCES
American Studies 0323
Anthropology
- Archaeology 0324
- Cultural 0326
- Physical 0327

Business Administration
- General 0310
- Accounting 0272
- Banking 0770
- Management 0454
- Marketing 0338

Canadian Studies 0385
Economics
- General 0501
- Agricultural 0503
- Commerce-Business 0505
- Finance 0508
- History 0509
- Labor 0510
- Theory 0511

Folklore 0358
Geography 0366
Gerontology 0351
History
- General 0578
- Ancient 0579
- Medieval 0581
- Modern 0582
- Black 0328
- African 0331
- Asia, Australia and Oceania 0332
- Canadian 0334
- European 0335
- Latin American 0336
- Middle Eastern 0333
- United States 0337

History of Science 0585
Law 0398
Political Science
- General 0615
- International Law and Relations 0616
- Public Administration 0617

Recreation 0814
Social Work 0452
Sociology
- General 0626
- Criminology and Penology ... 0627
- Demography 0938
- Ethnic and Racial Studies 0631
- Individual and Family Studies 0628
- Industrial and Labor Relations 0629
- Public and Social Welfare 0630
- Social Structure and Development 0700
- Theory and Methods 0344

Transportation 0709
Urban and Regional Planning 0999
Women's Studies 0453

THE SCIENCES AND ENGINEERING

BIOLOGICAL SCIENCES
Agriculture
- General 0473
- Agronomy 0285
- Animal Culture and Nutrition 0475
- Animal Pathology 0476
- Food Science and Technology 0359
- Forestry and Wildlife 0478
- Plant Culture 0479
- Plant Pathology 0480
- Plant Physiology 0817
- Range Management 0777
- Wood Technology 0746

Biology
- General 0306
- Anatomy 0287
- Biostatistics 0308
- Botany 0309
- Cell 0379
- Ecology 0329
- Entomology 0353
- Genetics 0369
- Limnology 0793
- Microbiology 0410
- Molecular 0307
- Neuroscience 0317
- Oceanography 0416
- Physiology 0433
- Radiation 0821
- Veterinary Science 0778
- Zoology 0472

Biophysics
- General 0786
- Medical 0760

EARTH SCIENCES
Biogeochemistry 0425
Geochemistry 0996
Geodesy 0370
Geology 0372
Geophysics 0373
Hydrology 0388
Mineralogy 0411
Paleobotany 0345
Paleoecology 0426
Paleontology 0418
Paleozoology 0985
Palynology 0427
Physical Geography 0368
Physical Oceanography 0415

HEALTH AND ENVIRONMENTAL SCIENCES
Environmental Sciences 0768
Health Sciences
- General 0566
- Audiology 0300
- Chemotherapy 0992
- Dentistry 0567
- Education 0350
- Hospital Management 0769
- Human Development 0758
- Immunology 0982
- Medicine and Surgery 0564
- Mental Health 0347
- Nursing 0569
- Nutrition 0570
- Obstetrics and Gynecology .. 0380
- Occupational Health and Therapy 0354
- Ophthalmology 0381
- Pathology 0571
- Pharmacology 0419
- Pharmacy 0572
- Physical Therapy 0382
- Public Health 0573
- Radiology 0574
- Recreation 0575
- Speech Pathology 0460
- Toxicology 0383

Home Economics 0386

PHYSICAL SCIENCES
Pure Sciences
Chemistry
- General 0485
- Agricultural 0749
- Analytical 0486
- Biochemistry 0487
- Inorganic 0488
- Nuclear 0738
- Organic 0490
- Pharmaceutical 0491
- Physical 0494
- Polymer 0495
- Radiation 0754

Mathematics 0405
Physics
- General 0605
- Acoustics 0986
- Astronomy and Astrophysics 0606
- Atmospheric Science 0608
- Atomic 0748
- Electronics and Electricity 0607
- Elementary Particles and High Energy 0798
- Fluid and Plasma 0759
- Molecular 0609
- Nuclear 0610
- Optics 0752
- Radiation 0756
- Solid State 0611

Statistics 0463

Applied Sciences
Applied Mechanics 0346
Computer Science 0984
Engineering
- General 0537
- Aerospace 0538
- Agricultural 0539
- Automotive 0540
- Biomedical 0541
- Chemical 0542
- Civil 0543
- Electronics and Electrical 0544
- Heat and Thermodynamics ... 0348
- Hydraulic 0545
- Industrial 0546
- Marine 0547
- Materials Science 0794
- Mechanical 0548
- Metallurgy 0743
- Mining 0551
- Nuclear 0552
- Packaging 0549
- Petroleum 0765
- Sanitary and Municipal 0554
- System Science 0790

Geotechnology 0428
Operations Research 0796
Plastics Technology 0795
Textile Technology 0994

PSYCHOLOGY
General 0621
Behavioral 0384
Clinical 0622
Developmental 0620
Experimental 0623
Industrial 0624
Personality 0625
Physiological 0989
Psychobiology 0349
Psychometrics 0632
Social 0451

Nom _____

Dissertation Abstracts International est organisé en catégories de sujets. Veuillez s.v.p. choisir le sujet qui décrit le mieux votre thèse et inscrivez le code numérique approprié dans l'espace réservé ci-dessous.

_____ ☐☐☐ U·M·I

SUJET — CODE DE SUJET

Catégories par sujets

HUMANITÉS ET SCIENCES SOCIALES

COMMUNICATIONS ET LES ARTS
Architecture 0729
Beaux-arts 0357
Bibliothéconomie 0399
Cinéma 0900
Communication verbale 0459
Communications 0708
Danse 0378
Histoire de l'art 0377
Journalisme 0391
Musique 0413
Sciences de l'information 0723
Théâtre 0465

ÉDUCATION
Généralités 515
Administration 0514
Art 0273
Collèges communautaires 0275
Commerce 0688
Économie domestique 0278
Éducation permanente 0516
Éducation préscolaire 0518
Éducation sanitaire 0680
Enseignement agricole 0517
Enseignement bilingue et multiculturel 0282
Enseignement industriel 0521
Enseignement primaire. 0524
Enseignement professionnel 0747
Enseignement religieux 0527
Enseignement secondaire 0533
Enseignement spécial 0529
Enseignement supérieur 0745
Évaluation 0288
Finances 0277
Formation des enseignants 0530
Histoire de l'éducation 0520
Langues et littérature 0279
Lecture 0535
Mathématiques 0280
Musique 0522
Orientation et consultation 0519
Philosophie de l'éducation 0998
Physique 0523
Programmes d'études et enseignement 0727
Psychologie 0525
Sciences 0714
Sciences sociales 0534
Sociologie de l'éducation 0340
Technologie 0710

LANGUE, LITTÉRATURE ET LINGUISTIQUE
Langues
- Généralités 0679
- Anciennes 0289
- Linguistique 0290
- Modernes 0291

Littérature
- Généralités 0401
- Anciennes 0294
- Comparée 0295
- Médiévale 0297
- Moderne 0298
- Africaine 0316
- Américaine 0591
- Anglaise 0593
- Asiatique 0305
- Canadienne (Anglaise) 0352
- Canadienne (Française) 0355
- Germanique 0311
- Latino-américaine 0312
- Moyen-orientale 0315
- Romane 0313
- Slave et est-européenne 0314

PHILOSOPHIE, RELIGION ET THÉOLOGIE
Philosophie 0422
Religion
- Généralités 0318
- Clergé 0319
- Études bibliques 0321
- Histoire des religions 0320
- Philosophie de la religion 0322

Théologie 0469

SCIENCES SOCIALES
Anthropologie
- Archéologie 0324
- Culturelle 0326
- Physique 0327

Droit 0398
Économie
- Généralités 0501
- Commerce-Affaires 0505
- Économie agricole 0503
- Économie du travail 0510
- Finances 0508
- Histoire 0509
- Théorie 0511

Études américaines 0323
Études canadiennes 0385
Études féministes 0453
Folklore 0358
Géographie 0366
Gérontologie 0351
Gestion des affaires
- Généralités 0310
- Administration 0454
- Banques 0770
- Comptabilité 0272
- Marketing 0338

Histoire
- Histoire générale 0578
- Ancienne 0579
- Médiévale 0581
- Moderne 0582
- Histoire des noirs 0328
- Africaine 0331
- Canadienne 0334
- États-Unis 0337
- Européenne 0335
- Moyen-orientale 0333
- Latino-américaine 0336
- Asie, Australie et Océanie 0332

Histoire des sciences 0585
Loisirs 0814
Planification urbaine et régionale 0999
Science politique
- Généralités 0615
- Administration publique 0617
- Droit et relations internationales 0616

Sociologie
- Généralités 0626
- Aide et bien-être social 0630
- Criminologie et établissements pénitentiaires 0627
- Démographie 0938
- Études de l' individu et de la famille 0628
- Études des relations interethniques et des relations raciales 0631
- Structure et développement social 0700
- Théorie et méthodes. 0344
- Travail et relations industrielles 0629

Transports 0709
Travail social 0452

SCIENCES ET INGÉNIERIE

SCIENCES BIOLOGIQUES
Agriculture
- Généralités 0473
- Agronomie. 0285
- Alimentation et technologie alimentaire 0359
- Culture 0479
- Élevage et alimentation 0475
- Exploitation des pâturages 0777
- Pathologie animale 0476
- Pathologie végétale 0480
- Physiologie végétale 0817
- Sylviculture et faune 0478
- Technologie du bois 0746

Biologie
- Généralités 0306
- Anatomie 0287
- Biologie (Statistiques) 0308
- Biologie moléculaire 0307
- Botanique 0309
- Cellule 0379
- Écologie 0329
- Entomologie 0353
- Génétique 0369
- Limnologie 0793
- Microbiologie 0410
- Neurologie 0317
- Océanographie 0416
- Physiologie 0433
- Radiation 0821
- Science vétérinaire 0778
- Zoologie 0472

Biophysique
- Généralités 0786
- Medicale 0760

SCIENCES DE LA TERRE
Biogéochimie 0425
Géochimie 0996
Géodésie 0370
Géographie physique 0368
Géologie 0372
Géophysique 0373
Hydrologie 0388
Minéralogie 0411
Océanographie physique 0415
Paléobotanique 0345
Paléoécologie 0426
Paléontologie 0418
Paléozoologie 0985
Palynologie 0427

SCIENCES DE LA SANTÉ ET DE L'ENVIRONNEMENT
Économie domestique 0386
Sciences de l'environnement 0768
Sciences de la santé
- Généralités 0566
- Administration des hôpitaux 0769
- Alimentation et nutrition 0570
- Audiologie 0300
- Chimiothérapie 0992
- Dentisterie 0567
- Développement humain 0758
- Enseignement 0350
- Immunologie 0982
- Loisirs 0575
- Médecine du travail et thérapie 0354
- Médecine et chirurgie 0564
- Obstétrique et gynécologie 0380
- Ophtalmologie 0381
- Orthophonie 0460
- Pathologie 0571
- Pharmacie 0572
- Pharmacologie 0419
- Physiothérapie 0382
- Radiologie 0574
- Santé mentale 0347
- Santé publique 0573
- Soins infirmiers 0569
- Toxicologie 0383

SCIENCES PHYSIQUES
Sciences Pures
Chimie
- Généralités 0485
- Biochimie 487
- Chimie agricole 0749
- Chimie analytique 0486
- Chimie minérale 0488
- Chimie nucléaire 0738
- Chimie organique 0490
- Chimie pharmaceutique 0491
- Physique 0494
- PolymÈres 0495
- Radiation 0754

Mathématiques 0405
Physique
- Généralités 0605
- Acoustique 0986
- Astronomie et astrophysique 0606
- Électronique et électricité 0607
- Fluides et plasma 0759
- Météorologie 0608
- Optique 0752
- Particules (Physique nucléaire) 0798
- Physique atomique 0748
- Physique de l'état solide 0611
- Physique moléculaire 0609
- Physique nucléaire 0610
- Radiation 0756

Statistiques 0463

Sciences Appliqués Et Technologie
Informatique 0984
Ingénierie
- Généralités 0537
- Agricole 0539
- Automobile 0540
- Biomédicale 0541
- Chaleur et thermodynamique 0348
- Conditionnement (Emballage) 0549
- Génie aérospatial 0538
- Génie chimique 0542
- Génie civil 0543
- Génie électronique et électrique 0544
- Génie industriel 0546
- Génie mécanique 0548
- Génie nucléaire 0552
- Ingénierie des systèmes 0790
- Mécanique navale 0547
- Métallurgie 0743
- Science des matériaux 0794
- Technique du pétrole 0765
- Technique minière 0551
- Techniques sanitaires et municipales 0554
- Technologie hydraulique 0545

Mécanique appliquée 0346
Géotechnologie 0428
Matières plastiques (Technologie) 0795
Recherche opérationnelle 0796
Textiles et tissus (Technologie) 0794

PSYCHOLOGIE
Généralités 0621
Personnalité 0625
Psychobiologie 0349
Psychologie clinique 0622
Psychologie du comportement 0384
Psychologie du développement 0620
Psychologie expérimentale 0623
Psychologie industrielle 0624
Psychologie physiologique 0989
Psychologie sociale 0451
Psychométrie 0632

ASSESSMENT AND COMPARISON OF EXISTING PROCEDURES TO EVALUATE PERFORMANCE OF ARRESTERS IN A WET-POLLUTED ENVIRONMENT

BY

MAREK KORNOWSKI

A Thesis submitted to the Faculty of Graduate Studies of the University of Manitoba in partial fulfillment of the requirements for the degree of

MASTER OF SCIENCE

ABSTRACT

These studies investigate existing procedures to evaluate stable performance of arresters under wet and polluted conditions. Procedures proposed by IEC, IEEE and Japanese Standards were applied to distribution class arresters housed in EPDM and energized with negative dc voltage, and then the behavior of arresters under these procedures was evaluated.

Suggestions have been made about the suitability of application of methods designed for ac voltage testing to distribution class arresters energized with dc voltage.

ACKNOWLEDGEMENT

My profound gratitude to Dr. M. R. Raghuveer for his invaluable inspiration, guidance and advice through the course of this work.

Many thanks to Manitoba Hydro for provision of financial assistance through the Manitoba Hydro Research Committee and to NSERC for their funding of this work.

Acknowledgement is also given to Bowthrope EMP Limited of United Kingdom for providing EPDM arresters.

My grateful acknowledgement to the technician of High Voltage Lab, Mr. John Kendall of the University of Manitoba for supplying the equipment and help in setting up the experimental circuits.

My appreciation to my wife for her encouragement and support throughout the course of my studies.

Table of Content

List of Figures

List of Tables.

Chapter 1 INTRODUCTION

1.1. General.

The first commercial metal oxide surge arresters were placed in service on transmission systems in 1976. They offer significant advantages over silicon carbide arresters including superior protective characteristics, improved reliability because of design simplicity, superior performance in low impedance circuits (e.g., cable and capacitor applications), and superior energy absorbing capability under polluted conditions. Although the new arresters were a considerable departure from the gapped silicon carbide arresters then in use, they were accepted rapidly by utility engineers because of the advantages listed above, and because they were subjected to a rigorous program of analysis and tests to demonstrate their suitability for service. Operating experience since 1976 indicates that the analysis and test program yielded realistic results.

A few years later metal oxide arresters were introduced to meet the need for better protection of cables used in underground distribution system. It was recognized that the low protective levels required for cables would result in temporary over voltage capability for the arresters lower than desirable for some applications, and the over voltage failures might occur on some systems. Operating experience has shown that the arresters did reduce equipment failures, and while some over voltage failures have occurred, the improvement in protection has been sufficient to result in widespread application of riser pole arresters.

During the last few years, metal oxide arresters have been designed for the protection of overhead distribution equipment, and these arresters are replacing silicon carbide arresters on many systems. Experience has shown that most failures of silicon carbide arresters occur because of reduction of spark–over voltage due to moisture or contamination ingress inside the arrester. This can cause a repetitive spark–overs at or near normal operating voltage. Because metal oxide valve elements are more nonlinear than silicon carbide elements, gaps are

not required in metal oxide arresters designed with protective characteristics approximately the same as silicon carbide arresters. Elimination of gaps results in significant improvement in reliability. Because the experience with metal oxide distribution arresters is limited, the most realistic method available for estimating the long run frequency of surge failures of metal oxide arresters is to compare their surge discharge capability to that of silicon carbide arresters [1].

Since the last few years metal oxide arresters are being housed in polymeric insulation. The advantages of choosing polymer instead of porcelain as the housing material for arresters are, light weight, shorter length of arrester possible due to the use of an insulated mounting bracket, reduced risk of shattering and explosion of the housing during arrester failure, improved resistance to moisture ingress due to close fitting provided by the polymer, etc. Presently, polymer housed arresters are available up to 36 kV rating, and there are plans to manufacture them for higher voltages. Currently available arresters use either an EPM or an EPDM polymer, and it is expected that silicone rubber housed arresters will be available shortly [2].

Considerable amount of service experience and laboratory tests have demonstrated that there are two types of polymers, namely silicone rubber and ethylene propylene rubber (EPR, which is the generic name for EPM and EPDM polymers), that are well suited for outdoor applications. A major concern which still remains in the use of these materials is their behavior under combined high electric stress, moisture and outdoor contamination. Corona and dry bands arcing are promoted under such conditions. Unlike with porcelain, corona on polymers can cause degradation in the form of radial cracks, and pin holes, and dry band arcing can cause degradation in the form of tracking and erosion *.

Metal oxide arresters for higher voltage ratings are made by stacking multiple low voltage

* Tracking is defined as the formation of the conducting layer of carbon deposit formed on the surface due to polymer degradation. Erosion is defined as the loss of material with time.

sections. For a constant diameter, the electric field near the high voltage electrode will increase with the applied voltage, thereby increasing the risk of occurrence corona at operating voltage.

It would be valuable to determine the highest voltage class polymer housed arresters which could be used without corona problems.

In polymer housed arresters, the housing fits more snugly and tightly to the metal oxide column than is obtained with porcelain, hence providing a greater resistance to moisture ingress. However, this also increases the capacitance between housing and the arrester column. Consequently, there is a concern by the users that under contaminated conditions the internal arrester current may be affected by the external leakage current (mostly in ac). This could result in heating the zinc oxide blocks and eventual failure of the arrester. If this is true, an evaluation of the effect of contamination on the internal current should be performed.

Another problem with the use of polymers is the lack of a meaningful laboratory tests to predict the performance in service. Dry band arcing is largely controlled by the surface electric stress, which varies for different devices. Although there is data available for polymer outdoor insulation, this may not be applicable to polymer housed surge arresters [2].

Field experience has shown that the performance of insulators subjected to the effect of atmospheric agents, especially pollution and wetting, is one of the weak conditions for dc system reliability.

In general the accumulation of the contaminant is higher on insulators in dc systems than in ac ones, enhancing the importance of the pollution problems. Furthermore the distribution of the contaminant tends to be more non–uniform in the dc than in the ac cases. These facts were, at least partly duplicated in laboratory making use of dust chamber contamination method [3].

In addition, tests carried out with procedures proposed for standardization [4] have shown that the pollution strength under dc voltage is generally lower than under ac one with the same pollution degree, again underlining the importance of pollution problems for dc sys-

tem.

The applied test procedures were generally just extended from the ac applications and their representativeness with the respect to the peculiarities of dc voltage could necessitate a further investigation.

1.2. General properties of the metal oxide surge arrester.

1.2.1. Microstructure.

The metal oxide material is a ceramic made by mixing ZnO with small amounts of additive materials, such as Bi_2O_3, CoO_2, Cr_2O_3, MnO and Sb_2O_3, granulating the mixture, then drying it, pressing it into discs, and finally sintering it [5].

The ZnO grains (about 10 μm diameter) have a low resistivity and are surrounded by a granular layer, which is a high resistive oxide (about 0.1 μm thick). The two are strongly bonded to each other. The disc can be represented by the equivalent circuit shown in Figure 1.1.

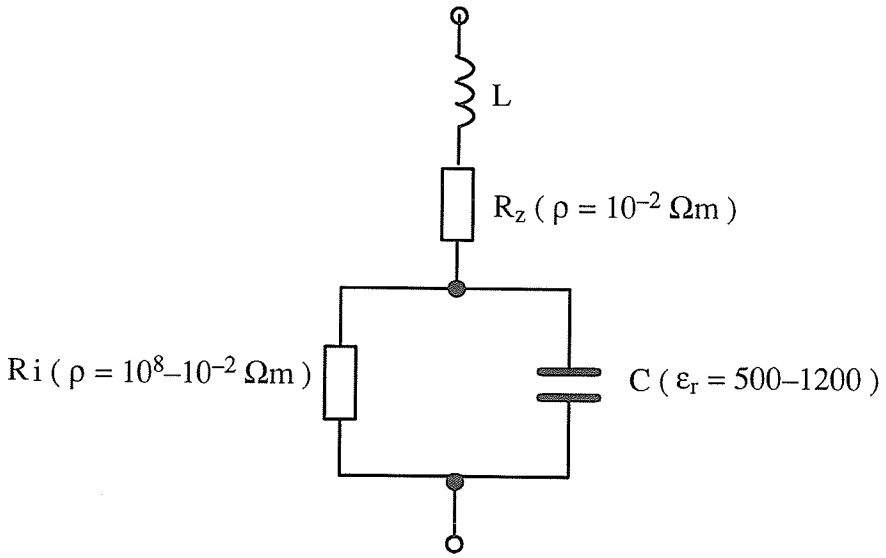

Fig. 1.1. Equivalent circuit of a metal oxide disc [5].

R_i in this figure represents the nonlinear resistance of the granular layers, where the resistivity ρ changes from 10^8 Ωm for low electric field stress to just below 0.01 Ωm for high stress. The granular layer has a relative dielectric constant between 500 and 1200 depending of the manufacturing process. R_z is the resistance of the ZnO grains with the resistivity of about 0.01 Ωm. L represents the inductance of the metal oxide disc and is determined by the geometry of the current flow path.

1.2.2. Volt–current characteristic.

The volt–current characteristic of MOSA is shown in Figure 1.2. Based on the conduction mechanism of the microstructure the V–I characteristic is divided into three regions:

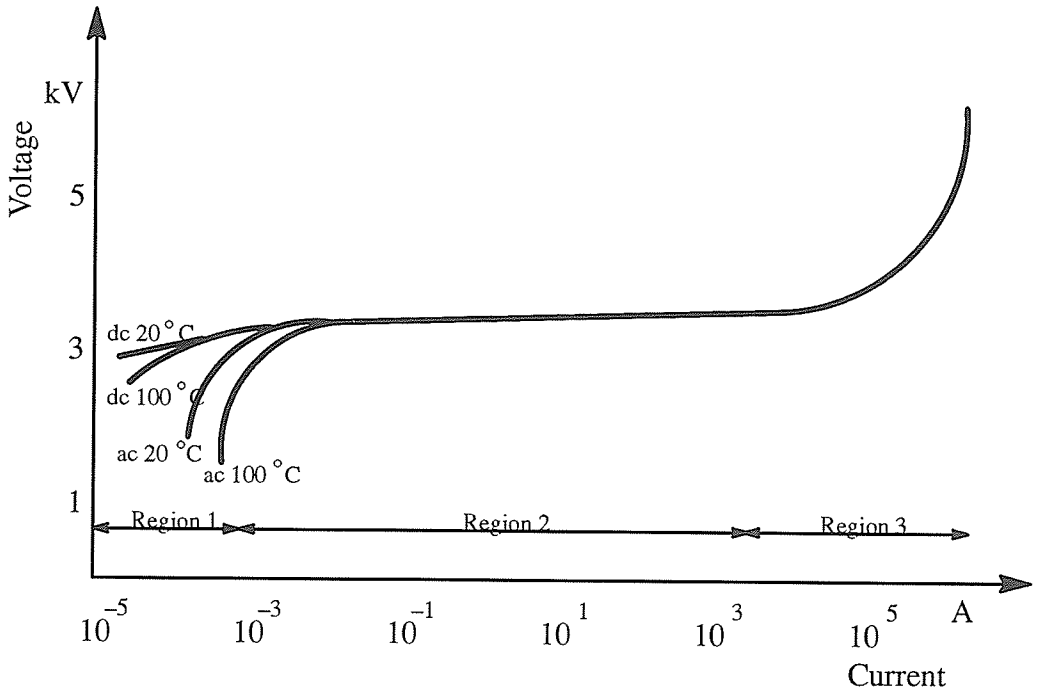

Fig. 1.2. Typical volt–current characteristics of one specific metal oxide disc (80 mm diameter, 20 mm height).

a) Low electric field region (Region 1).

The conduction mechanism in this region is explained by means of energy barriers in the granular layer. These barriers prevent electrons from moving from one grain to another. An applied electric field has the effect of lowering these barriers and electrons pass over them thermally.This is called Schottky emission (as in semiconductor diodes, transistors, etc.) and gives rise to a small current through the material.

The current density is given approximately by equation 1.1 [5].

$$J_r = J_0 \exp\left[-\frac{\sqrt{Ee^3/4\pi\epsilon} - \Phi_B}{kT}\right] \qquad (1.1)$$

where J_0 is constant depending on the material and the geometry of the granular layer, Φ_B the potential barrier, E the electric field stress, e the electron charge, ε the dielectric constant, k the Boltzman's constant and T the absolute temperature.

Higher temperatures increase the energy of the electrons and they can pass over the barrier more easily.

b) Medium electric field region (Region 2).

When the electric field in the granular layer reaches about 100 kV/mm electrons move through the barriers by the tunnel effect represented by equation 1.2 [5].

$$J_r = J_0 \exp\left(-(A\Phi_B^{3/2}/E)\right) \qquad (1.2)$$

where J_0 and A are constant for a specific material.

c) High electric field region (Region 3).

In this region the voltage drop at the barrier due to the tunnel effect is small and the voltage dropped across the resistance R_z of the ZnO grains dominates. The current then gradually approaches the linear relation with the voltage described by equation 3.

$$I = k\,V^{\alpha} \qquad (1.3)$$

where k and α are constants for a specific material. The applicable exponent α depends on the conduction region and can vary between 3 and 50. Even in a specific region generalized numbers are not applicable and the actual arrester characteristics are developed from the determined constants.

1.2.3. Implications.

In regions 1 and 2 of the V–I characteristic the voltage applied to the arrester drops across the granular layer. Consequently, suitable measures have to be applied along the outer surface of the discs, in order to prevent external discharges across the outer wedges between the ZnO grains.

In order to keep the power dissipation in a metal oxide arrester due to the system operating voltage small, the continuous operating voltage of the arrester has to be chosen in region 1. In this region the peak value of current is usually well below 1 mA.

The value of the current through the metal oxide varistor in region 1 depends on the granular layer and is thus influenced by the manufacturers selection of the materials and production technique.

The dispersion of the current characteristics means, that the arrester's supervision by means of current measurements is only possible, when the current is measured in service installation at the same new arrester. The temperature according to Figure 1.2 has to be observed taking into account that the current can change by several % per °C (typically 3 %). The initial and comparison measurements have to be carried out at approximately the same ambient temperature after obtaining the thermal equilibrium of the arrester.

The protection characteristics of the arrester are determined by the voltage–current characteristic in regions 2 and 3. In these regions the influence of temperature has disappeared and the deviation from the linear voltage distribution along the arrester is only determined by the dispersion of the voltage–current characteristic. It can be assumed that the dispersion is small and the voltage distribution is linear.

1.2.4. Thermal stability.

When a steady state thermal analysis is conducted as shown in Figure 1.3 the power dissipation–temperature curve P–T is the heat generation curve of metal oxide element and the heat loss temperature curve Q–T is the heat dissipation curve of the heat dissipation system of MOSA. There are two intersections of the two curves: point A represents stable balance conditions and the point B represents instability threshold balance conditions.
When MOSA is operating at point B, even if the heat generation of the ZnO element is increased slightly, the thermal run away is bound to occur. In general the design is such that the ZnO element of MOSA always remain at the operating point A; that is, they are in stable conditions. The energy difference between two points (A,B) is called allowable surge energy. The larger the energy difference between A and B the larger the capacity of the surge ener-

gy for MOSA. It can be guaranteed that MOSA returns to (or approaches) point A provided that the surge energy does not exceed the allowable value [5].

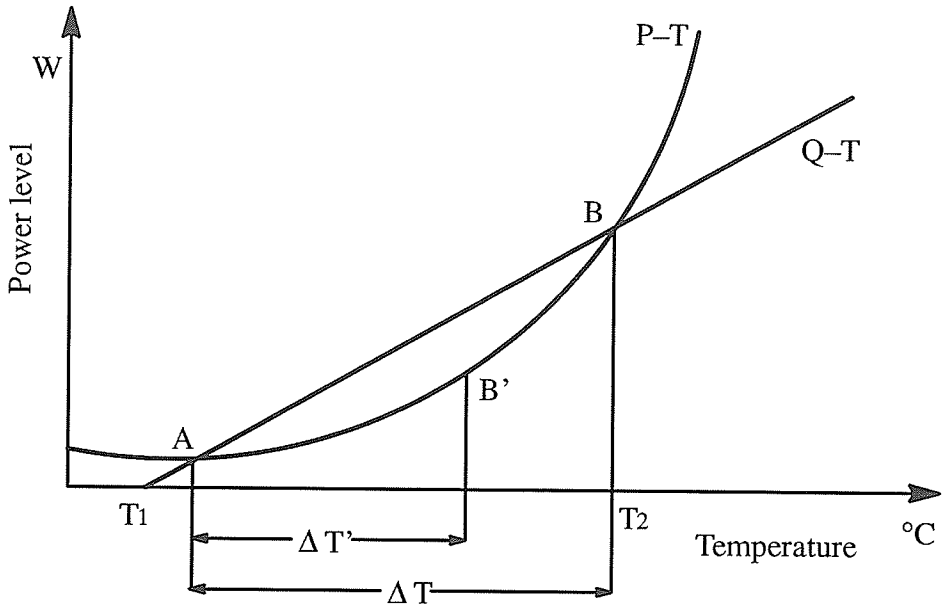

Fig. 1.3. Evaluation of MOSA steady state stability using the heat loss–input characteristic [6].

As shown in Figure 1.2 and Eq. 1.1 the current and thus also the power dissipation in the arrester at the operating voltage increases with the temperature with an exponent greater than 1. The dissipated power has to be transferred from the arrester blocks via the arrester housing and via the connections to the surrounding air. To achieve thermal stability, the power transfer to the environment for a given temperature must exceed the sum of the input power formed by the power dissipation and the possible radiations.

The temperature, at which thermal instability begins depends on the arrester construction i.e. the heat transfer conditions, the material characteristic, and the applied operating voltage. The energy necessary to reach this temperature depends on the initial temperature of the re-

sistor blocks, which may not be equal over the complete arrester and depends on the time taken to dissipate this energy in the arrester. The unequal initial temperatures may originate from the nonlinear voltage distribution along the arrester which is, in particular, possible, when conductive surfaces e.g. by pollution influence this distribution. The time taken to expend a high energy inside an arrester can vary between some 10 μs due to lighting currents to several seconds due to temporary over voltages. In general it can be assumed that the shorter times create the more severe conditions, owing to possible unequal temperatures within the blocks and absence of heat transfer to the surroundings.

The voltage–current characteristic of the metal oxide material offers the degree of nonlinearity necessary to fulfil the mutually contradicting requirements of a low protection level at high current values and a low current, i.e. a low power dissipation, at the system operating voltage. Surge arresters using this material, therefore, can be connected to the system without series spark gaps disconnecting the varistors from the operating voltage.

Structure of and the current conduction mechanism through the material make evident that a metal oxide arrester without series gaps can represent a reliable equipment in the system, if its voltage–current characteristics remain stable with time and if they are selected adequately with respect to the voltage stresses in service.

A metal oxide arrester can be thermally unstable only at high temperatures. Generally, varistor temperatures far above 100 °C are necessary. At such temperatures the voltage distribution is linear, even if the temperature is not absolutely the same in all resistors. The thermal stability, therefore, is not affected by the surge arrester grading and what is important, can be tested at continuous operating voltage.

1.2.5. Pollution effect on MOSA.

When polluted metal oxide arrester is energized, a leakage current will flow in the pollution layer, if the layer is wetted by fog, rain or wet snow. This leakage current will be unevenly distributed along the circumstance of the insulator. As the housing diameter is varying, the leakage current density and consequently the power dissipation and drying of the pollution layer will vary along the arrester. Dry bands are established with the consequence that the external voltage distribution will differ from the voltage distribution along the stack of the varistors inside the arrester. Radial voltage differences are established along the arrester resulting in the transfer of current from the pollution layer outside to the varistor inside via the capacitive coupling. This means that the varistors shunting the dry bands may be stressed by a considerably higher current than what is normal for dry and clean housings. In addition, a part of the external leakage current on one unit may flow through the varistors in another unit via the metal flanges that represent a galvanic connection between external pollution layer and the varistors.

Depending on the arrester design the consequence of this behavior may be that the increased varistor temperature may cause thermal instability, if combined with over voltages and faults in the network. This will require that the varistor temperature increase caused by pollution has to be an important parameter in the operating duty test of a metal oxide surge arrester. The difference between the voltage distributions along the varistor column and along the outside housing surface of the arrester causes a radial voltage stress, which may initiate internal partial discharges changing the composition of the gas within the arrester. If the varistors are not effectively sealed by a tight cover on the surface, this may lead to their deterioration. In addition, possible deposits on the varistor surfaces may cause increased surface conductivity on the varistors due to partial discharges, in the case when the interior of the arrester is not kept sufficiently dry.

In principle both effects are separate and the surface conditions giving rise to one of the two effects can be different [5].

1.2.6. Information obtained from field tests.

From natural pollution tests on metal oxide arresters without gaps it is observed that the heating of the varistor may be nonlinearly distributed along the arrester (see chapter 3). What part of the arrester (top, middle or bottom) reaches the highest temperature varies from one exposure to another. It seems to vary randomly. Furthermore, the temperature may stay uniform within the arrester for a long time and may then became non–uniform or it may be non–uniform already after a much shorter time of exposure. The time of occurrence of the maximum temperature also varies randomly. There are indications from field tests that high temperatures are most probably generated during a relatively small numbers of incidents of external pollution explaining these inconsistent observations [5].

Tests are being conducted in different locations with varying pollution conditions ranging from clean environments far away from cities and industrial centers to locations where the MOSA can be stressed beyond thermal run away. This indicates that it would be unrealistic to apply the same pollution requirements to all arrester independent of their location. Consequently, a relevant procedure for classification of pollution severity (pollution zones) with respect to MOSA stresses has to be established.

It may also happen that more energy is accumulated by the arrester due to many small leakage current pulses than due to few with high amplitude. However, the distribution of these current pulses in time is very important with respect to the possible cooling of the MOSA. Consequently, the current pulse amplitude, the current pulse duration of pollution activity have all to be considered when determining the arrester stress.

This leads to the need of a new classification of pollution severity with regards to stress on metal oxide surge arresters. The commonly used Equivalent Salt Deposit Density (ESDD) is not relevant if the intensity and duration of pollution activity is not defined. Very high expected external currents appearing during short periods of time will for instance not be decisive in determining MOSA thermal stability under polluted conditions.

1.2.7. Artificial pollution tests.

Artificial pollution test procedures have been devised by CSA, ANSI/IEEE, IEC and Japanese Standards to evaluate the ability of arrester to perform stably in a wet and polluted environment. It is important to compare existing procedures and assess them because many uncertainties exist and satisfactory pollution test procedure has yet to be worked out.
An artificial pollution test procedure must satisfy three criteria [7] :

i) The test must be reliable; arresters which pass the laboratory test must not fail under service conditions.

ii) The test should not be too stringent. Adoption of very stringent test procedures will result in conservative designs.

iii) The test must to some degree, simulate the naturally occurring service conditions; otherwise overly stringent conditions will be imposed on arrester components.

A high resistor temperature may be obtained by several of the artificial pollution test methods used at present by different laboratories.
In this study some of the main and common test procedures were investigated. The arrester was tested in accordance with following methods:

1) Solid Deposit Method proposed by IEC.

2) Dip Test – modified version of Partial Wetting Test.

3) Wet Slurry Test proposed by IEEE.

4) Partial Wetting Test proposed by IEEE.

5) Test Method in accordance with Japanese Standards.

6) Salt Fog Test proposed by IEC.

Each method was repeated with different pollution levels, some of them with different voltage levels and with two arresters in series. Some of the methods were modified to investigate

the behavior of the arrester in severe conditions. The description of every method, proposed modification, results of the tests obtained in our laboratory and in other laboratories will be presented in chapter 4.

Chapter 2 EXPERIMENTAL SETUP AND APPARATUS.

2.1. ZnO Surge Arrester specimens.

a) Polymeric housed arrester.

The polymeric housed gapless ZnO arrester (type HEA 12) used in this test was manufactured in the United Kingdom by Bowthrope EMP Limited. The polymeric housing material is Ethylene Propylene Diene Monomer (EPDM) – the hydro–carbon rubber.

The arrester comprises of high strength core which is homogeneously wrapped in cured resin impregnated fibre glass to prevent the ingress of moisture and the entrapment of voids. Aluminium heat sinks are placed between metal oxide elements to dissipate the heat generated during operations.

Arrester's Technical Details.

Rated voltage	: 12 kV rms
Maximum Continuous Operating Voltage	: 9 kV rms
Rated frequency	: 60 Hz
Steep current discharge	
current 10 kA	: 42.4 kV crest
Discharge voltages (8 x 20)	
i) at 5 kA	: 34.8 kV crest
ii) at 10 kA	: 38.5 kV crest
iii) at 20 kA	: 43.1 kV crest
Temporary over voltage capability	
1 second	: 15 kV rms
Length	: 226 mm

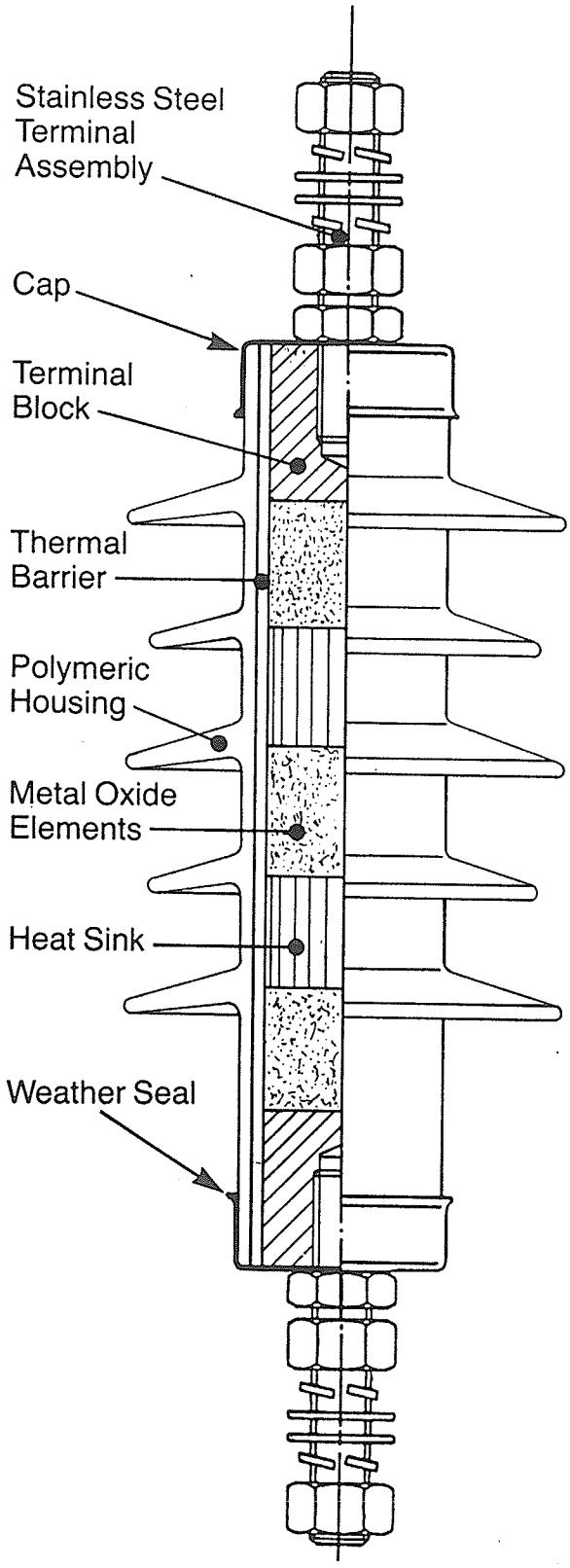

Fig. 2.1. EPDM Arrester Specimen.

Total creep distance	: 420 mm
Weight	: 2.5 kg
Diameter of ZnO blocks	: 42 mm
Operating temperature range	: – 40 to + 110 °C

b) Specimen preparation.

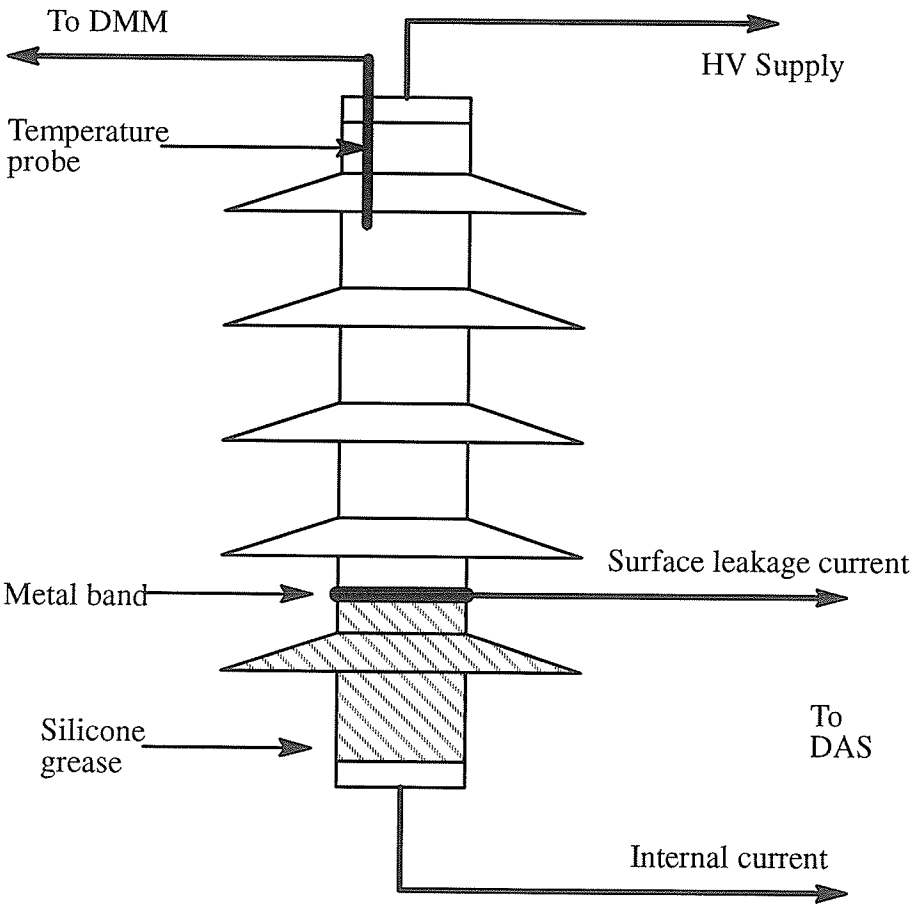

Fig. 2.2. Surge arrester specimen for artificial pollution test.

The arrester specimen was prepared to monitor the internal block and surface leakage cur-

rents as shown in Figure 2.2. For measuring the internal current the ground electrode was connected to a 50 Ω coaxial cable. A metal band was inserted above the bottom shed and connected to a 50 Ω coaxial cable to transmit the surface leakage current. To assure good electrical contact between the metal band and arrester housing, silver paint was applied between the contact surfaces. The part of arrester between the metal band and bottom electrode was greased using non conductive silicon grease to insulate the internal current from the surface leakage current.

For measuring the temperature of the top ZnO block a hole was drilled from the top cap of arrester to the ZnO block.

2.2. High Voltage dc Supply.

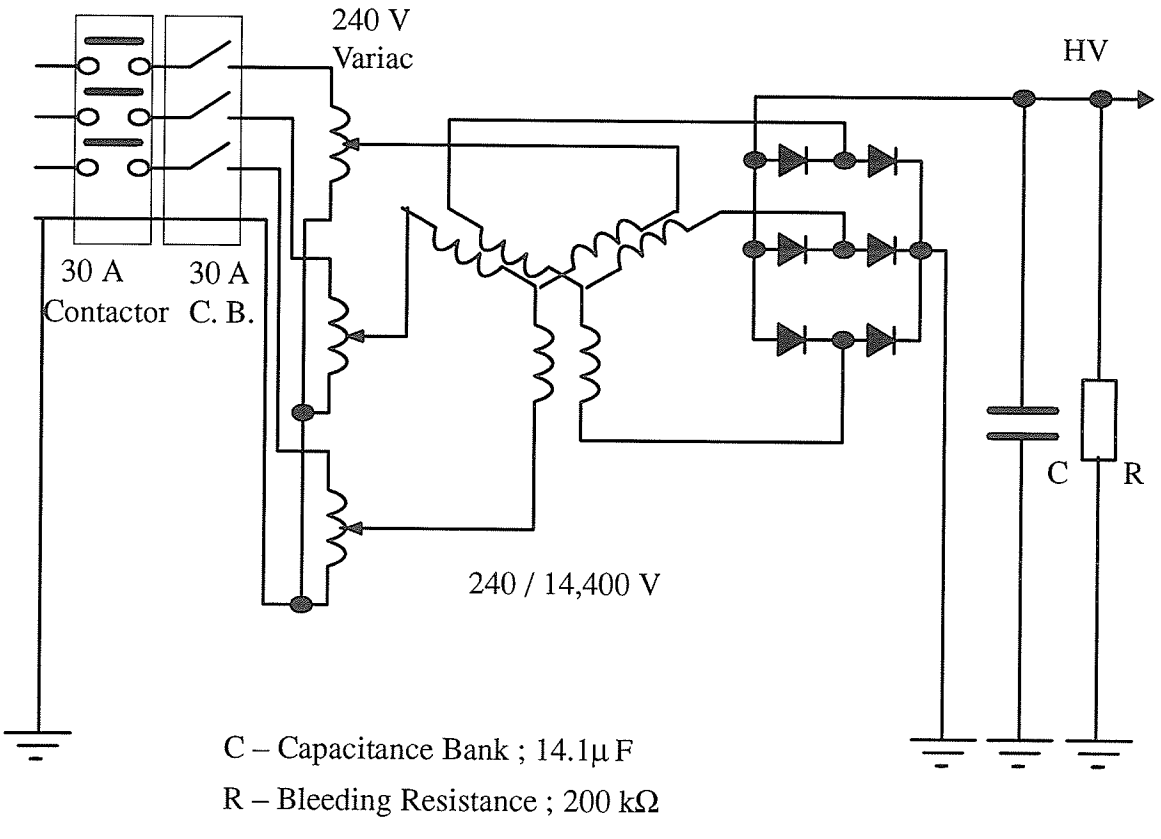

Fig 2.3. Schematic diagram of the HVDC Source.

A three phase full wave rectified dc source shown in Figure 2.3 supplied a negative polarity voltage. The source consists of a transformer bank with three single phase distribution transformers, high voltage rectifier bridge and a capacitor bank.

The single phase distribution transformers were connected in a star configuration. From the high voltage side of the transformer bank high voltage ac was supplied to the three phase full wave rectifier consisting of six HV rectifiers. To maintain a reasonable constant voltage in the presence of discharges, a capacitor bank of 14.1 μF was incorporated in the output voltage.

The output voltage was controlled by a 0 to 240 V three phase variac and protected by a 30 A magnetic circuit breaker.

A bleeding resistor of 200 kΩ was coupled between the dc terminal and the ground.

The bleeding resistor was inserted in the circuit for two very important reasons:

– to improve voltage regulation,

– to improve the relation between voltage regulation and dc output current. This characteristic consists of two linear portions, of which the first one applies for small currents is much steeper (see Figure 2.4). The application of bleeding resistance brings the operating point closer to the higher current region and makes the characteristic smoother.

The dc source was grounded automatically after each operation by the 30 kΩ resistor.

The specifications of the main components of the source are described as follows:

Transformer parameters:

single phase ONAN Distribution Transformer produced by Carte Electric:

Transformer ratio	: 14.4 kV / 240 V
kVA rating	: 10 kVA
Impedance at 85 °C	: 2.04 %
BIL	: 125 kV

Insulation class	: 18 kV

Rectifier parameters:

Peak Inverse Voltage	: 60 kV
Current rating:	
– natural convection 25 °C	: 1.5 A
– forced air	: 3 A
– in oil	: 3.8 A
Over current rating:	
– 1cycle surge	: 150 A

Capacitor parameters:

Capacitance	: 4.7 μF
Rated voltage	: 30 kV dc

2.3. Source requirements.

The general requirements for sources are the stable voltage supply and the relatively low ripple content. Additionally a dc source for testing contaminated insulators should be capable of providing leakage current pulses without excessive voltage drop, which can interfere with arc growth.

Although standardization of dc source requirements is not finalized the following requirements are generally recommended in pollution tests:

i) the maximum voltage drop must not exceed 10 % ,

ii) the mean voltage drop must not exceed 5 % ,

iii) the ripple content must not exceed 10 % .

Voltage drop.

The voltage drop of the dc current source was assessed by performing a resistive load test.

Resistive Load Test: The open circuit voltage of the source was set for 10 kV and resistive loads were connected to the source. The voltage drop was measured using a Tektronix digital oscilloscope. The graph of the voltage drop vs current for the source is shown in Figure 2.4. The voltage drop reaches values of 8 % for currents up to 300 mA.

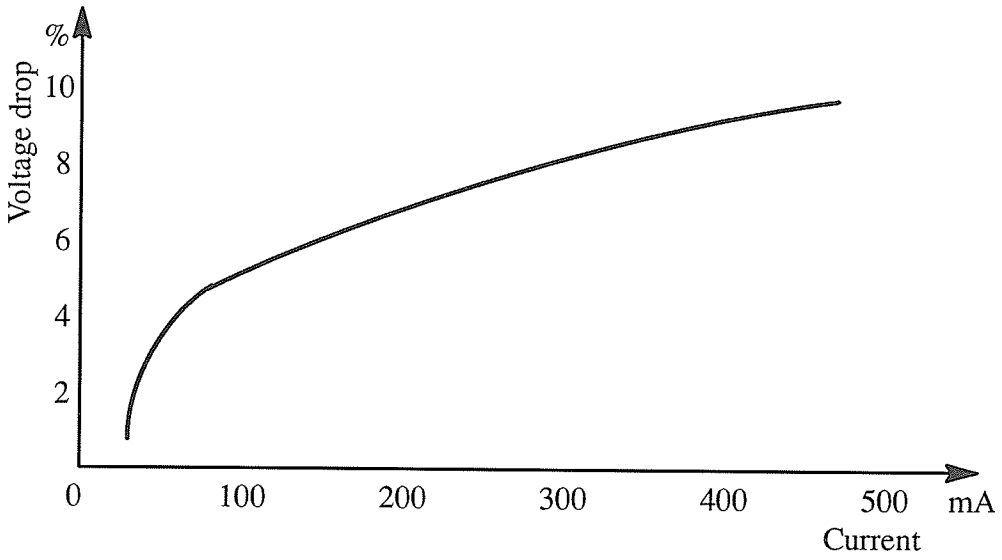

Fig. 2.4. Voltage drop vs current for the resistive load test.

2.4. Fog chamber.

The artificial pollution tests were carried out in a fog chamber of dimension of 180 x 180 x 230 cm as shown in Figure 2.5. Fog was generated by two air atomizing nozzles located 20 cm from the base of the chamber supplied with compressed air and distilled water using the syphon method.

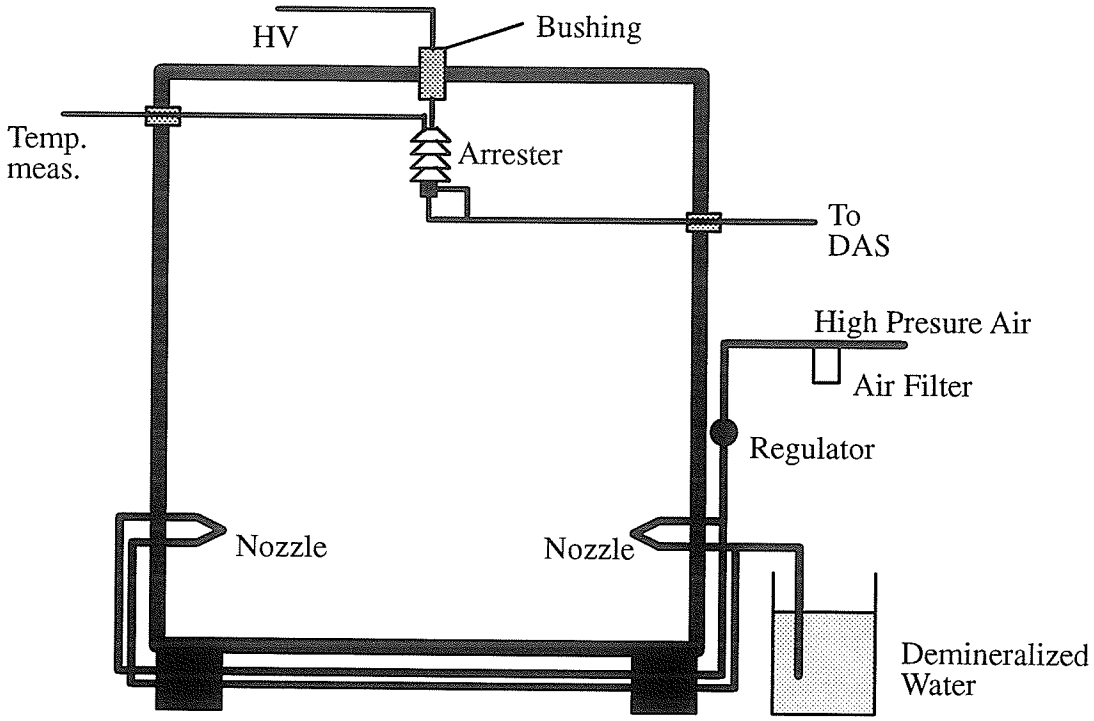

Fig. 2.5. Schematic diagram of the Fog Chamber.

Nozzle parameters:

Atomizing air:

Air Capacity – 1.9 Standard Cubic Feed per Minute at 35 p.s.i.

Liquid:

Liquid Capacity – 0.65 Gallons per Hour for siphon Height of 12".

Spray Angle : 19°.

During a test the fog gradually filled the chamber starting from the base. The arrester was located at the height of 200 cm above the base. The air pressure was set at a constant value of 35 p.s.i. The air supply system consisted of the 2.5 hp air compressor, air filter and regula-

tor. The syphon water head was kept constant at 12". The quantity of distilled water used to produce fog was 6 liters per hour.

Fog chamber characteristics.

To check that the fog distribution complies with standards, the Layer Conductance Test was performed [8]. According to the IEEE Task Force to Refine the Clean Fog Test Parameters, the rate of wetting shall be such that the time from 10 % of maximum surface conductance to 90 % of maximum surface conductance should have a target time of 25 minutes while an acceptable range should be from 10 to 35 minutes.

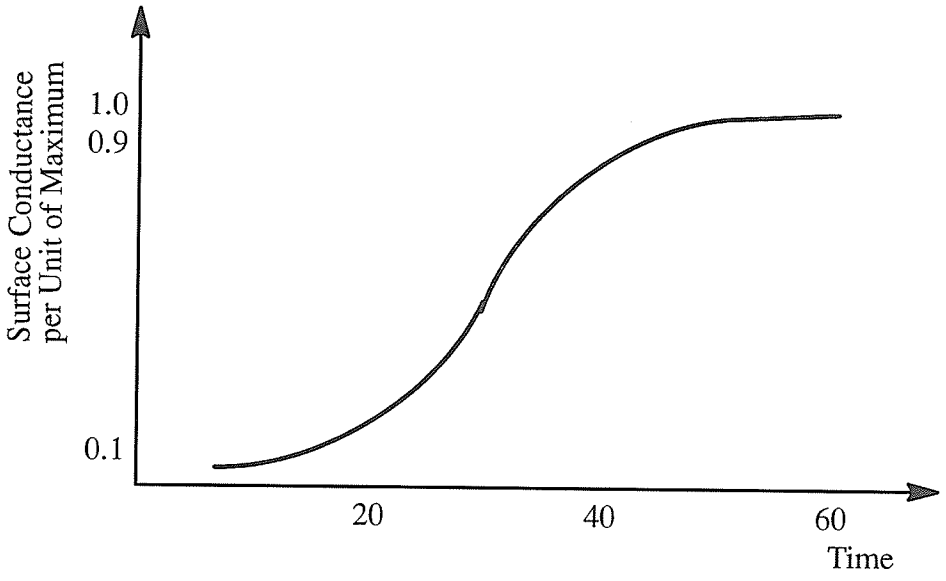

Fig. 2.6. Surface leakage current vs time obtained from the layer conductance test.

Layer Conductance Test: During the test the polluted insulator was energized at 1 kV and clean fog was applied. The layer conductivity of the polluted insulator was assessed by measuring the surface leakage current. The results of this test are shown at Figure 2.6, where the surface leakage current vs time is presented.The time from 10 % of maximum surface con-

ductance to 90 % of maximum surface conductance is 22.4 minutes and is within the acceptable range.

2.5. Data Acquisition System.

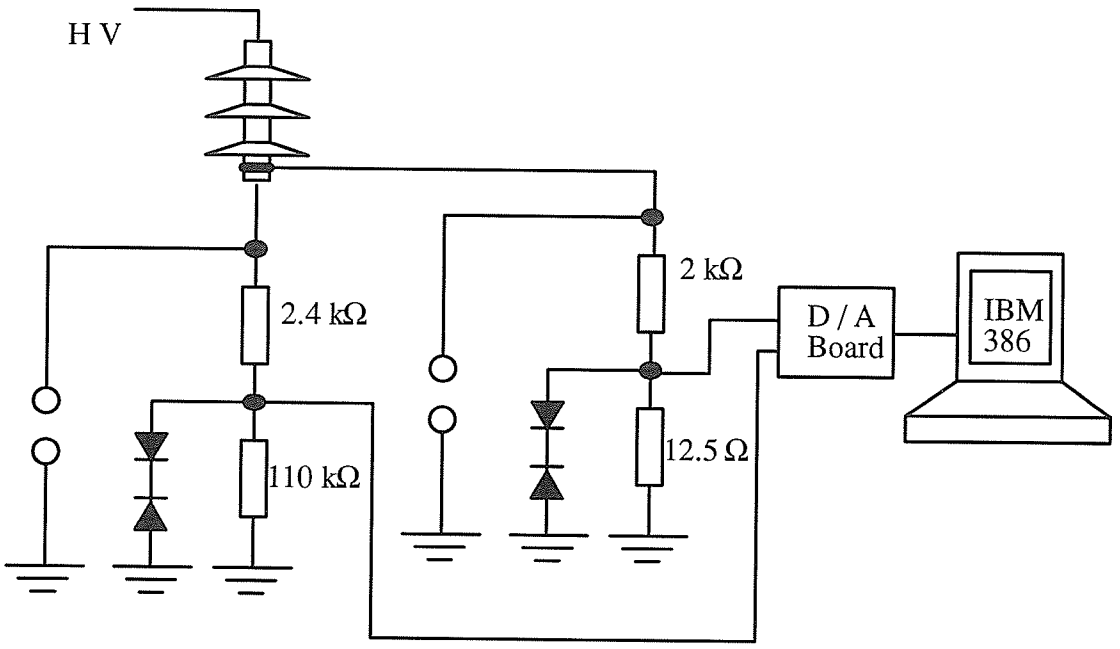

Fig. 2.7. Data Acquisition System.

A system capable of data storage analysis was necessary because of the large number of data samples to be stored and analyzed. Data acquisition, storage, and analysis were done using the Data Acquisition System (DAS) shown in Figure 2.7. The main components of the DAS are Analog to Digital (A/D) board, IBM 386 personal computer, measuring shunt and protection circuit.

The internal and surface leakage currents from the arrester specimen were transmitted to low inductive precision shunt resistors of value 110 kΩ and 12.5 Ω respectively, using two coax-

ial cables. The analog voltage signals from the shunt resistors were converted to digital signals using the A/D board and were stored in the IBM 386 PC.

a) Analog to Digital Board.

The A/D board utilized was the AT–MIO–16F–5 from National Instruments Corporation. The AT–MIO–16F–5 is a high performance multifunction analog, digital and timing input/output board for personal computer.

Specifications of AT–MIO–16F–5:

Number of input channels	: 16 single–ended, 8 differential
Analog resolution	: 12–bit, 1 in 4,096
Relative accuracy	: ± 1.5 LSB maximum over temperature
(nonlinearity + quantization error)	: ± 0.8 LSB typical
Differential analog input ranges	: ± 5 V or 0 to 10 V; software selectable
Over voltage protection	: ± 15 V power off; ± 25 V power on
Common mode rejection ratio	: 78 dB minimum; 90 dB typical; gain = 0.5
	84 dB minimum; 96 dB typical; gain = 1
	90 dB minimum; 102 dB typical; gain = 2
	94 dB minimum; 110 dB typical; gain > 2
Input impedance	: 100 GΩ in parallel with 50 pF
Gain ranges	: 0.5, 1, 2, 5, 10, 20, 50 and 100;
	software selectable
Gain accuracy	:
gain = 1	± 0.5 %; adjustable to < ± 0.01 %
gain ≠ 1	± 0.5 %

System Noise	: 0.2 LSB rms for gains 0.5 to 50; dither off
	0.4 LSB rms for gain 100; dither on
	0.5 LSB rms; dither on
Impulse settling time	: 5 μs maximum to ± 0.5 LSB for all gains and ranges

Two channels with single ended connection were used to acquire the two input voltage signals. Single ended connections are those in which all AT–MIO–16F–5 analog input signals are referenced to one common ground. The input signals are tied to the positive (+) input of the instrumentation amplifier, and their common ground point is tied to the negative (–) input of the instrumentation amplifier.

b) Personal Computer.

The IBM 386 Personal Computer (PC) accompanied with an in line EPSON 810 dot matrix printer was used with the A/D board to store and analyze the acquired data.

Specifications of the PC:

Clock speed	: 33 MHz
Random Accesses Memory (RAM)	: 8 MB
Hard disc memory	: 124 MB

c) Protection Circuit.

The DAS was protected against damages caused by over voltages which would develop in the event of a flashover of the test sample.

A combination of the spark gap and 4.7 V back–to–back Zener diodes was used on the A/D input as shown in Figure 2.7. Sphere spark gaps were calibrated for 500 V and accompanied with parallel resistances of 2 kΩ for surface leakage current and 112.4 kΩ for internal cur-

rent.

d) Noise Elimination.

For eliminating superimposed noise signals in the two current signals, signal conditioners model 5B41–03 manufactured by Analog Devices Inc. were added to the input circuit. Signal isolation is provided by transformer coupling, using a proprietary modulation technique for linear stable performance. A demodulator at the output side of the signal transformer recovers the original signal, which is then filtered and buffered to provide a clean, low impedance output.

Specifications of the signal conditioner:

Input span limits	: ± 0.5 V to ± 10 V
Output ranges	: – 5 V to + 5 V or 0 to + 5 V
Accuracy	: ± 0.05 % span ± 0.05 % (V_Z)
	V_Z – input voltage that results in a 0 V output
Nonlinearity	: ± 0.02 % span
Band width, – 3 dB	: 10 kHz
Power supply voltage	: + 5 V ± 5 %
Input resistance	: 650 kΩ

e) Software Development.

LAB WINDOWS software package in Quick Basic environment was utilized to develop software for data acquisition and analysis. Software programs are included in Appendix A. LAB WINDOWS is an innovative program development software package for test and measurement applications. The package enhances microsoft Quick Basic and C languages with an interactive development environment, function panels to generate source code and libraries for data acquisition, instrument control, data analysis and presentation.

Data Acquisition.

A software program was developed to acquire analog voltage signals, to convert these analog signals to digital signals and to store the data on the PC hard disk as binary files. The data acquisition command Scan–to–disk performs a synchronous, multiple channel scanned data acquisition operation and simultaneously saves the acquired data in a disk file.

Software selectable gain for the input channels of A/D board was chosen as 1 with a sample rate of 4 ksamples / second per channel.

Pulse Detection.

A software program was developed to detect the surface leakage current pulses based on the five point gradient method.

Five point gradient method: the gradients of five consecutive sample points were calculated. If these four gradients had positive values, the first sample point was selected as the pulse starting point. Then the current corresponding to that point was regarded as a reference current for the particular pulse. The sample point at which the current was equal or less than the reference current was selected as the end point of the pulse. After detecting a pulse, sample points of the pulse were stored in the binary file. In addition pulse height, pulse duration and pulse start time were calculated and stored in separate binary files. The algorithm for the pulse detection is shown in Figure 2.8.

Pulse Data Analysis.

Pulse data analysis comprises of cumulative charge calculation of the two currents and the statistical analysis of the surface leakage current pulses.

The cumulative charges of the internal current and surface leakage current pulses were calculated from the current time integral $\int I\,dt$ based on the formula for discrete integral for the i^{th} element.

$$y(i) = \Sigma \left[x(j-1) + 4x(j) + x(j+1) \right] \frac{dt}{6} \qquad (2.1)$$

where,

$X(-1) = X_{initial}$

$X(n) = X_{final}$

Statistical analysis was developed to calculate the maximum, minimum, mean and standard deviation of pulse amplitude, duration and start time of each pulse to generate histograms and cumulative graphs of pulse amplitude, duration and time.

The following formula were applied to calculate the mean and standard deviation.

$$Mean = \Sigma \frac{x(i)}{n} \qquad (2.2)$$

$$Std.\ Dev. = \sqrt{\Sigma \frac{[x(i) - Mean]^2}{n}} \qquad (2.3)$$

The histograms were obtained by counting the number of times that the elements in any array fall in the i^{th} interval.

$$hist(i) = \Sigma\, y[x(j), i] \qquad (2.4)$$

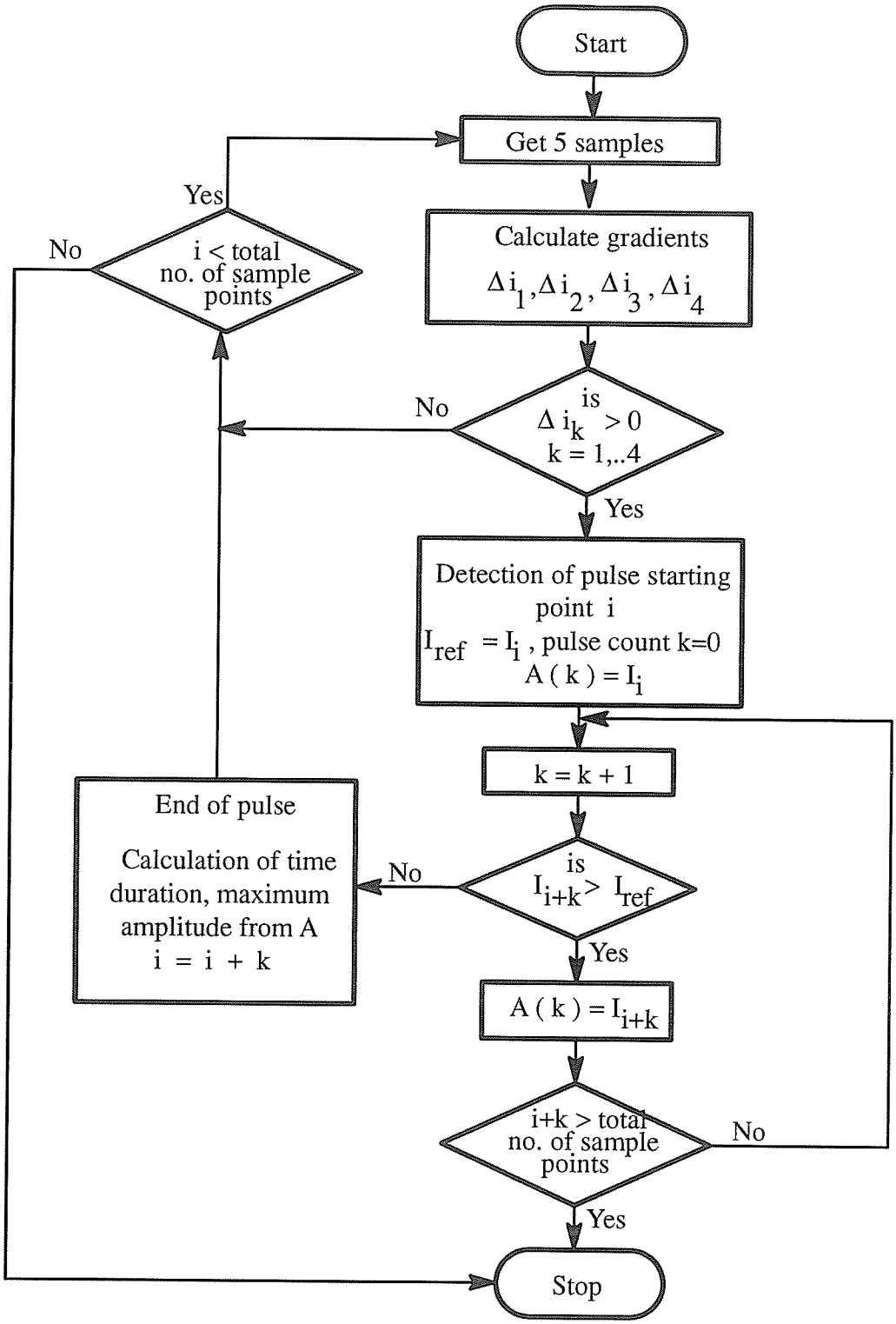

Fig. 2.8. Pulse detection algorithm.

2.6. Temperature measurement.

The temperature of the arrester was measured by three different methods:

a) Using a temperature probe with a multimeter.

A type K Thermocouple probe connected to a digital multimeter was used to measure the top block temperature of the arrester. The probe was inserted into arrester as shown on Figure 2.2.

Thermocouple specifications:

Type	: K (Chrome Alumel)
Tip Temperature Range	: 0 °C to 540 °C
Resolution	: 1 °C

Digital multimeter specifications for temperature measurements:

Range	: –50 °C to +1370 °C
Resolution	: 1 °C
Accuracy	:
–20 °C to 350 °C	± 0.5% reading + 2 digits
350 °C to 500 °C	± 1.75% reading + 2 digits
501 °C to 1370 °C	± 2.0% reading + 2 digits

b) Using infrared temperature measuring device.

The infrared non contact temperature measuring device, AGA Thermopoint 80 was used to measure temperature at different locations on the arrester surface. The Thermopoint 80 is a hand held instrument designed to measure surface temperature of the objects without contact. The instrument measures temperature by sensing the infrared energy emitted by an object or material, computes the surface temperature and displays the result on a liquid crystal display. It operates within the temperature range from –30 °C to 1100 °C and is designed to carry out accurate measurements from a minimum distance of 60 cm.

c) Using the relation between the internal current and the temperature of ZnO block.

Before the test the relation between the internal current and the temperature of ZnO block was found for a clean arrester. Then after each test, the temperature of internal blocks could be found by measuring the internal current.

The application of this method was very inaccurate because of the influence of the surface leakage current. The non–conducting silicon grease was not able to eliminate the surface current component. For this reason the internal current measurement always was not without error.

Chapter 3 FLASHOVER MECHANISM OF POLLUTED ARRESTER UNDER DC VOLTAGE.

Due to the lack of understanding and experience about the mechanisms which govern the flashover process on polluted EPDM insulators under dc voltages this chapter presents a literature review of research conducted in Japan and in the USA on HVDC porcelain and glass insulators.

The surface flashover of polluted insulation is a complex phenomenon, involving several variables. The flashover process develops in five main stages [9].

1. Surface contamination deposition.
2. Wetting of contamination layer with consequent formation of a conductive layer on insulator surface.
3. Formation of dry bands associated with a drying effect by surface leakage current with non–uniform density along the insulator surface.
4. Partial arc formation bridging the dry bands.
5. Arc elongation to complete short circuit of the insulation.

3.1. Surface contamination deposition; contamination pattern of dc insulators.

The first stage of the flashover process under pollution is the accumulation of contaminants over the surface of the insulation under voltage. Information was found in the literature about the types and degrees of contamination observed in some installations in USA and Japan. The first results presented were obtained at Sylmar dc Converter Station [10], the southern terminal of the +/– 500 kV HVDC Pacific Intertie, situated next to a busy interstate highway and inside a farming area.

An outdoor insulator testing rack consisting of 11 insulator strings was constructed and energized directly from the pole of the operating transmission line. Glass and porcelain insulators were tested. Also a string of dc suspension insulators was energized, at the same locations, at 230 kV ac at an approximately equivalent voltage stress as for dc energized insulators, for the same period.

The following observations were made:

– for the dc energized insulators the amount of soluble contaminants (expressed in ESDD) collected by the bottom surface of an insulator was much higher than that collected by the top surface. After two years the bottom surface accumulated 3 times more contaminants than the top one. After three years the ratio increased to 10 times. Rain had an effective cleaning action on the top surface but the effect of natural cleaning on the bottom surface is much reduced. After rainfall the amount of soluble contaminant level decreased more than 5 times at the top surface but to half of the previous level at the bottom surface.

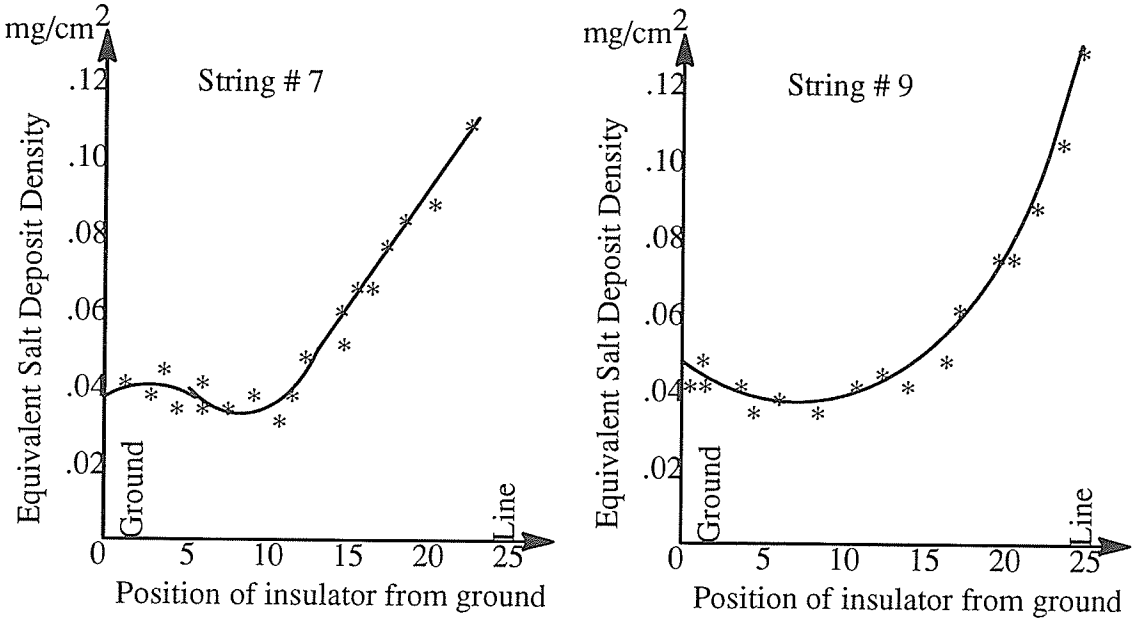

Fig. 3.1. Distribution of surface contaminant along the string of insulators after 38 months of exposure[10].

– nitrate salts accounted for over 50 % of the total contamination, probably due to automobile emission and agricultural pollution. The paper [10] suggests that during corona, ions N_2+, $NO+$, N_2H+, NO_2-, NO_3- are formed, which with suitable reacting agents can contribute to an increase of concentration of NO_3- ions.

– the amount of contaminants collected was different for insulator positions along the string. This pattern is noted mainly in the bottom surface of the insulators. The insulators close to the energized and ground terminals collected much more contaminants than those in the middle of the string. Figure 3.1 shows the distribution for two different insulators strings.

Tab. 3.1. Amount of contaminant collected by insulators energized in ac , dc and non–energized [10].

	TIME OF EXPOSURE = SIX MONTHS		
	dc voltage (0.8 kV/ in)	ac voltage (0.88 kV/ in)	non–energized dc field
ESDD (mg/cm^2)	0.0508 (max)	0.0105 (max)	0.016 (av)

– the ac energized string presented an entirely different pattern. The top surfaces, on the av–erage, accumulated 50 % more contaminant than the bottom ones. The amount of collected contaminant, however, was much less than for the dc string during the same time and loca–tion. Table 3.1 shows the ESDD values measured. It also shows the ESDD level for a non–energized string placed close to the test set–up, situated in the dc field. Chemical analysis was not performed for the ac energized insulator in order to verify if the composition of the contaminant layer was similar to that of the dc energized insulators. It is suggested that under dc the electrostatic forces have a dominating role, whereas, under ac, forces due to ac and gravity predominate and govern position of particles over the surfaces of insulators.

– for the dc energized strings the amount of collected contaminants increases with the volt age stress. The glass insulators collected more contaminant than the porcelain ones, even when the voltage level was lower.

Another paper [11] presents the results of measured contaminant levels on bus support and disconnect switches post insulators of four different HVDC Converter Station in USA, with operating voltage +/– 500 kV. Although the number of measurements was limited, as these stations are in operation and samples could be taken only during short maintenance periods, the following main conclusions are derived:

– the contaminant level on the top surfaces of the sheds increases downward towards ground, due to effect of rain.
– the amount of contaminant collected by the bottom part of sheds was on the average 35% higher than that for the top surface of sheds. The distribution of contamination on the bot– tom surface of sheds was practically uniform along the column.
– the contamination deposition was uniform along the circumference of the insulator.
– no difference was observed between the positive and negative polarity energized insula – tors.
– the accumulation of contaminants increases more linearly with the applied stress; for insu– lators submitted to the same average stress, those energized with higher voltages collect more pollution.

In order to measure the degree of contamination collected by dc insulators in Japan, four testing stations were mounted; three close to the sea and one inland [12, 13].The applied voltage was +/– 250 kV in one station (Takeyama, close to the coast) and +/– 280 kV in the other three. Some of the insulators were energized for more than five years.

The following information was obtained from the measurements:

Coastal Stations,

– no significant difference was observed between contamination levels collected by energized and unenergized insulators. The suggested reason is that, close to the sea, the contamination process is rapid, caused by the strong winds from the sea which carry the salt to be deposited.

– for short periods (some days) of observation the amount of contamination in the layer was almost constant along the insulator strings. However, when long periods were considered (some years) there was an increase of the pollution level on insulators close to the energized terminal.

– for short periods (some days) of observation there was no significant difference between top and bottom surface contamination levels. However, after one to three months there was an increase in the contamination level on the bottom surface as compared to the top ones; contamination levels were 2 to 5 times higher at bottom surface on average.

Inland station (Yonezawa testing station, 70 km from the coast). This station is located in a rural area far away from any industrial contamination source.

– the effect of the dc voltage on contamination collection was observed only on insulators close to the energized and ground end of the string under test.

– the amount of insoluble contaminants on the bottom surface of the dc energized insulators was 1.2 to 1.4 greater than for non energized ones. This value has a tendency to increase as the exposure period becomes shorter. The contamination levels (ESDD) on the bottom surface were 3 to 5 higher times than those observed on the top surfaces for those insulators close to the string ends, whereas no practical differences were observed for the unit in the middle of the string.

– no significant influence was observed in the contamination levels when the voltage stress was increased from 90 kV/m to 120 kV/m.

Another significant natural pollution study was performed in the USA by BPA and ASEA in a test rack at Big Eddy Test Center [14]. Tests were performed on different types of station insulators using a + / – 600 kV source, with 1.5 A continuous rating and voltage drop less than 5 % when 100 mA pulses are drawn by the load. Insulators were energized at different voltage levels: –100 kV, + 250 kV and + / – 500 kV. The following main results were obtained:

– pollution distribution is uneven along the insulators and around their circumference due to electric field and wind effects. Higher concentration occurs at ends of the strings. See Figure 3.2.

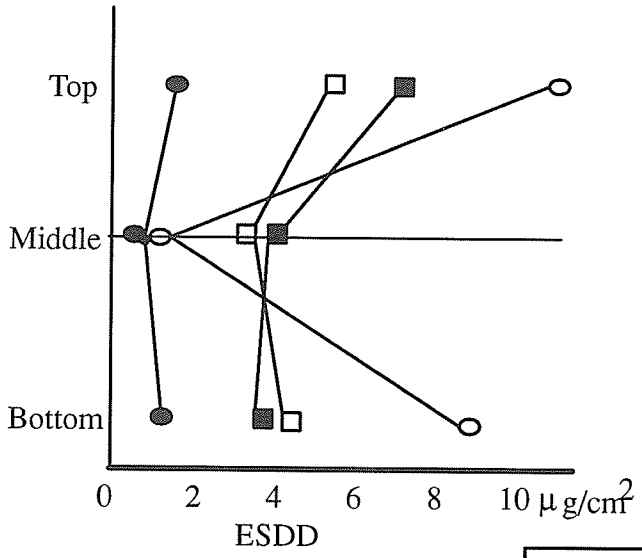

shed	stress mm/kV	surface
A	32	porc.
A	32	RTV
B	32	porc.
A	20	porc.
A	V=0	porc.

Fig. 3.2. Pollution distribution along insulators after 18 months [14].

– energized insulators collected approximately 3 times more contamination than non energized ones.

– self cleaning designs (it is not explained how the insulators are designed to have this characteristic) are effective in limiting the amount of pollution collected. In these insulators final pollution levels, which are dependent on weather conditions were attained in less than 3 months.

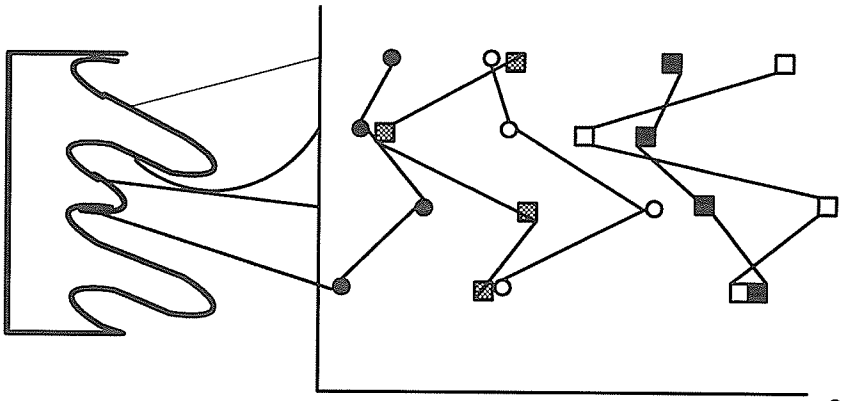

	stress mm/kV	surface	shed no.
○	32	porc.	53
■	32	RTV	53
▩	32	RTV	35
●	32	porc.	35
□	16	porc.	43

Fig. 3.3. Pollution distribution after three months of service.

– RTV and non ceramic insulators collect 1.5 to 2.0 times more pollution than porcelain but are more easily cleaned by wind and rain.

– the pollution level at top and bottom of sheds are different and change with insulator type.

Figure 3.3 shows the distribution obtained one month after measurable rain precipitation.

– the measured pollution levels and leakage currents were very low. Even during adverse weather conditions, current pulses were below 1 mA, however several flashovers were obtained during experiments. Those flashovers occurred on highly stressed insulators under heavy rain in combination with wind. Some occurred also under ice conditions at low pollution levels. Again it should be noted that there was a limitation of the power supply used which could inhibit pollution flashover development.

As a conclusion to this section it can be said that the results of the experiments conducted at different locations are, in general, in agreement. Differences occur in some aspects of the contamination process but this can occur due to the lack of understanding of the physical process for pollution deposition under HVDC.

No theoretical study was found in the literature about the surface contamination collection process under dc voltages, which, as seen from the field data is dependent on the electric field. The mechanism of pollution deposit is enhanced by ions generated due to corona on the high voltage conductors. If this mechanism is better understood, designs could be proposed which make dc insulators less sensitive to the pollution accumulation [9].

3.2. Mechanism of wetting the contamination layer.

A polluted insulator under dry condition has an electric strength very close to that of a clean one. When the pollution layer is wetted, the surface resistance decreases, increasing the surface current and eventually a flashover develops.

In nature, it is observed that polluted insulators flashover under very humid conditions, such as under drizzle and fog, or after sunset when the humidity increases.

Three main processes occur which cause wetting of the insulation contamination layer. The first one is the moisture absorption by the soluble and non–soluble components of the pollution layer. The intensity of moisture absorption depends on the chemical constitution of the pollution layer [9]. For example, NaCl rapidly absorbs moisture at the ambient humidity higher than 75 %. Other salts or salt compositions can have even higher hygroscopicity than NaCl [15].

The second process is the condensation of water over the insulator surface when the ambient temperature is higher than the insulator's one. This process is mainly influenced by the temperature difference between the insulator and the fog.

The third is wetting by collision of water droplets with the insulator surface, for example during rain.

During steam fog wetting method used in artificial pollution tests, similar phenomena occur as those in nature. The three main humidification processes are present; condensation being the major wetting factor.

Another wetting method, also used in the laboratory, is the cold fog method. This method was used for wetting the contamination layer on the polluted arrester in the solid deposit method conducted in this experiment. With standard equipment for fog generation water droplets are produced with average radius $\approx$31.4 μm and with a radius dispersion $\approx$18.8 μm. These parameters are much higher than those for droplets generated by the steam fog method, i.e. average radius $\approx$10.3 μm and radius dispersion $\approx$4.6 μm [9]. Due to these differences, humidification by cold fog is much faster than that by steam fog; its major wetting mechanism is the collision of the water droplets with the insulator surface. The minimum surface resistance is attained in less than 30 minutes. Also the washing of the pollution layer is a faster process.

Condensation is the major wetting mechanism during the steam fog wetting, and is due to the fact that water droplets have more uniform dimensions, and are of smaller sizes; this wetting process is much slower. The time to attain minimum surface resistance is larger than 40

minutes. Also the washing process is slower, resulting in leakage currents with longer duration. Due to these characteristics the steam fog method is preferred and it results in lower flashover voltages with less dispersion than the cold fog method.

3.3. Dry band formation.

The voltage gradient to initiate a discharge process in air is about 30 kV/cm. High voltage dc insulators are designed with an average working voltage gradient of about 330 V/cm or even less (arrester used in this experiment has an voltage gradient 290 V/cm). It can be concluded that in order to initiate flashover the voltage distribution along the insulator must be highly non–uniform. Some non–uniformity is expected because of insulator shape but the main factor which causes non–uniformity and consequently the appearance of highly stressed areas is the formation of dry bands.

When the pollution layer becomes wet, the surface resistance decreases and the surface leakage current increases. The current density is higher at some areas of the insulator surface, usually, where the insulator has a smaller diameter. In these areas, the drying effect of the leakage current overcomes the wetting effect of the fog and a dry band is formed, whose length can now increase with time. In suspension insulators, the dry bands usually forms around sharp edges.

As the resistance of the dry band is much higher than the resistance of the conductive layer across the rest of the insulating distance, almost the entire applied voltage is dropped across the dry band. When the dry band can not sustain the voltage across it, a partial arc is triggered and bridges the dry band. The applied voltage is then distributed across the wet area. Eventually the arc propagates across the rest of insulating distance leading to flashover. It is not clear from the analyzed literature what the initial condition is which triggers the arc across the dry band. Figure 3.4 shows qualitatively the process of dry band formation and breakdown on a polluted insulating strip.

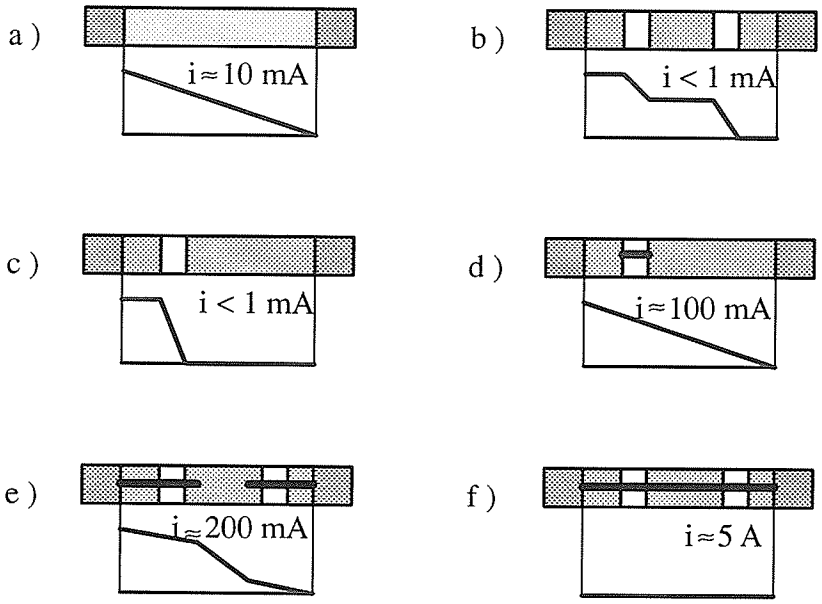

a) Wetting begins.

b) Dry bands form.

c) One dry band predominates.

d) Dry band flashes over.

e) Arc extend.

f) Flashover complete.

Fig. 3.4. Typical voltage distributions on a polluted strip [16].

One or more dry bands are formed even when the electrodes and the insulator are designed in order to have uniform current density along the insulating distance. This occurs probably due to the local non–uniformity of the pollution layer and the wetting process.

Due to the complexity of the arcing phenomena along contaminated surfaces, the models presented in literature are based on experiments with very simple insulator shapes (cylinder, rectangular plate, circular plate) and many simplified assumptions have to be made in order

that a mathematical model can be obtained.

The flashover voltage of polluted insulator is a statistical variable with significant dispersion, even when obtained in tests under controlled conditions. Some simplifications are made to obtain the model of flashover on polluted insulators, such as:

– simplicity of the insulator shape,

– uniformity of the pollution layer,

– linearity of surface resistivity due to thermal process and non–uniform wetting,

– no multiple arcing burning in series or in parallel,

– no influence of supply circuit parameters on the insulator behavior during the artificial tests.

These simplifications do not exist in a real complex case.

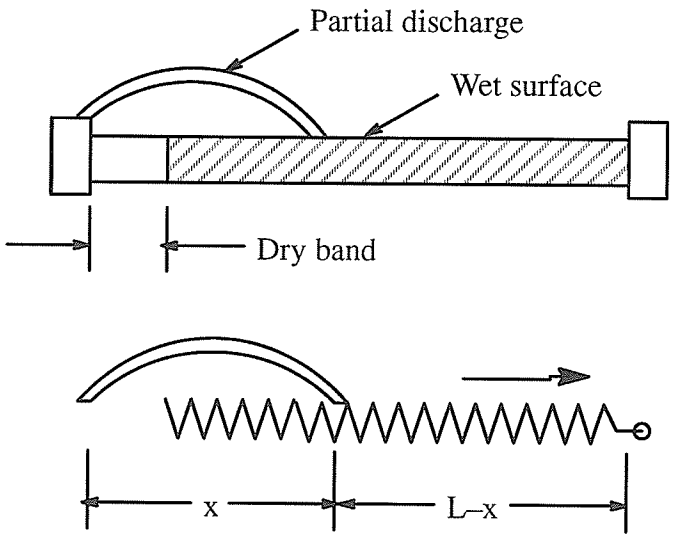

Fig. 3.5. Model of the flashover process proposed by Obenaus [17].

Arcing models have to take into account three aspects:

– a criterion to determine the minimum voltage necessary to trigger the partial arc across the dry band,

– a criterion to determine the minimum necessary voltage to maintain the partial arc in series

with the wetted contaminated layer,

– a criterion for arc propagation along the insulator surface.

The models presented in literature in general focus on the second aspect of the arcing phenomena.

In this thesis one particular model proposed by Obenaus in 1958 [9] will be presented. The model of the flashover process assumes an arc in series with a resistance as seen in Figure 3.5. The arc represents the partial flashover which bridges the dry band and the series resistance represents the series unbridged wetted polluted portion of the insulator.

The arc voltage can be expressed as:

$$V_{arc}=xNi^{-n}+V_e \qquad (3.1)$$

Where n and N are constant for the static arc characteristic in air, V_e is the electrode voltage drop, the sum of cathode and anode arc voltage drop, which, for an electrolyte was measured to be ≈830 V. Normally this voltage drop can be neglected, except for multiple arcs burning in series. Then:

$$V=xNi^{-n}+iR_p \quad \text{, or}$$

$$x=(i^n/N)(V-iR_p) \qquad (3.2)$$

where R_p is the resistance of pollution layer.

The maximum arc length that can be sustained in the circuit is determined by differentiating x with regard to i and equating to zero. For obtaining the critical current i_{cx} Eq. 3.2 must be differentiated with regard to x and equating to zero.

$$i_{cx}=V^n/R_p{}^{n+1} \qquad (3.3)$$

The critical arc length is given by substitution of (3.3) in (3.2):

$$x_c=(1/R_p)(V^{n+1}/N)(n^n/(n+1)^{n+1}) \qquad (3.4)$$

Now the minimum direct voltage V_{cx} necessary to sustain an arc of length x in series with the resistance R_p can be determined from (3.4):

$$V_{cx}=x^{1/(n+1)}N^{1/(n+1)}R_p{}^{n/(n+1)}(n+1)/(n^{n/(n+1)}) \qquad (3.5)$$

Reference [16] considers for the wet layer a uniform pollution resistance per unit leakage path:

$$R_p=r_p(L-x) \qquad (3.6)$$

Then:

$$V=xNi^{-n}+ir_p(l-x) \qquad (3.7)$$

The minimum voltage necessary to maintain an arc of the length x can be calculated by differentiating V with regard to i and equating to zero. The following expression is obtained for the corresponding current:

$$i_{cx}=[(nNx)/r_pL-r_px)]^{1/(n+1)} \qquad (3.8)$$

The critical voltage can be obtained by substitution of (3.8) in (3.7) and is given by:

$$V_{cx}=(n+1)\,(Nx)^{1/(n+1)}\,[r_p(L-x)/n]^{n/(n+1)} \qquad (3.9)$$

Figure 3.6 shows a curve for the relation between V_{cx} and x.

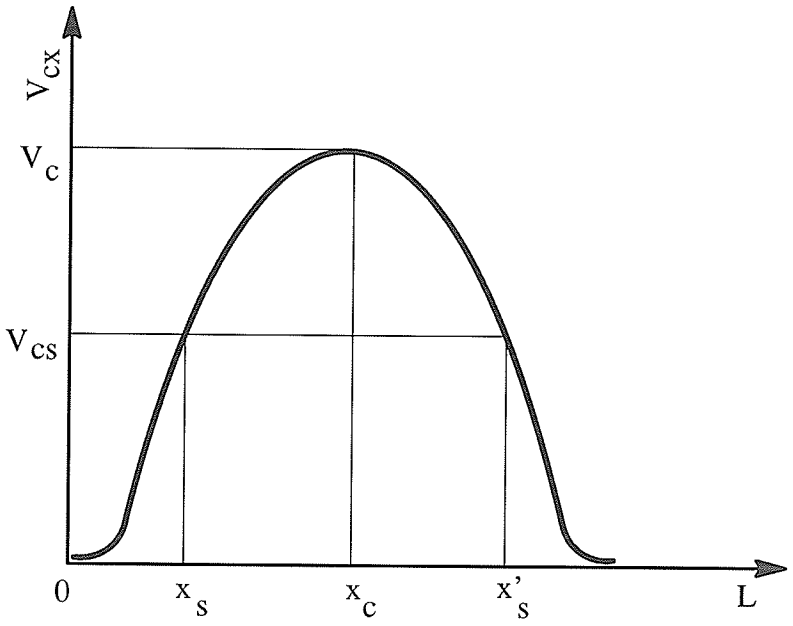

Fig. 3.6. Dependence of the critical voltage necessary to sustain a dc arc on the arc length according to Alston–Zoledziowski [18].

The maximum value for V_{cx} can be calculated by maximizing V_{cx} in relation to x:

$dV_{cx}/dx=0$ which results in:

$$x_c=L/(n+1) \qquad (3.10)$$

The maximum value V_c then is given by:

$$V_c = LN^{1/(n+1)} r_p^{n/(n+1)} \qquad (3.11)$$

If a voltage V_{cs} is applied to the insulator (Figure 3.6), the discharge being quite short initially, the discharge can grow until $x=x_s$. It cannot grow further because the voltage required to maintain conduction exceeds V_{cs} . However, if the discharge length exceeds x_s', initially, further increase of x will reduce the burning voltage so that the discharge can grow to a flashover.

From (3.7) and (3.8) the critical current can be obtained as:

$$i_c = (N/r_p)^{1/(n+1)} \qquad (3.12)$$

The critical current is independent of the leakage length L.

Some other models of arc propagation are presented in references [19], [20], [21], [22].

Chapter 4 PERFORMANCE OF MOSA IN A WET–POLLUTED CONDITIONS.

This chapter includes the results of artificial pollution tests, their description and proposed modifications of these procedures.

Whenever available, the results of the tests carried out in other laboratories are included. An extensive literature search showed that the performance of distribution class arresters in polluted conditions energized with dc voltage has not yet been investigated. Therefore only the results of the tests performed on transmission class arresters (MCOV over 100 kV) energized with ac voltage are included. This makes comparison of our results with those obtained in other laboratories very difficult. These results are presented to show the thermal behavior of metal oxide arresters in a wet–polluted conditions.

The available experience and knowledge of ac pollution testing should not be directly applied to HVDC arresters design. Because of the lack of tests procedures estabilishing the performance of distribution class metal oxide arresters in a wet–polluted environment under dc voltage procedures suggested by IEC and IEEE for the tests under ac voltage will be described. These procedures were studied in order to establish correlation between the natural contamination performance and the laboratory performance.

The test procedures which have been considered were:

1) Solid Deposit Method proposed by IEC.

2) Wet Slurry Test Method proposed by IEEE.

3) Partial Wetting Test Method proposed by IEEE.

4) Dip Test Method – modified version of Partial Wetting Test.

5) Test method in accordance with Japanese Standards.

6) Salt Fog Test Method proposed by IEC.

During these tests many results were collected, among which the most important are current–

time integral ($\int I\,dt$) and surface and top block temperature rise.

In this work results obtained from application of artificial test procedures proposed by IEC, IEEE or Japanese Standards will be described. Certain procedures were modified; corresponding test results are also included and discussed.

4.1. Solid Deposit Method.

4.1.1. Solid Deposit Method proposed by standards.

The Solid Deposit Test was conducted in accordance with IEC Publication 507 [23].

a) Compositions of the contaminating suspension.

The suspension was prepared using the following components:

- 40 g Kaolin,
- 1000 g demineralized water,
- a suitable amount of salt (NaCl),
- photo–flo solution.

To achieve the reference layer conductivity or Equivalent Salt Deposit Density in contaminating the arrester, an appropriate value of volume conductivity of the prepared suspension is required. This was provided by adjusting the amount of salt in the suspension itself.

b) Application of the pollution layer.

The liquid containing the contaminant was applied by spraying the dry insulator which was previously cleaned. To obtain a reasonably uniform layer, the arrester was always sprayed with a fixed number of coats (2) and squeezes (40). To avoid dripping after the application of each coat the arrester was dried using a hand held dryer. During spraying and drying the arrester was rotated at a constant speed of 3 rpm. After this process, the arrester was allowed to dry overnight before each test.

c) Wetting of the pollution layer.

The arrester was wetted in the fog chamber described in section 2.4 using fog generated with nozzles spraying warm water.

After a certain degree of wetting of the pollution layer was reached, moisture from the edges of the arrester sheds started to drip; some pollution content was removed from the layer and progressive washing of arrester was obtained.

d) Equivalent Salt Deposit Density (ESDD).

For every Solid Deposit Test two arresters with the same shape were washed, dried and polluted in exactly the same manner. Then, one arrester was used to perform Solid Deposit Test and the second one to measure ESDD.

The deposit was removed and carefully collected from the surface of the arrester and then dissolved in a known quantity (500 ml) of demineralized water. The resulting solution was thoroughly stirred before measuring its conductivity σ_0 at the temperature t. The salt solution concentration S_a (mass of NaCl in the unit of volume of solution) was determined by use of the following expression [23]:

$$S_a = (6.31\ \sigma_{20}\ 10^{-3})^{1.042}\ 10 \qquad 4.1$$

where σ_{20} was obtained from formula:

$$\sigma_{20} = \sigma_0\ [\ 1 - b\ (\ t - 20\ )] \qquad 4.2$$

with:

t – solution temperature,

σ_0 – conductivity at temperature t,

b – factor depending on temperature t as given in Table 4.1.

Tab. 4.1. Variation of factor b with temperature.

t [°C]	b
0	0.03675
10	0.02817
20	0.02277
30	0.01905
40	0.01632

For other values of temperature t, the factor b was obtained by linear interpolation.

e) Test procedure.

The test voltage was applied to a dry arrester in its test position and fog was admitted at a steady rate. The Standard states that the voltage should be maintained until flashover occurs or for 120 minutes from the start of the test.

Tests were performed with three different levels of ESDD:

– light 0.01 – 0.06 mg/cm^2,

– moderate 0.06 – 0.1 mg/cm^2,

– heavy 0.1 – 0.4 mg/cm^2.

To find the influence of the thickness of pollution layer tests were performed with three different levels of kaolin in suspension:

– light 20 g/l,

– moderate 40 g/l , proposed by standards,

– heavy 160 g/l.

All tests were repeated three times.

During the tests the internal and surface current data was stored. After the tests the following were developed:

– histograms of scintillation pulse amplitude, number and time duration,

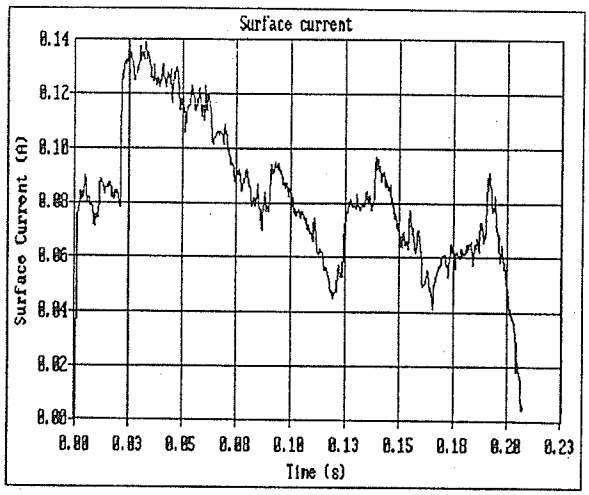

Fig. 4.1. An example of surface current pulse.

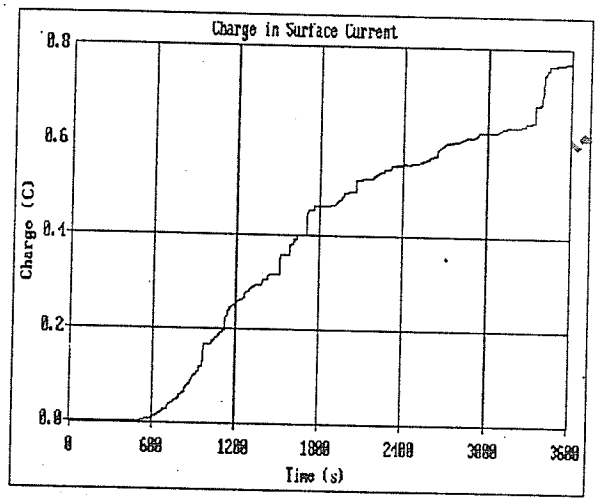

Fig. 4.2. An example of charge in surface current.

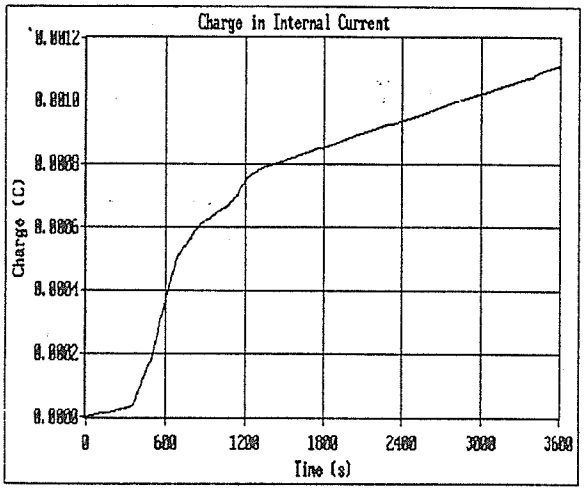

Fig.4.3. An example of charge in internal current.

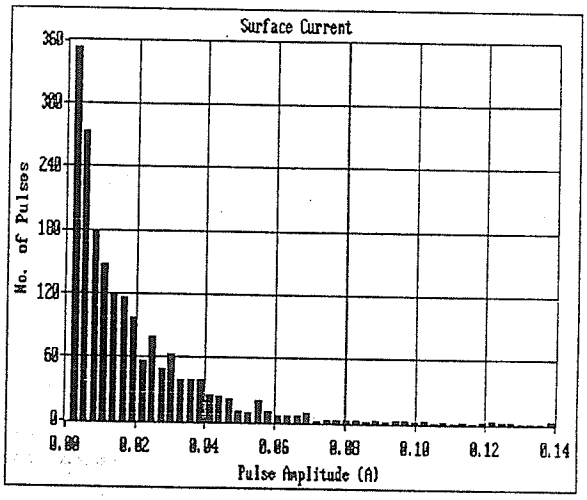

Fig. 4.4. An example of histogram of scintil–lation pulse amplitude.

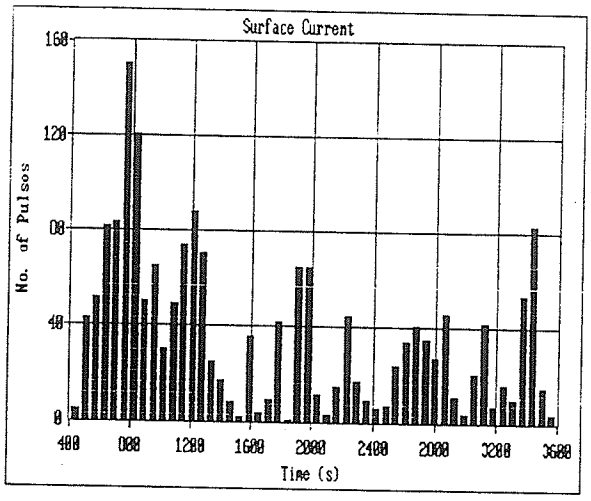

Fig.4.5. An example of histogram of number of scintillation pulses.

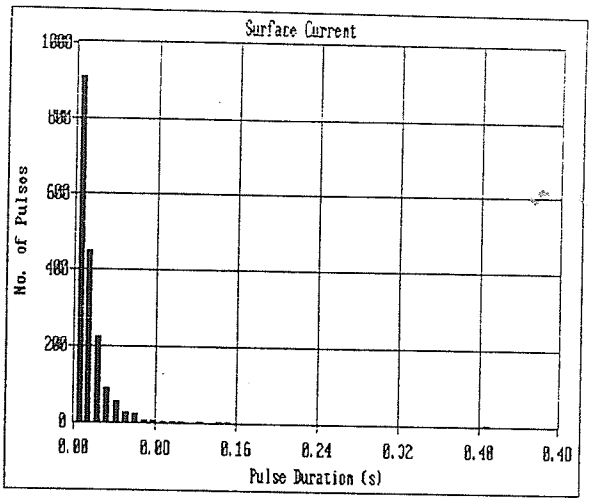

Fig.4.6. An example of histogram of scintillation pulse time duration.

– current–time integral ($\int I\,dt$) for both currents,

– changes in top block temperature.

Selected examples of surface current pulse, histograms of scintillation pulse amplitude, number and time duration and the charge in surface and internal currents are presented in Figures 3.1 to 3.6.

The results obtained with the Solid Deposit Method with different ESDD and different level of kaolin are shown in Tables 4.2 and 4.3.

Additionally Solid Deposit Tests were conducted with some modifications in the method of application of the pollution layer (non–uniform pollution) and in the test procedure.

Tab. 4.2. Solid Deposit Method results for different ESDD.

ESDD [mg/cm^2]	$Q_{surf.}$ [C]	$Q_{int.}$ [C]	No. of pulses	Max. ampl [mA]	Max. dur. [s]	Temp. incr. [°C]
0.055	0.0465	0.00094	745	27.73	0.274	0
0,059	0.0132	0.00046	348	12.1	0.88	0
0.05	0.193	0.00053	607	48.4	0.831	0
0.062	0.09	0.0057	228	35.5	0.753	0
0.082	0.4988	0.0009	1950	86.33	O.487	0
0.085	0.477	0.00128	2149	70.31	0.876	0
0.159	0.934	0.0027	1700	152.7	0.463	0
0.16	1.237	0.0039	1415	167.58	0.371	0
0.19	0.772	0.0011	1827	140.2	0.458	0

Tab.4.3. Solid Deposit Method results for different level of kaolin.

Kaolin [g/l]	ESDD [mg/cm^2]	$Q_{surf.}$ [C]	$Q_{int.}$ [C]	No. of pulses	Max. ampl. [mA]	Max. dur. [s]	Temp. incr [°C]
160	0.08	0.302	0.00077	609	96.48	0.47	0
160	0.091	0.829	0.00047	883	100.0	0.68	0
20	0.09	0.356	0.00093	1170	31.64	0.449	0

4.1.2. Modified Solid Deposit Methods – non–uniform pollution.

The arrester was polluted non–uniformly in several different ways:

I. Only bottom or only top parts of the sheds were polluted in the moderate ESDD level. The way of pollution application is presented at Figure 4.7. During these tests, surface leakage current was very small because of the high resistance of the clean parts of sheds. In half of the test a few small scintillation pulses were observed in the middle of the arrester. There was no temperature increase noticed in any of these tests.

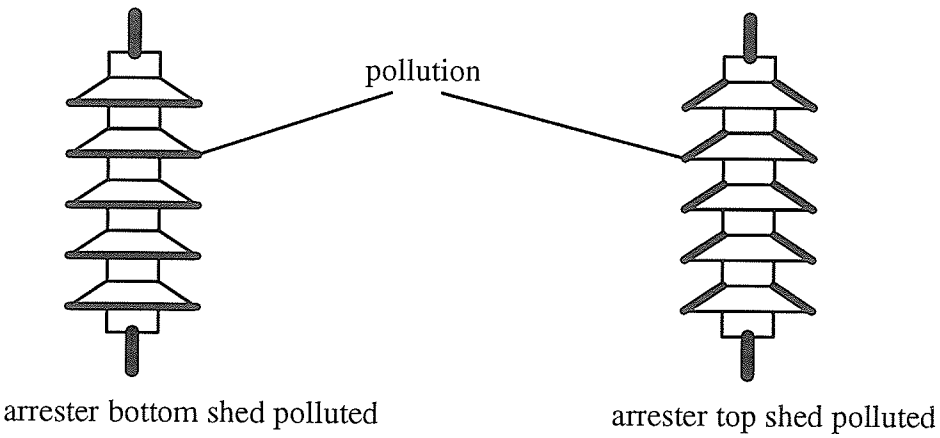

Fig. 4.7. Non–uniform pollution of the arrester.

II. Half of the arrester was polluted.

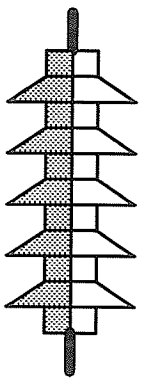

Fig. 4.8. Non–uniform pollution of the arrester – half polluted.

Figure 4.8 shows the type of non–uniformity considered. During these tests, pulses appeared only at the polluted side of the arrester, mostly at the bottom end. These were small in amplitude and short in duration. Results of these tests are presented in Table 4.4.

Tab. 4.4. Solid Deposit Method results – arrester half polluted.

ESDD [mg/cm^2]	$Q_{surf.}$ [C]	$Q_{int.}$ [C]	No. of pulses	Max. ampl. [mA]	Max. dur. [s]	Temp. incr. [°C]
0.054	0.01	0.00057	318	9.37	0.153	0
0.066	0.027	0.00043	481	10.57	1.149	0
0.06	0.073	0.0038	361	15.6	1.886	0

III. Arrester was polluted non–uniformly: top and bottom – moderate ESDD,
middle – light ESDD.

The manner of pollution application is presented in Figure 4.9 and the results are included in Table 4.5.

Test III Test IV

Fig. 4.9. Non–uniform pollution application for tests III and IV.

During these tests, pulses developed mostly in the middle and at the second and third shed from the bottom of the arrester.

Tab. . 4.5. Solid Deposit Method – arrester polluted in a "U" shape (Test III).

ESDD [mg/cm^2]	$Q_{surf.}$ [C]	$Q_{int.}$ [C]	No. of pulses	Max. ampl. [mA]	Max. dur. [s]	Temp. incr. [°C]
T – 0.065 M – 0.06 B – 0.095	0.313	0.0005	1820	71.8	0.433	0
T – 0.085 M – 0.06 B – 0.08	0.786	0.00067	2765	83.2	0.616	0
T – 0.075 M – 0.058 B – 0.085	0.45	0.00088	1772	81.64	0.606	0

IV. Arrester was polluted non–uniformly: top – moderate ESDD,

middle – light ESDD,

bottom – heavy ESDD.

During this test, pulses appeared both at the top and at the bottom of the arrester. The position of the pulses did not change during the test duration; only their intensity decreased with time of voltage application. The manner of pollution application is shown in Figure 4.9–Test IV. and results are presented in Table 4.6.

Tab. 4.6. Solid Deposit Method – arrester polluted non–uniformly (Test IV).

ESDD [mg/cm^2]	$Q_{surf.}$ [C]	$Q_{int.}$ [C]	No. of pulses	Max. ampl. [mA]	Max. dur. [s]	Temp. incr. [°C]
T – 0.08 M – 0.06 B – 0.15	0.353	0.00061	1037	21.87	0.824	0
T – 0.085 M – 0.059 B – 0.17	0.171	0.00052	1576	30.86	0.622	0
T – 0.08 M – 0.058 B – 0.15	0.449	0.00054	1208	36.72	0.351	0

4.1.3. Modified Solid Deposit Method – two arrester units in series.

Two arresters connected in series were supplied with 18 kV negative dc voltage. In these tests the surface current terminal was removed and the non–conductive silicone grease was not applied. Throughout these tests temperature of the arresters before, during and after the test was monitored.

Tests were conducted for two different cases:

I. top arrester – clean,
   bottom arrester – polluted (ESDD – 0.085 mg/cm^2).

II. top arrester – polluted (ESDD – 0.08 mg/cm^2),
   bottom arrester – polluted (ESDD – 0.055 mg/cm^2).

During these tests no temperature increase was observed. In the first case weak and very short pulses were observed at the bottom arrester. In the second case, pulses were stronger and appeared on both arresters, but were concentrated mostly at the top of the bottom arrester.

4.1.4. Modified Solid Deposit Method – modifications in the test procedure.

In order to extend the time duration of the test and to avoid quick washing of the polluted arrester surface fog was not supplied continuously. The voltage was applied during the whole time.

Again several different cases were tested:

I. Arrester polluted uniformly (ESDD – 0.18 mg/cm^2).

During this test, it was found that the scintillation pulses were strong and could last up to three hours only when the period on/off for the fog supply was around 16 min. (8 min. on and 8 min. off). In this way the process of arrester washing was slowed down. Data was collected once every hour of the test for a period of one cycle. The results are presented in Table

4.7.

Tab. 4.7. Solid Deposit Method – fog supplied at intervals, single arrester.

Time duration [min.]	$Q_{surf.}$ [C]	$Q_{int.}$ [C]	No. of pulses	Max. ampl. [mA]	Max. dur. [s]	Temp. incr. [°C]
36 – 52	0.105	0.00011	108	60	0.406	0
88 – 104	0.031	0.0001	60	46	0.159	0

II. Two arresters in series polluted non–uniformly in the "U" shape.

The arresters in this test were energized for three hours with fog supplied with 16 min on/off periods. Data was collected for 16 min during each hour. The test was performed twice for two different levels of pollution:

1) top arrester ESDD:
   top – 0.158 mg/cm^2,
   middle – 0.12 mg/cm^2,
   bottom – 0.158 mg/cm^2.

   bottom arrester ESDD:
   top – 0.09 mg/cm^2,
   middle – 0.06 mg/cm^2,
   bottom – 0.09 mg/cm^2.

The results are presented in Table 4.8.

Tab.4.8. Solid Deposit Method – fog supplied at intervals; two arresters in series; test No. 1.

Time duration [min.]	$Q_{surf.}$ [C]	$Q_{int.}$ [C]	No. of pulses	Max. ampl. [mA]	Max. dur. [s]	Temp. incr. [°C]
16 – 32	0.203	0.00092	282	73	0.266	0
80 – 96	0.167	0.00095	82	106	0.708	0
144 – 160	0.091	0.0011	143	63	0.434	0

2) top arrester ESDD:

top – 0.14 mg/cm^2

middle – 0.08 mg/cm^2

bottom – 0.14 mg/cm^2

bottom arrester ESDD:

top – 0.06 mg/cm^2

middle – 0.03 mg/cm^2

bottom – 0.06 mg/cm^2

Test results are presented in Table 4.9.

Tab.4.9. Solid Deposit Method – fog supplied at intervals; two arresters in series; test No. 2.

Time duration [min.]	$Q_{surf.}$ [C]	$Q_{int.}$ [C]	No. of pulses	Max. ampl. [mA]	Max. dur. [s]	Temp. incr. [°C]
16 – 32	0.144	0.00014	174	83	0.355	0
80 – 96	0.087	0.00008	50	90	0.147	0
144 – 160	0	0.00002	0	0	0	0

During this test, discharges appeared mostly at the top part of the bottom arrester. They become weaker with time and disappeared within the third hour, especially in the second test where the ESDD was lower. The temperature of the arrester did not increase in this test.

III. Two arresters in series polluted uniformly with different ESDD levels.

The arresters were polluted with following ESDD:

top arrester – 0.158 mg/cm^2,

bottom arrester – 0.08 mg/cm^2.

During this test, pulses occurred along both arresters but were not able to heat them. The re–

sults of this test are shown in Table 4.10.

Tab.4.10. Solid Deposit Method – fog supplied at intervals, two arresters polluted uniformly in series.

Time duration [min.]	$Q_{surf.}$ [C]	$Q_{int.}$ [C]	No. of pulses	Max. ampl. [mA]	Max. dur. [s]	Temp. incr. [°C]
18 – 34	0.225	0.0012	261	125	0.651	0
80 – 96	0.326	0.00008	92	177	0.407	0
146 – 162	0.136	0.00007	48	45	0.257	0

IV. Single arrester energized at $\sqrt{2}$ times the MCOV .

This test followed the procedure proposed by standards. The results are presented in Table 4.11.

Tab. 4.11. Solid Deposit Method – arrester energized at $\sqrt{2}$ times the MCOV.

ESDD [mg/cm^2]	$Q_{surf.}$ [C]	$Q_{int.}$ [C]	No. of pulses	Max. ampl. [mA]	Max. dur. [s]	Temp. incr. [°C]
0.015	1.43	0.0022	477	0.237	0.603	3

During this test a very slight temperature increase was noticed. The top block temperature rise is shown in Figure 4.10.

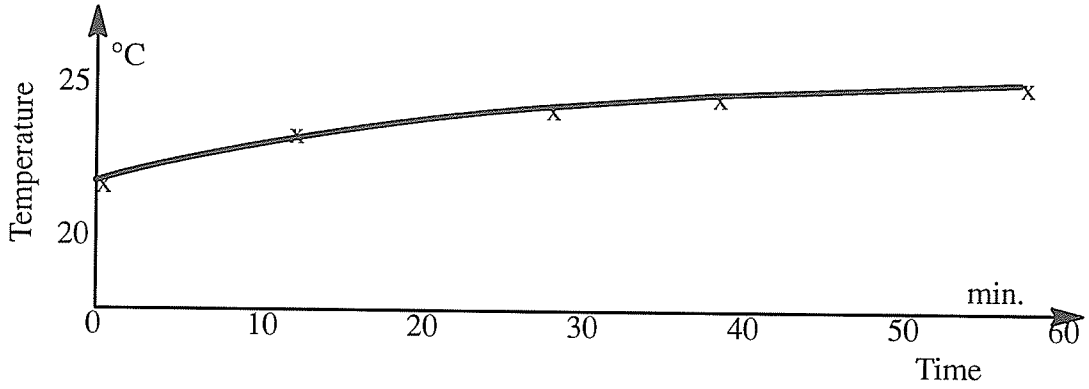

Fig. 4.10. Temperature increase of the arrester energized at MCOV x $\sqrt{2}$.

4.1.5. Solid Deposit Method tests performed in other laboratories.

References [24] and [25] describe the use of the Solid Deposit Method in other laboratories, and the results are included in Table 4.12.

Tab. 4.12. Results of Solid Deposit Tests.

Reference number	MCOV [kV]	Temp. incr. [°C]	Remarks
[24]	245 ac	70	ESDD – 0.15 mg/cm^2 ; bottom or top unit polluted; test duration two hours; larger temperature rise when top unit polluted.
		20	ESDD – 0.15 mg/cm^2 ; one arrester uniformly polluted; test duration two hours.
[25]	110 ac	26 – top 24 – bottom	Modified Solid Deposit Method; each test consisted of two wetting and drying cycles. Time duration and ESDD are not specified.
	220 ac	25 – top 23 – bottom	

4.2. Wet Slurry Method.

4.2.1. Wet Slurry Method proposed by standards.

The Wet Slurry Test was conducted in accordance with the procedure developed by the IEEE Surge Protective Devices Working Group [26].

a) Compositions of the contaminating suspensions.

The suspension was prepared using the following compositions:

- 40 g Kaolin,
- 1000 g demineralized water,
- 18 g salt (NaCl) – very heavy pollution,
- photo–flo solution.

b) Test procedure.

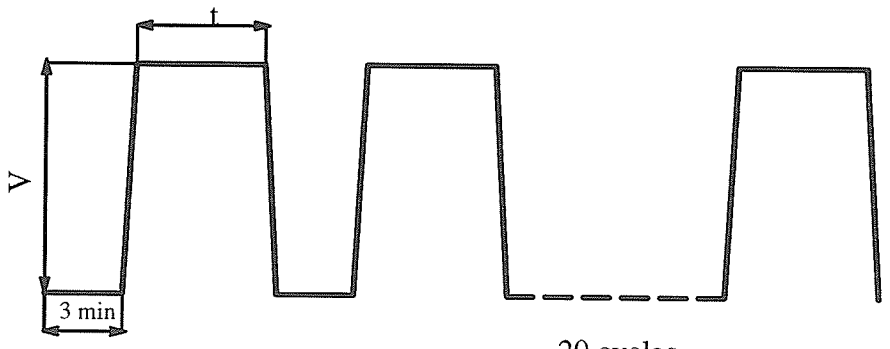

Fig. 4.11. Wet Slurry Test method diagram.

The clean and dry arrester was polluted in the fog chamber in its test position. Pollution was applied by spraying the arrester uniformly until the solution was dripping from the surface.

After completion of the slurry application a 3 minute drip time was allowed. Then the arrester was energized at its MCOV level. After 15 minutes the arrester was de–energized and re–sprayed to begin the next slurry cycle. This procedure was repeated 20 times for a total energization time of 5 hours. After completion of the 20th slurry cycle, MCOV was maintained at the arrester for a minimum duration of 30 minutes or until arrester demonstrated thermal stability. The above procedure is shown diagrammatically in Figure 4.11. Thermal stability was determined by measurement of internal current and the top block temperature. After each cycle the temperature of the arrester was measured by a temperature probe (top block temperature) and infrared gun (surface temperature).

4.2.2. Modified Wet Slurry Methods.

In order to find the performance of MOSA in very stringent conditions some modifications in test procedure were applied:

a) Time of voltage application was reduced.

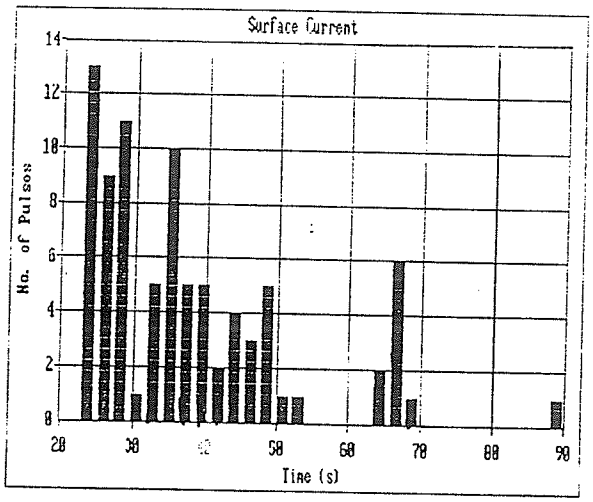

Fig.4.12. Intensity of scintillation pulses during Wet Slurry Test.

During the Wet Slurry Test (as recommended by standards) it was found that scintillation pulses at the surface of the arrester occurred only within the first few minutes during each cycle (see Figure 4.12). After a short time when the arrester dryed out, the leakage current was very small and the arrester cooled down. To avoid too extensive cooling, time of voltage application was reduced first to 7 minutes and then to 4 minutes.

b) Tests were performed with arrester energized at $\sqrt{2}$ times the MCOV .

All available test procedures for evaluating the performance of metal oxide arresters use ac voltage. Because for ac application MCOV refers to the r.m.s. value, some tests were performed to determine the performance of the arrester energized at a voltage which refers to ac maximum value.

4.2.3. Results.

I. Single arrester energized at MCOV; time of voltage application 15 min.

During each period of this test there were many heavy and long scintillation pulses observed along the arrester. After 1 to 4 min. a long dry band appeared at one of the sheds (usually at the top one) and within one minute the pulses disappeared.
The temperature increased during pulsing and then decreased. With increasing number of cycles the pulses became stronger and longer in duration, but they still lasted only 2 to 3 minutes. The behavior of scintillation pulses was very similar in all Wet Slurry Tests.
During this test, the pulse data was collected and analyzed only for the 14th and the 18th cycle. The results presented in Table 4.13 show a slight top block temperature increase of 4 and 6 °C after the 14th and 18th cycle respectively. A maximum top block temperature rise of 7 °C occurred after the 20th cycle.

Tab. 4.13. Wet Slurry Method; single arrester energized at MCOV; time of voltage application 15 min.

Cycle No.	$Q_{surf.}$ [C]	$Q_{inter.}$ [C]	No. of pulses	Max. ampl. [mA]	Max. duration [s]	Top block temp. incr. [°C]	Surface temp. incr. [° C]
14	0.45	0.0028	85	105.8	1.46	4	N/A
18	0.95	0.0023	93	181.6	1.97	6	N/A

II. Single arrester energized at MCOV; time of voltage application 7 min.

During this test pulse data was collected and analyzed for the 3rd, 8th, 13th and 19th cycle. The results are shown in Table 4.14. The maximum top block temperature increase was noticed after the 20th cycle.

Tab. 4.14. Wet Slurry Method; single arrester energized at MCOV; time of voltage application 7 min.

Cycle No.	$Q_{surf.}$ [C]	$Q_{inter.}$ [C]	No. of pulses	Max. ampl. [mA]	Max. duration [s]	Top block temp. incr. [°C]	Surface temp. incr. [° C]
3	1.437	0.0012	173	192	1.73	4	N/A
8	0.89	0.0009	112	166	0.95	7	N/A
13	0.45	0.0011	101	144	1.05	6	N/A
19	1.116	0.0017	115	164	1.74	6	N/A

III. Single arrester energized at MCOV; time of voltage application 4 min.

Within this test pulse analysis was performed after the 3rd, 8th, 13th and 18th cycle. The re-

sults are presented in Table 4.15.

Tab. 4.15. Wet Slurry Method; single arrester energized at MCOV; time of voltage application 4 min.

Cycle No.	$Q_{surf.}$ [C]	$Q_{inter.}$ [C]	No. of pulses	Max. ampl. [mA]	Max. duration [s]	Top block temp. incr. [°C]	Surface temp. incr. [°C]
3	1.875	0.00005	97	200	1.33	5	7
8	0.713	0.00002	56	234	1.56	9	9
13	0.576	0.00003	97	188	1.41	6	6
18	0.648	0.00002	75	311	1.8	8	13

The maximum top block temperature increase of 9 °C occurred during the 8th and 17th cycle and the maximum surface temperature increase of 13 °C was observed after the 4th, 15th and 18th cycle.

IV. Single arrester energized at $\sqrt{2}$ times the MCOV; time of voltage application 4 min.

Tab. 4.16. Wet Slurry Method; single arrester energized at $\sqrt{2}$ times the MCOV; time of voltage application 4 min.

Cycle No.	$Q_{surf.}$ [C]	$Q_{inter.}$ [C]	No. of pulses	Max. ampl. [mA]	Max. duration [s]	Top block temp. incr. [°C]	Surface temp. incr. [°C]
3	1.566	0.0011	286	330	1.71	8	9
8	0.803	0.0008	59	180	1.40	11	7
13	0.293	0.0006	55	95	1.69	11	6
18	0.874	0.0009	95	247	1.0	13	9

In this test pulse data was stored and analyzed for the 3rd, 8th, 13th and 18th cycle. The maximum top block temperature increase of 13 °C occurred during the 18th cycle and the maxi-

mum surface temperature increase of 9 °C was noticed after the 3rd and 4th cycle. By measuring the surface temperature it was found that the largest temperature rise occurred in those places where dry bands and scintillation pulses were observed. Results of this test are presented in Table 4.16.

V. Two arresters in series energized at 18 kV; time of voltage application 7 min.

For this test both arresters were polluted. The top block temperature was measured at the top arrester, and surface temperature on both arresters. The highest top block temperature rise of 7 °C was observed during the 19th and 20th cycle and surface temperature after each of the three latest cycles. The results of this test are shown in Table 4.17.

Tab. 4.17. Wet Slurry Method; two arresters in series energized at 18 kV; time of voltage application 7 min; test No. 1.

Cycle No.	$Q_{surf.}$ [C]	$Q_{inter.}$ [C]	No. of pulses	Max. ampl. [mA]	Max. duration [s]	Top block temp. incr. [°C]	Surface temp. incr. [°C]
3	0.474	0.0016	120	115	0.538	2	3 top arrester
8	0.131	0.0011	153	61	0.677	3	4 bottom arrester
13	0.540	0.0002	122	91	1.3	7	5 top arrester
19	0.457	0.0019	129	117	1.2	6	5 bottom arrester

In order to check which arrester was exposed to more severe pollution conditions this experiment was repeated. The results from the second test are included in Table 4.18.

In both tests the maximum surface temperature of the arresters depended on where the dry band had formed earlier, but most frequently the hottest spots appeared on the bottom part of the top arrester or on the top part of the bottom arrester.

During the second test the arresters' temperature increased more. The maximum top block temperature increase reached 8 °C in the 19th cycle and maximum surface temperature rise

of 6 °C was noticed after the 18th and 19th cycle.

Tab. 4.18. Wet Slurry Method; two arresters in series energized at 18 kV; time of voltage application 7 min; test No. 2.

Cycle No.	$Q_{surf.}$ [C]	$Q_{inter.}$ [C]	No. of pulses	Max. ampl. [mA]	Max. duration [s]	Top block temp. incr. [°C]	Surface temp. incr. [° C]
3	0.946	0.00049	289	123	1.51	6	4 top arrester
8	1.052	0.0001	217	132	0.89	7	5 top arrester
13	0.682	0.0003	122	172	0.93	6	3 both arresters
18	0.801	0.0003	75	205	1.39	7	6 top arrester

4.2.4. Wet Slurry Tests performed in other laboratories.

Two papers [24] and [26] have discussed the Wet Slurry Tests and the results are shown in Table 4.19.

Tab. 4.19. Results of Wet Slurry Tests performed in other laboratories.

Reference number	MCOV [kV]	Max. temp. increase [° C]	Remarks
[26]	140 ac	23 – top 26 – bottom	IEEE 5–hours Wet Slurry Test procedure was applied; ESDD was not specified.
	210 ac	34 – top 23 – middle >20 – bottom	
[24]	245 ac	65	ESDD – 0.015 mg/cm – bottom unit polluted; modified method – pollution was applied twice and then arrester was energized for 15 and 20 minutes.
	245 ac	22	ESDD – 0.015 mg/cm – arrester polluted uniformly; modified method – arrester polluted and energized for 10 min. and then six times polluted and energized for 20 min.

4.3. Partial Wetting Test.

4.3.1. Partial Wetting Test Method proposed by standards.

The Partial Wetting Test was conducted in accordance with IEEE Standards for Metal Oxide Surge Arresters for ac Power Circuits [27].

This test was performed to examine the effects of abnormal wetting on the polluted arresters. It simulates the performance of transformer–mounted arrester adjacent to a deluge system that malfunctions and sprays water over the bottom section of a contaminated arrester. Alternatively, it could represent the performance of pedestal–mounted contaminated arrester in a fog. In this way the bottom section of the arrester is wetted [26].

In both of these cases, the wet contaminated bottom section of the arrester may force substantial surface leakage currents to flow through the inside elements of the dry top section. If the contamination level is severe, external flashover of the arrester housing can occur. Less severe contamination can, in the case of metal oxide arresters, cause substantial heating of the arrester top section, promoting thermal instability [26].

a) Test procedure.

The clean and dry arrester was energized at MCOV. After at least one hour the arrester was de–energized and the contaminant was applied to the entire surface of the lower half of the arrester, including the undersides of the sheds. The coating was applied heavily enough to form drops of the slurry at the skirts of the housing. The contamination was applied by spraying. Within three minutes of contamination application, the arrester was energized at MCOV. The measurements of leakage current, top block and surface temperature were made at the end of 15 minutes of energization.

After the measurements the arrester was polluted again and energized at MCOV in the same way as before. After each step, the temperatures and the internal current were measured.

According to standards the arrester shall have passed this test if [27] :

i) it demonstrates thermal stability,

ii) no flashovers occurs, or

iii) there is no physical damage to the internal parts as evidenced by inspection.

The contamination suspension components are described in Section 4.2.1.

4.3.2. Results.

The Partial Wetting Test was performed with the arrester energized at MCOV and $\sqrt{2}$ times the MCOV.

No changes in internal current, top block temperature and surface temperature were observed before, during and after the test.

4.4. Dip Test.

The Dip Test was proposed by our laboratory as a modified version of Partial Wetting Test.

4.4.1. Dip Test procedure.

A clean and dry arrester was dipped into the water with sodium chloride (NaCl) and energized at MCOV. For this test the amount of salt was proposed as 1 g/l which gave a resistivity of 480 Ωcm.

The internal current, the top block temperature and the surface temperature were measured before, during and after the test. The criteria for passing the test were the same as for the Partial Wetting Test.

4.4.2. Results.

As in the case of the Partial Wetting Test no difference in internal current and no rise of top block or surface temperature was observed.

4.5. Test method in accordance with Japanese Standards.

This test was performed in accordance with Japanese Standard "Electrical Standards for Arresters" [28]. This procedure is designed for ac voltage.

During the test the top block and surface temperatures were measured, and a full pulse analysis was performed.

This test was conducted to verify that no discharges occur in internal parts and that there is no flashover on the insulator surface under rated voltage on the polluted arrester [26].

4.5.1. Japanese Test procedure.

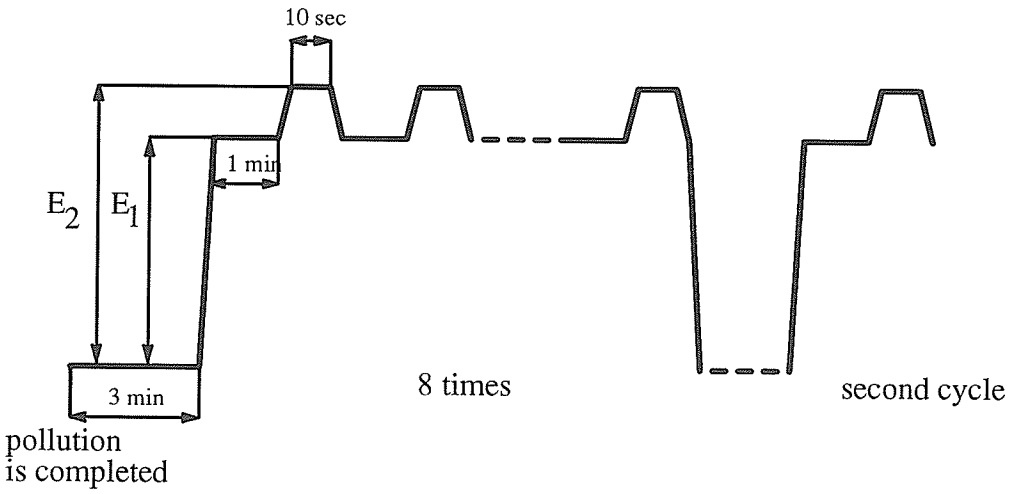

Fig. 4.13. Japanese Test Method diagram [28].

A clean and dry arrester was polluted in a fog chamber in its test position. Pollution was applied by spraying the arrester uniformly until the solution was dripping from the surface.

After the completion of slurry application a 3–minute drip time was allowed. Then the arrester was energized in accordance with the procedure shown in Figure 4.13. The test consisted of four cycles.

According to above standards:

$E_1 = 7.24$ kV is the maximum voltage / $\sqrt{3}$,

where max. voltage for 12 kV rated arrester is 12.55 kV [29], and

$E_2 = 9.48$ kV is a rated voltage x 82 %.

For this test the arrester was sprayed with a solution of 18 g of salt per liter of water which represents a contamination level of 0.1 mg/cm^2.

4.5.2. Results.

During this test data was collected separately for every cycle. After that full pulse analysis was performed.

Tab.4.20. Japanese Test Method results.

Cycle No.	$Q_{surf.}$ [C]	$Q_{inter.}$ [C]	No. of pulses	Max. ampl. [mA]	Max. duration [s]	Top block temp. incr. [°C]	Surface temp. incr. [°C]
1	2.912	0.00006	303	321	1.97	5	5
2	1.416	0.00007	183	236	1.62	6	5
3	0.330	0.00008	128	61	1.87	7	6
4	0.948	0.00006	142	376	1.59	9	8

During this test scintillation pulses were observed mostly at the beginning of each cycle. As in the Wet Slurry Test they were observed during the first few minutes until the arrester dryed out. The total time of voltage application in one cycle was 7 min and 20 sec. After the fourth cycle the arrester's temperature increased by 9 °C inside and by 8 °C on the surface.

4.6. Salt Fog Test.

The Salt Fog Test was conducted in accordance with IEC Publication 507 [23].

4.6.1. Salt Fog Test procedure.

This procedure was developed for testing insulators under pollution. The main part of it was the withstand test. Because of the electrical properties of the arrester, the withstand test could not be applied to it. Therefore in this experiment the procedure was modified and the thermal properties of the arresters were investigated under negative dc voltage at the MCOV level. The Salt Fog Test was performed in the fog chamber described in chapter 2.4 using the fog generated by nozzles spraying a solution of water with salt. The test was performed for three different levels of solution salinity: 20, 56 and 160 g of salt per liter.

The time duration for this test was 2 hours, but because of the computer memory capacity the data was collected for the first hour only. The top block temperature was controlled throughout the time of test duration.

4.6.2. Results.

Tab. 4.21. Salt Fog Test results.

Solution salinity [g/l]	Solution conduct. [S/m]	$Q_{surf.}$ [C]	$Q_{int.}$ [C]	No. of pulses	Max. ampl. [mA]	Max. duration [s]	Top block temp. incr. [°C]
20	2.9	0.121	0.0042	883	8.5	0.78	5
56	7.4	0.00048	0.0016	29	2.7	0.06	2
160	17.8	0.0076	0.0005	84	11.7	0.2	1

During these tests, the surface current was very weak, consisting of small a number of short pulses. In the Salt Fog Method the separation of internal and surface currents was difficult

because of the deposit of a conducting salt layer on the silicon grease surface. As a result, the arrester internal current observed on the scope was larger and contained more pulses than in the other experiments.

The largest temperature increment was observed for the lowest solution salinity. This is probably due to the fact that at the lower salinity level the pollution deposit is more non–uniform. Than the probability of dry bands and scintillation pulses is higher. At the higher salinity level the surface pollution and the current distribution are more uniform. The results of the Salt Fog Test are shown in Table 4.21.

4.6.3. Salt Fog Tests performed in other laboratories.

As was mentioned before there are no results available for distribution class arresters. All published data for transmission class arrester corresponded to ac voltage. Four papers [24], [26], [30] and [31] were located which discuss results of the Salt Fog Test.

Tab. 4.22. Results of Salt Fog Tests performed in other laboratories.

Reference number	MCOV ac [kV]	Max. temp. increase [C]	Remarks
[26]	140	23 – 29	salinity 56 g/l ; duration 60 min ; max. temperature on bottom unit.
	210	40 – 46	salinity 56 g/l ; duration 10 hours ; max. temperature on top unit.
[30]	292	40	salinity 14 g/l ; duration 10 hours ; max. temperature on top unit.
		50	salinity 56 g/l ; duration 5 hours ; max. temperature on top unit.
[24]	145	70	salinity 40 g/l ; duration 2 hours.
[31]	275	120	salinity 1.5 g/l ; duration 2.5 hours.

4.7. Non–polluted arrester energized at 15 kV.

This test was conducted in order to check the possibility of heating the arrester by a higher internal current.

During this test the voltage was increased gradually from 9 to 15 kV. The internal current increased 17 times and at 15 kV reached the value of 1.75 μA. Then the voltage was maintained at 15 kV for one hour. During this time current did not increase further. The relation between current and voltage for the arrester energized at a temperature of 21 °C is shown at Figure 4.14.

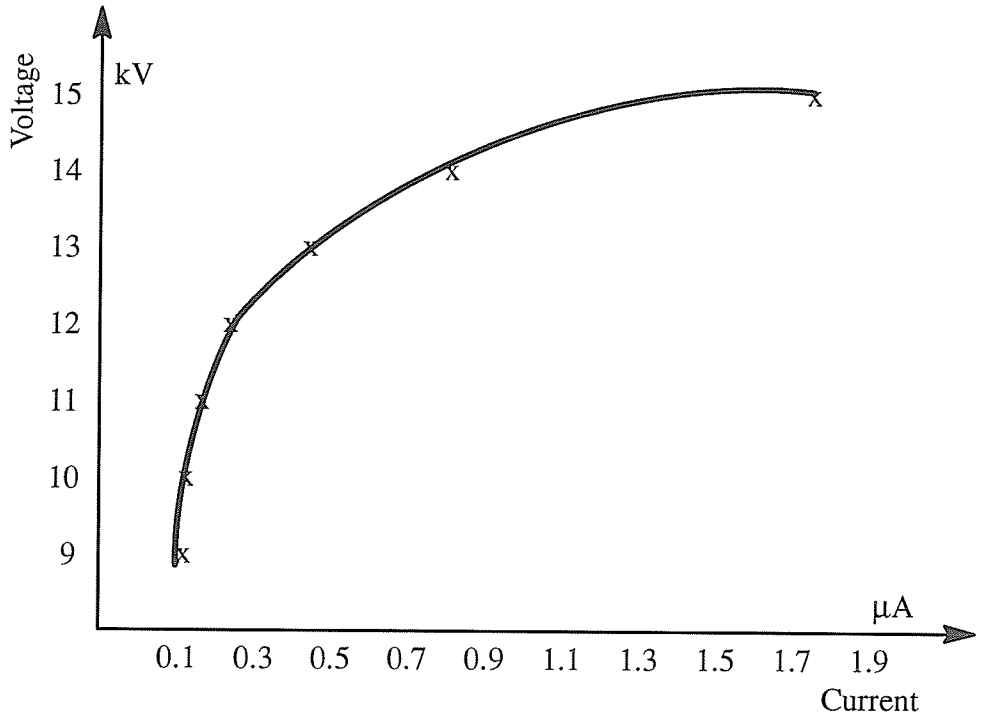

Fig. 4.14. Non–polluted arrester at 21 °C ; V–I characteristic.

The surface and the top block temperature did not increase during this test. Even though that the current increased 17 times the power dissipation inside arrester was still very small. It was in the milliwatts range.

4.8. Summary of the results of performed tests.

In this part all results obtained in the various tests are presented. In some cases small modifications were made to make the comparison easier. Because in almost every test the time duration of voltage application was different, two of the main parameters: the charge in the surface current and number of pulses were normalized to the value per one minute. In the case when test was performed two or three times only one result is presented. For tests which consisted of several cycles the highest temperature increment is shown.

Tab. 4.23. Results of performed tests.

Applied procedure	$Q_{surf.}$ [C]	No. of pulses	Max. ampl. [mA]	Max. dur. [s]	Top bl. tem. inc. [°C]	Surface tem. inc. [°C]
Solid Deposit Method						
ESDD – light	0.0032	10	48.4	0.083	0	N/A
ESDD – moderate	0.0023	32	86.33	0.487	0	N/A
ESDD – heavy	0.02	23	167.58	0.371	0	N/A
Kaolin – heavy	0.014	15	100.0	0.68	0	N/A
Kaolin – light	0.0059	19	31.64	0.499	0	N/A
arrester top shed polluted.	0	0	0	0	0	N/A
arrester bottom shed pol.	0	0	0	0	0	N/A
arrester half polluted.	0.0012	6	15.6	1.866	0	N/A
arrester polluted in unif. "U" shape.	0.013	46	83.2	0.616	0	N/A
arrester polluted in non–uniform "U" shape.	0.0075	29	36.72	0.351	0	N/A
single arrester ; fog supplied with breaks.	0.0065	7	60.0	0.406	0	N/A
two arresters in series ; fog supplied with breaks.	0.013	17	73.0	0.266	0	N/A
single arrester energized at $\sqrt{2}$ MCOV.	0.024	8	237.0	0.603	3	N/A

Table 4.23 continued

Applied procedure	$Q_{surf.}$ [C]	No. of pulses	Max. ampl. [mA]	Max. dur. [s]	Top bl. temp. inc. [°C]	Surface temp. inc. [°C]
Wet Slurry Method						
arrester energ. at MCOV. volt. applied for 15 min.	0.063	6	181.6	1.97	6	N/A
arrester energ. at MCOV. volt. applied for 7 min.	0.205	28	192	1.73	7	N/A
arrester energ. at MCOV; volt. applied for 4 min.	0.296	24	200	1.33	8	13
arr. energ. at $\sqrt{2}$ MCOV; volt. applied for 4 min.	0.391	71	330	1.71	13	9
two arresters in series; volt. applied for 7 min.	0.15	31	132	0.89	7	6
Partial Wetting Test						
arrester energ. at MCOV.	0	0	0	0	0	0
arr. energ. at $\sqrt{2}$ MCOV.	0	0	0	0	0	0
Dip Test						
arrester energ. at MCOV.	0	0	0	0	0	0
Japanese Standards	0.399	41	321	1.97	9	8
Salt Fog Test						
fog conduct. – 2.9 S/m	0.002	15	8.5	0.87	5	N/A
fog conduct. – 7.4 S/m	0.00001	0.5	2.7	0.06	2	N/A
fog conduct. – 17.8 S/m	0.00012	1.5	11.7	0.2	1	N/A

The histograms of scintillation pulse amplitude, time duration and number and charge in the surface current for tests presented above are included in Appendix B.

Chapter 5 ELECTROSTATIC FIELD ANALYSIS.

This chapter includes the results of Electrostatic Field Analysis conducted by use of computer software package "ALGOR". Voltage and the Electric Field distribution along the non–polluted arrester were calculated using the Finite Element method.

Voltage and Electric Field distribution.

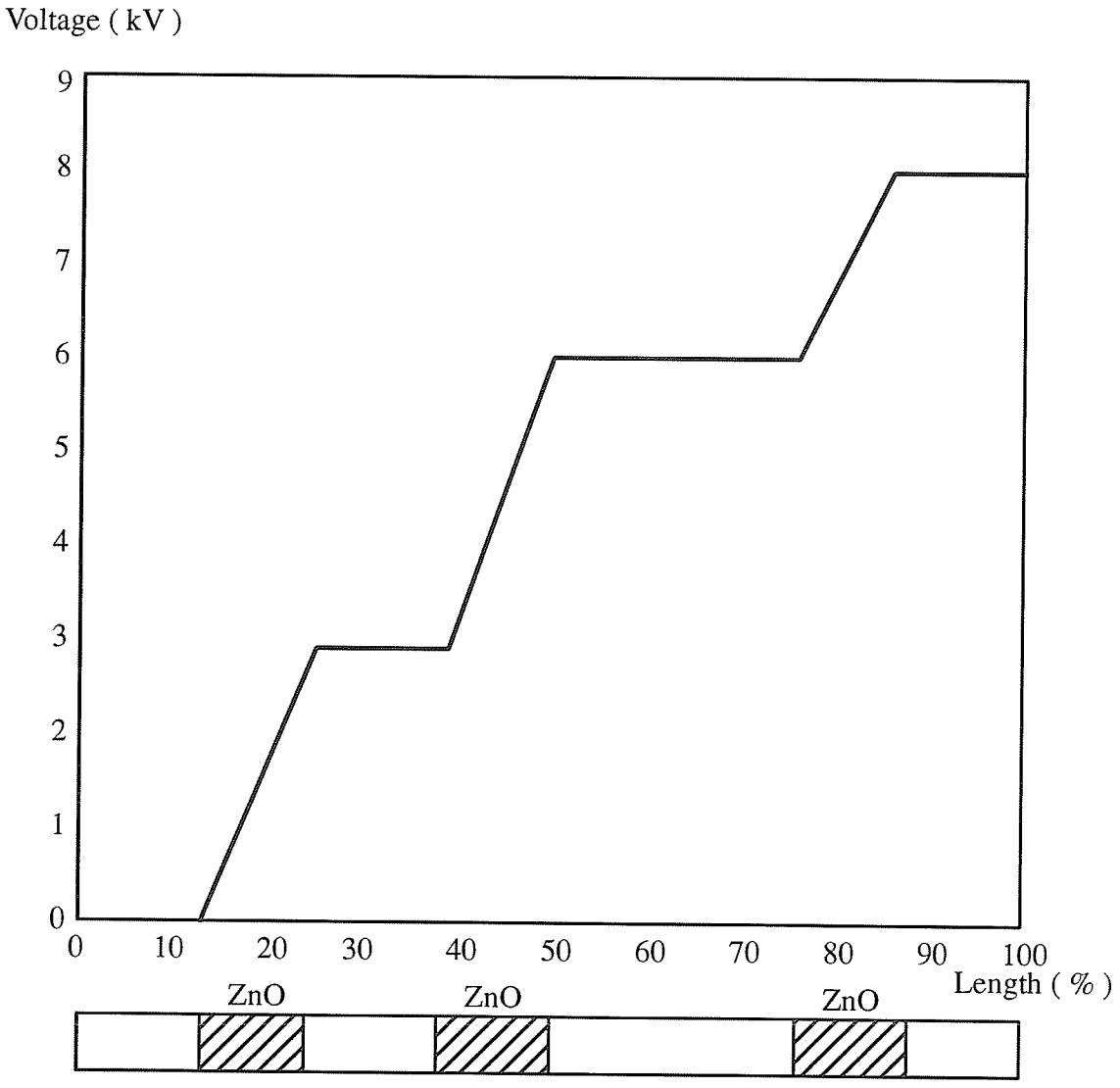

Fig. 5.1. Voltage distribution along EPDM arrester.

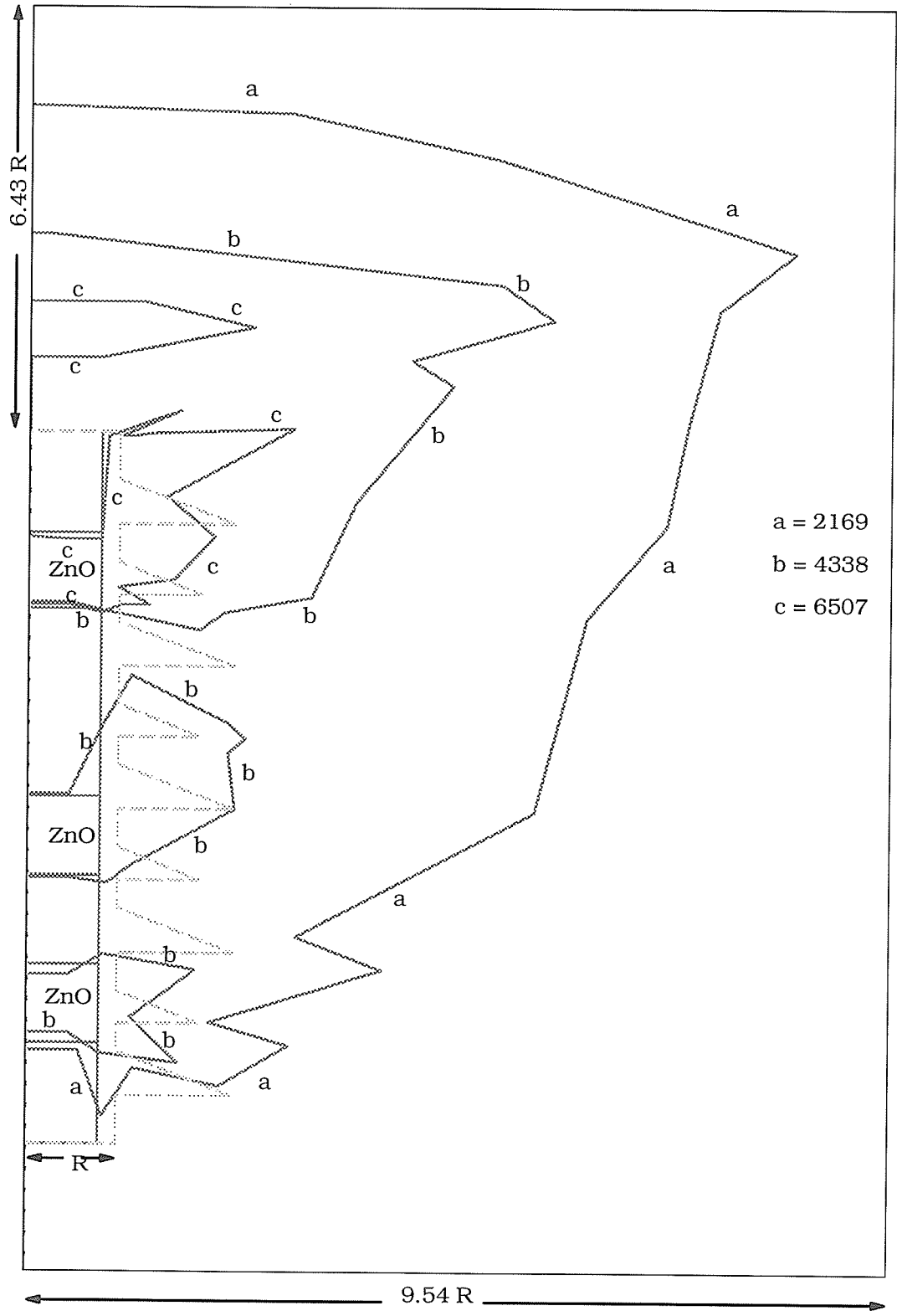

Fig. 5.2. Electric Field distribution outside the EPDM arrester.

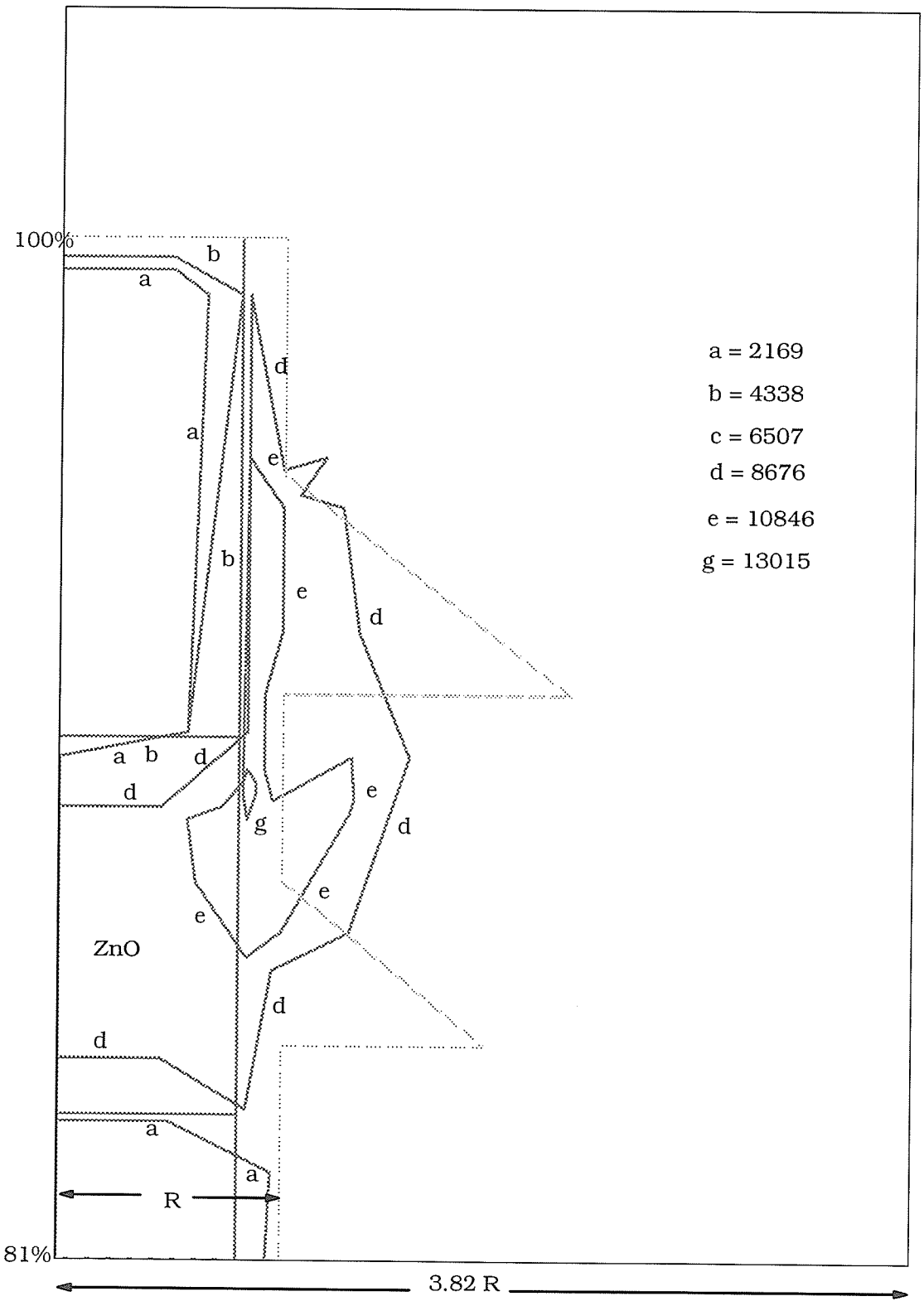

Fig. 5.3. Electric Field distribution of the upper part of the EPDM arrester.

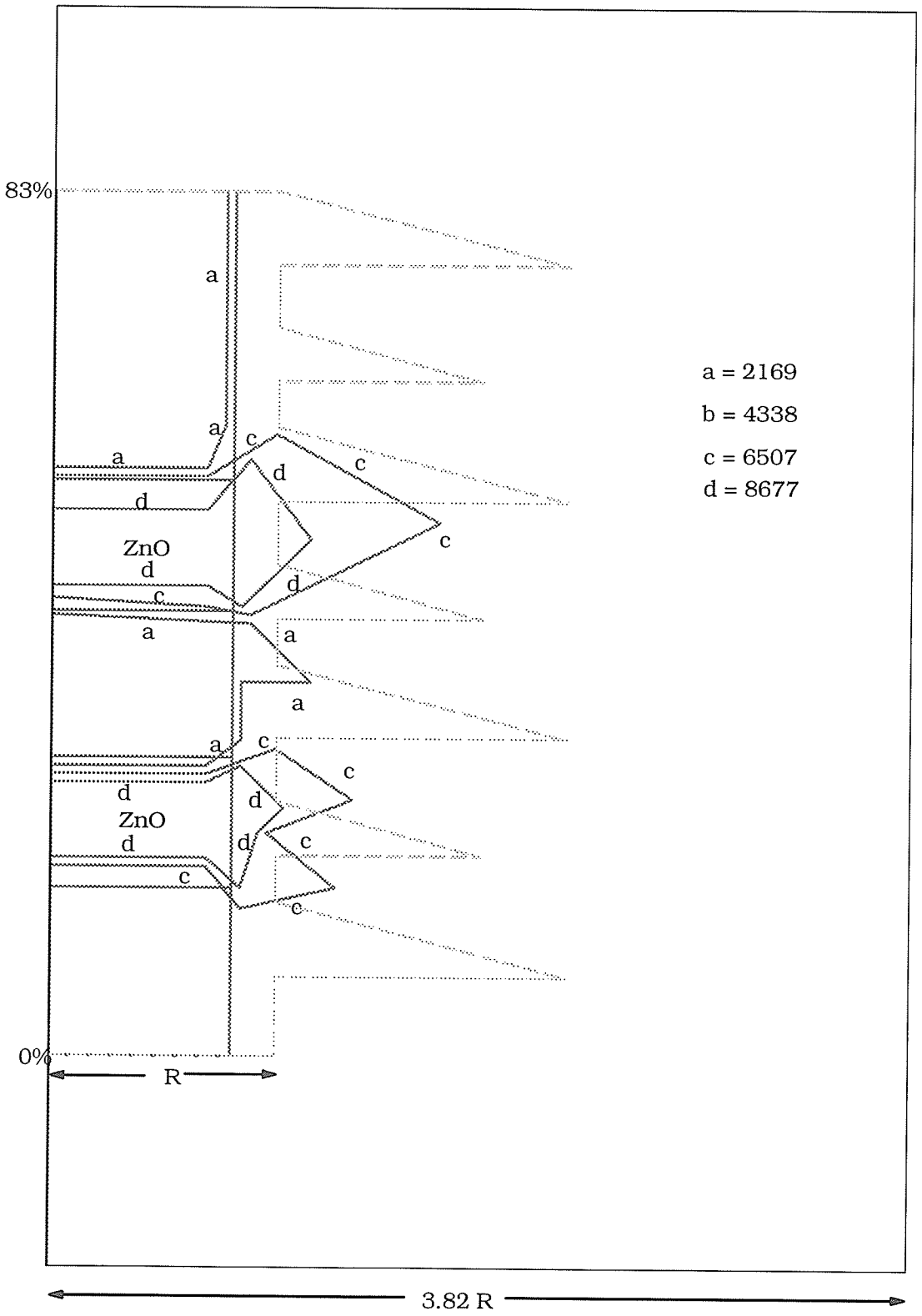

Fig. 5.4. Electric Field distribution of the lower part of the EPDM arrester.

Chapter 6 CONCLUSIONS.

The purpose of this study was to assess and compare existing procedures evaluating the ability of distribution class arresters energized with dc voltage to perform stably in a wet–polluted environment.

Chapter 1 introduces the scope of metal oxide surge arresters housed in EPDM and presents short review of their general properties including V–I characteristic, thermal stability and pollution effects.

Chapter 2 comprises the bulk of work related to this study i.e. the experimental work which consisted of setting up the testing circuit, constructing the fog chamber and developing the data acquisition system.

In chapter 3, a flashover mechanism of polluted arrester proposed by Obenaus is developed. Additionally in this chapter a short literature review of research conducted in Japan and in the USA on HVDC porcelain and glass insulators is presented.

In chapter 4, the results of artificial pollution tests, their description and proposed modifications are described. Whenever available, the results of tests carried out in other laboratories are attached. The conclusions which are presented below are composed mostly of the results obtained from this chapter.

Chapter 5 includes the results of Electric Field Analysis conducted by use of computer software ALGOR. The electric field and voltage distribution along the polluted arrester are analyzed.

From the conducted research and results obtained one main conclusion can be derived:

The distribution class arresters energized with dc voltage are heated only by scintillation pulses developed on the surface. The internal current even under highly non–uniform voltage distribution is unable to heat arrester. This has been shown in a test described in Section 4.7, where the non polluted arrester was energized at a voltage 25% above the rated voltage.

The internal current rose 17 times but the dissipated power inside arrester was still very small, in the milliwatts range. These findings were confirmed by results obtained from artificial pollution tests conducted in this work. Whenever the temperature of the arrester increased it was caused by arcing at the arrester's surface.

Because of these facts all of the procedures tested cannot be directly applied to distribution class arresters energized with dc voltage. These procedures assess arresters mostly according to their thermal behavior and exclude tests in which arresters run away thermally. This work showed that distribution class arresters energized with dc voltage will never run away thermally unless complete flashover occurs.

In many publications a large temperature increment was observed, even up to 120 °C [28]. This can be explained by the following:

a) under ac applied voltage the current from the surface of the arrester can flow to the metal oxide blocks by capacitive coupling,
b) with transmission class arresters tested the power power dissipated inside arrester was larger,
c) transmission class arresters are of larger size and voltage distribution can be more non–uniform.

From the results obtained and the available literature the following additional conclusions can be drawn:

1. The Solid Deposit Test should not be longer than two hours in duration (Section 4.1 and paper [28]). Longer fog application will result in washing off of the pollution layer. The test can be extended only if the fog is not applied continuously.
2. From publications [24, 28, 30] it can be concluded that the temperature rise of the arrester is higher when the bottom unit is polluted more heavily.
3. Papers [24, 27, 28] propose that in the Salt Fog Test the temperature rise is larger for higher conductivity of the contaminating liquid, but results from Section 4.6.2 and from

publication [29] show that the highest temperature rise occurred for the smallest solution salinity. This can be explained by the fact that at the lower salinity the pollution deposits are more non–uniform. In this case the probability of dry bands and scintillation pulses formation is higher. When the salinity level and fog intensity are too large dry bands cannot be formed and the uniform current flows along the surface of the arrester.

REFERENCES.

[1] E.C. Sakshang, et. al. "Metal oxide arresters on distribution systems; fundamental considerations", IEEE Trans. Vol. 4, No. 4, October 1989, pages 2076 – 2082.

[2] V. Chaudhry, et. al. "Electrical performance of polymer housed Zinc Oxide arrester under Contaminated Conditions", IEEE, Power Engineering Society, 1990 Summer Meeting, Minneapolis, July 15–19, 1990.

[3] D. Perin, et. al. "Comparison of standard and not standard pollution test methods with particular reference to dc voltage", ISH New Orleans, August 28 – September 1, 1989.

[4] IEC 36 (Secretariat) 64, "Draft revision of IEC Publication 507", January 1987.

[5] A. Schei, et. al. "Metal oxide surge arrester in ac systems", CIGRE, Working Group 06 of Study Committee 33.

[6] W. Yuanfang, et. al. "Study of thermal stability of metal oxide surge arrester", ISH Braunschweig, August 24–28, 1987.

[7] M. R. Raghuveer, "Performance of polymeric and porcelain housed gapless MOA", proposals for research, April 1991.

[8] "Minutes of the Meeting of the IEEE Task Force to Refine the Clean Fog Test Parameters", meeting held at IREQ, Varennes, Quebec on 10. 04. 1983.

[9] F. Chagas, "Flashover mechanisms of polluted insulators under dc voltage", proposals for research project on dc polluted insulation.

[10] T.C. Cheng, et. al. "Pollution performance of dc insulators under operating conditions", IEEE Trans. Vol. EI–16, No. 3, June 1981, pages 154 – 164.

[11] H. M. Schneider, "Measurements of contamination on post insulators in HVDC converter stations", IEEE Trans. Vol. 3, No. 1, January 1988, pages 398 – 404.

[12] T. Kawamura, et. al. "DC pollution performance of insulators", CIGRE 1984, Paper 33 – 10.

[13] K. Takasu, et. al. "Natural contamination test with dc voltage energization at inland ar–

eas", IEEE Trans. Vol. 3, No. 4, October 1988, pages 1847 – 1853.

[14] W. Lampe, et. al. "Long term tests on HVDC insulators under natural conditions at Big Eddy Test Center", IEEE Trans. Vol. 4, No. 1, January 1982.

[15] K. Chrzan, et. al. "Hygroscopic properties of pollutants on HV insulators", IEEE Trans. Vol. EI–24, No. 1, February 1989, pages 107 – 112.

[16] B.F. Hampton, "Flashover mechanism of polluted insulation", Proc. IEEE, Vol. 111, No. 5, May 1964, pages 985 – 990.

[17] "Applications of insulator in a contaminated environment", IEEE Trans. Vol. 98, No. 5, September 1979, pages 1676 – 1695.

[18] F.A.M. Rizk, "Mathematical models for pollution flashover", Electra 1981, Vol. 78, pages 71 – 103.

[19] S. Hesketh, "General criterion for the prediction of pollution flashover", Proc. IEE, Vol. 144, No. 4, April 1967, pages 531 – 532.

[20] A. Wilkins, et, al. "Arc propagation along the electrolyte surface", Proc. IEE, Vol. 118, No. 12, December 1971, pages 1866 – 1892.

[21] R. Wilkins, "Flashover voltage of high voltage insulators with uniform surface pollution film", Proc. IEE, Vol. 116, No. 3, March 1969, pages 457 – 465.

[22] F.A.M. Rizk, "Application of dimensional analysis to flashover characteristics of polluted insulators", Proc. IEE, Vol. 117, No. 12, December 1970, pages 2257 – 2260.

[23] Revision of IEC Publication 507, "Artificial pollution tests on high voltage insulators to be used on ac systems", Mannheim, April 1986.

[24] A. Bargigia, et. al. "Comparison of different test methods to assess the thermal stresses of metal oxide surge arresters under pollution conditions", IEEE 1992.

[25] M.N. Redrugina, et. al. "Contamination performance of zinc oxide arresters", ISH Dresden, August 26–30, 1991, pages 315 – 318.

[26] D.W. Lenk, "An examination of the pollution performance of gaped and gapless metal oxide station class surge arrester", IEEE Trans. Vol. PAS–103, No. 2, February 1984,

pages 337 – 344.

[27] IEEE Standard for Metal Oxide Surge Arrester for ac Power Circuits, ANSI/IEEE C62.11 – 1987.

[28] Electrical Standard for Arresters, The Institute of Electrical Engineers of Japan, JEC 203 – 1978.

[29] T. Takuma, et. al. "High Voltage and High Current Engineering", Morikuta Publishing Company, Tokyo 1988, page 18.

[30] E.G. Maier, et. al. "Voltage distribution and pollution performance of metal oxide ares–ters", CIGRE, Working Group 33 – 12.

[31] L.J. Sparrov, et. al. "U.K. experience in the investigation of the pollution performance of zinc oxide surge arresters". CIGRE, Working Group 33 – 07.

APPENDIX A

Appendix A contains the software programs developed for data acquisition and analysis. Table A.1 describes the programs developed for various objectives.

Table A.1 : List of software programs.

Program	Description
DATACQ	Data Acquisition.
PULDET	Pulse Detection.
PULANA	Pulse Data Analysis.

DATACQ

```
REM ********************* Program  no. 01 *********************************
REM
REM
REM This is the program that  calls the data acquisition library functions
REM for programming multiple A/D conversions and store in a disk file.
REM
REM ************************************************************************

CONST NUMCHANS = 2                    ' the # of channels we're scanning

CONST NUMPOINTS = 28800000            'total number of points to acquire

CONST RATE = 8000.0                   ' sampling rate

cls

i% = 0                                ' loop counter and array index
board% = 1                            ' slot/ID number of board
```

```
boardType% =11                    ' board code
k..err% = 0                       ' holds DOS LabDriver error code
DIM chans%(NUMCHANS – 1)          ' array storing channels
DIM gains%(NUMCHANS – 1)          ' array storing gains
numTimeOutTicks& = 0              ' tick count for Timeout_Config call
inputmode%=1
range%=10
polarity%=0
REM ————————————————————————————————————————

REM ********** Fill the channel and gain arrays for MIO–16 **************

i% = 0

WHILE i% < NUMCHANS
  chans%(i%) = i%
  gains%(i%) = 1
  i% = i% + 1
WEND

REM ********************** Board  initialization ****************************

k..err% = Init.DA.Brds% (board%, boardType%)
i..dummy% = AI.Config (board%, inputmode%,range%,polarity% )

REM ********************** Time out    calculation ****************************

numTimeOutTicks& = (NUMPOINTS / RATE) * 20

IF numTimeOutTicks& < 20 THEN
  numTimeOutTicks& = 20
END IF
  numTimeOutTicks& = –1

k..err% = Timeout.Config% (board%, numTimeOutTicks&)

print "err1=", k..err%

REM *************** Data  acquisition  to a disk file **********************

k..err% = SCAN.to.Disk% (board%, NUMCHANS, chans%(), gains%(), "dat", NUMPOINTS,
RATE, 0.0#, 0)

print "err2=", k..err%
print "NO=",NUMPOINTS
```

```
REM ********************** Done  with  program ******************************

k..err% = CloseInterfaceManager%

REM $INCLUDE: 'int1.inc'
REM $INCLUDE: 'int2.inc'
REM $INCLUDE: 'avg2.inc'
```

PULDET

```
REM ********************** Program  no. 02 A ******************************
REM
REM
REM This is the program that read the  data from the disk file to memory
REM buffers, analyse and store Pulse data in disk files.When no pulses
REM in internal current is accounted.
REM
REM ***************************************************************************

CONST RATE=8000                  ' sample rate

CONST LENGTH=16000               ' buffer length
CONST HLENGTH=8000

CONST REALRATE=RATE*0.5

DIM buf AS STRING * 32000        ' string for storing acquired data
DIM data.buf%(LENGTH)            ' buffer for storing acquired data

COMMON SHARED /data.buf/ data.buf%()

DIM d1.buf%(HLENGTH)
DIM d2.buf%(HLENGTH)

DIM v1.array#(8190)
DIM v2.array#(HLENGTH)

DIM time.array#(HLENGTH)

DIM u1#(HLENGTH)

DIM D#(8000)

DIM fu1#(HLENGTH)                ' buffer for storing pulses

DIM Vavg#(HLENGTH)               ' buffer for storing data in ch. 2
```

```
DIM y1#(HLENGTH)          ' buffer for storing inigrated values
DIM y2#(HLENGTH)          ' buffer for storing inigrated values

DIM pj&(4000)
DIM pk&(4000)

DIM fint1#(4000)
DIM fint2#(4000)

DIM cuch1#(4000)
DIM cuch2#(4000)

DIM x%(4000)

cls
n%=0                      ' no of cycles
i% = 0                    ' loop counter and array index
board% = 1                ' slot/ID number of board
boardType% =11            ' board code
k..err% = 0               ' holds DOS LabDriver error code
inputmode%=1              ' inputmode
range%=10                 ' range
polarity%=0               ' polarity

k%=LENGTH
l%=k%/2
m%=l%-1

REM ------------------------------------------------------------------------

REM ********** initializing the board************************************

k..err% = Init.DA.Brds% (board%, boardType%)
i..dummy% = AI.Config (board%, inputmode%,range%,polarity% )

REM ********** Open out put files for storing pulses**********************

hand1% = OpenFile% ("sf3u1", 2, 2, 1)

hand11% = OpenFile% ("sf3um1", 2, 2, 1)

hand12% = OpenFile% ("sf3td1", 2, 2, 1)

hand13% = OpenFile% ("sf3tp1", 2, 2, 1)

hand21% = OpenFile% ("sf3avg2", 2, 2, 1)
```

```
hpanel1% = LoadPanel ("int1.uir", HINA)
hpanel2% = LoadPanel ("int2.uir", HINB)
hpanel3% = LoadPanel ("avg2.uir", HAVG)

REM  *** Read  the  sample data from the disk file and into a memory buffer***

  Nu1&=0
  Num1&=0

  Fi1=0                    'addition of intigrated values
  Fi2=0                    'addition of intigrated values
  AVD=0

  nn%=1800
for n%=0  to 1799

  x%(n%)=(n%+1)*2          ' 2=(HLENGTH / REALRATE)

  p&=CLNG(n%)

  handle% = OpenFile% ("dat", 1, 2, 0)

  l..dummy& = SetFilePtr& (handle%,32000&*p&, 0)

  i..dummy% = ReadFile (handle%, buf$,32000)

  i..dummy% = Scan% (buf$, "%16000i[z]>%16000i", data.buf%())

  i..dummy% = CloseFile% (handle%)

REM ******************** Seperate  2  channels ******************************

  i..dummy% = SCAN.Demux (data.buf%(), k%, 2, 0)
  i..dummy% = Scan% (data.buf%(), "%*i>%*i",(l%),(l%), d1.buf%())
  i..dummy% = Scan% (data.buf%(), "%*i[i*]>%*i",(l%),(l%) ,(l%) , d2.buf%())

REM ********************** Scale  to  voltage ******************************

  k..err% = daq.scale% (board%, 1,l%, d1.buf%(),v1.array#() )
  k..err% = daq.scale% (board%, 1,l%, d2.buf%(),v2.array#() )

REM ********************** Inversion ***********************************

  CALL Abs1D (v1.array#(), l%, v1.array#())
  CALL Abs1D (v2.array#(), l%, v2.array#())

REM ********************** Multiplication ******************************
```

```
   CALL LinEv1D (v1.array#(),l% , 0.16, 0.0, v1.array#())
   CALL LinEv1D (v2.array#(),l% , 0.0000182, 0.0, v2.array#())

REM ********************* Convert  to  time  scale ***************************

 for i%= 0 to m%

        g#=i%/REALRATE
        h#=l%/REALRATE
        dd#=g#+h#*n%

        time.array#(i%)=dd#
 next i%

REM ******************** Channel 1  Pulse  Analysis**************************

jj%=0
jk%=0
kk%=0
i%=0

while i% <= 7995

        mi%=0

for ll%=i% to i%+3                                    'Differences for 5 pts.

    D#(mi%)=v1.array#(ll%+1)–v1.array#(ll%)
    mi%=mi%+1

next ll%

if D#(0) > 0 then
if D#(1) > 0 then
if D#(2) > 0 then
if D#(3) > 0 then

 VR1=v1.array#(i%)

 tp1=time.array#(i%)

 i..dummy%=FmtFile (hand13%,"%s<%f,",tp1)

while v1.array#(i%+1) > VR1

    kk%=kk%+1
    jj%=jj%+1
```

```
    u1#(kk%)=v1.array#(i%)–vR1
    fu1#(jj%)=u1#(kk%)

  i..dummy%=FmtFile (hand1%,"%s<%f,",u1#(kk%))

    i%=i%+1

  if i% > 7995 then
   v1.array#(i%+1) = –1
  end if

 wend

   if kk% > 0 then
    km1%=kk%
    um1=0
    td1=km1%/REALRATE

   for kk%= 1 to km1%

      if u1#(kk%) > um1  then
        um1=u1#(kk%)
      end if

   next kk%
   jk%=jk%+1

i..dummy%=FmtFile (hand11%,"%s<%f,",um1)
i..dummy%=FmtFile (hand12%,"%s<%f,",td1)

print "n=",n%,"vr1=",VR1,"um1=",um1 ,"td1=",td1,"tp1=",tp1

      kk%=0
      um1=0
  end if

end if
end if
end if
end if
   i%=i%+1

wend

   pj&(n%)=CLNG(jj%)
   pk&(n%)=CLNG(jk%)
```

```
    Nu1&=Nu1&+pj&(n%)
    Num1&=Num1&+pk&(n%)

REM ************************ Ch.1  Integration ******************************

if jj% > 0 then

dt1#=1/REALRATE                    'sampling interval ch.1
Init1#=fu1#(0)                     'initial condition ch.1
Final1#=fu1#(jj%-1)                'final condition ch.1

call Integrate (fu1#(),jj%,dt1#,Init1#,Final1#,y1#())

      fint1#(n%)=y1#(jj%-1)
      Fi1=Fi1+fint1#(n%)

end if

REM ***************** Channel 2   Average *********************************

Vad=0

for i%=0 to 7999
Vad=Vad+v2.array#(i%)
next i%

Vavg#(n%)=Vad/8000

i..dummy%=FmtFile (hand21%,"%s<%f,",Vavg#(n%))

AVD=AVD+Vavg#(n%)

REM ************************ Ch.2  Integration ******************************

dt2#=1/REALRATE                    'sampling interval ch.2
Init2#=v2.array#(0)                'initial condition ch.2
Final2#=v2.array#(7999)            'final condition ch.2

call Integrate (v2.array#(),8000,dt2#,Init2#,Final2#,y2#())

      fint2#(n%)=y2#(7999)
      Fi2=Fi2+fint2#(n%)

REM ********************** Plot  the  pulse  data ***************************

next n%
```

```
cuch1#(0)=fint1#(0)                    'Cumulative analysis

for i%=1 to nn%
cuch1#(i%)=cuch1#(i%-1)+fint1#(i%)
next i%

cuch2#(0)=fint2#(0)                    'Cumulative analysis

for i%=1 to nn%
cuch2#(i%)=cuch2#(i%-1)+fint2#(i%)
next i%

AVG2=AVD/nn%

print
print "No. of Surface Pulse Pts. =",Nu1&
print "No. of Surface Pulses    =",Num1&
print "Value of Surface Pulse Integration =",Fi1
print
print "Average Internal Current  =",AVG2
print "Value of Internal Current Integration =",Fi2

REM ****************** Plot  the  Integrated  Values ************************

i..dummy% = DisplayPanel (hpanel1%)
i..dummy% = PlotXY (hpanel1%, HINA.GRAPH,x%(), cuch1#(), nn%, 1, 4, 0, 0, 1, 6)
i..dummy% = GetKey
i..dummy% = OutputGraph (-1, "", 1, hpanel1%, HINA.GRAPH)

i..dummy% = DisplayPanel (hpanel2%)
i..dummy% = PlotXY (hpanel2%, HINB.GRAPH,x%(), cuch2#(), nn%, 1, 4, 0, 0, 1, 6)
i..dummy% = GetKey
i..dummy% = OutputGraph (-1, "", 1, hpanel2%, HINB.GRAPH)

REM ***************** Plot  the  1s  average  of  Internal  current ***************

i..dummy% = DisplayPanel (hpanel3%)
i..dummy% = PlotXY (hpanel3%, HAVG.GRAPH,x%(), Vavg#(), nn%, 1, 4, 0, 0, 1, 6)
i..dummy% = GetKey
i..dummy% = OutputGraph (-1, "", 1, hpanel3%, HAVG.GRAPH)

REM ********************** Done  with  program ****************************

k..err% = CloseInterfaceManager%
```

```
REM $INCLUDE: 'ama.inc'
REM $INCLUDE: 'amb.inc'
REM $INCLUDE: 'dua.inc'
REM $INCLUDE: 'dub.inc'
REM $INCLUDE: 'pta.inc'
REM $INCLUDE: 'ptb.inc'
REM $INCLUDE: 'cam.inc'
REM $INCLUDE: 'cdu.inc'
REM $INCLUDE: 'cti.inc'
```

PULANA

```
REM ********************** Program  no.  03 ********************************
REM
REM
REM This is the program  that  read the  Pulse data  from  disk files
REM to memory buffers and make Statistical Analysis – Histogram, Mean,
REM Std.Deviation, Maximum & Minimum, Cumilative analysis.
REM
REM ***************************************************************************

DIM um1.buf#(8000)                    'buffer to store pulse amplitude ch.1
DIM um2.buf#(8000)                    'buffer to store pulse amplitude ch.2

DIM td1.buf#(8000)                    'buffer to store pulse duration ch.1
DIM td2.buf#(8000)                    'buffer to store pulse duration ch.2

DIM tp1.buf#(8000)                    'buffer to store pulse time ch.1
DIM tp2.buf#(8000)                    'buffer to store pulse time ch.2

DIM hism1%(200),axim1#(200),cuam1%(200)
DIM hism2%(200),axim2#(200),cuam2%(200)

DIM hisd1%(200),axid1#(200),cudu1%(200)
DIM hisd2%(200),axid2#(200),cudu2%(200)

DIM hisp1%(200),axip1#(200),cuti1%(200)
DIM hisp2%(200),axip2#(200),cuti2%(200)

cls

hand11% = OpenFile% ("sf3um1", 1, 2, 1)
'hand21% = OpenFile% ("um2", 1, 2, 1)
```

```
hand12% = OpenFile% ("sf3td1", 1, 2, 1)
'hand22% = OpenFile% ("td2", 1, 2, 1)
hand13% = OpenFile% ("sf3tp1", 1, 2, 1)
'hand23% = OpenFile% ("tp2", 1, 2, 1)

nm1%=84                          'no. of elements in ch.1 amplitude file
intm1%=30                        'no. of intervals
nd1%=nm1%                        'no. of elements in ch.1 duration file
intd1%=intm1%                    'no. of intervals
np1%=nm1%                        'no. of elements in ch.1 time file
intp1%=intm1%                    'no. of intervals

'nm2%=                           'no. of elements in ch.2 amplitude file
'intm2%=200                      'no. of intervals
'nd2%=nm2%                       'no. of elements in ch.2 duration file
'intd2%=200                      'no. of intervals
'np2%=nm2%                       'no. of elements in ch.2 time file
'intp2%=200                      'no. of intervals

i..dummy% = OpenInterfaceManager

hpa1% = LoadPanel ("ama.uir",HAMA)
'hpa2% = LoadPanel ("amb.uir", HAMB)
hpa3% = LoadPanel ("dua.uir", HDUA)
'hpa4% = LoadPanel ("dub.uir", HDUB)
hpa5% = LoadPanel ("pta.uir", HPTA)
'hpa6% = LoadPanel ("ptb.uir", HPTB)

hdle1% = LoadPanel ("cam.uir",HCAM)
hdle2% = LoadPanel ("cdu.uir",HCDU)
hdle3% = LoadPanel ("cti.uir",HCTI)

REM **********Read data from disk files **********

i..dummy% = ScanFile% ((hand11%), "%s>%*f[x]",(nm1%), um1.buf#())
'i..dummy% = ScanFile% ((hand21%), "%s>%*f[x]",(nm2%), um2.buf#())
i..dummy% = ScanFile% ((hand12%), "%s>%*f[x]",(nd1%), td1.buf#())
'i..dummy% = ScanFile% ((hand22%), "%s>%*f[x]",(nd2%), td2.buf#())
i..dummy% = ScanFile% ((hand13%), "%s>%*f[x]",(np1%), tp1.buf#())
'i..dummy% = ScanFile% ((hand23%), "%s>%*f[x]",(np2%), tp2.buf#())
```

```
REM ***************** Histogram  for  pulse  amplitude **********************

call MaxMin (um1.buf#(),nm1%,max#,imax%,min#,imin%)
call Histogram (um1.buf#(),nm1%,min#,max#,hism1%(),axim1#(),intm1%)
CALL StdDev (um1.buf#(), nm1%, meanam1#, stdam1#)

cuam1%(0)=hism1%(0)                                    'Cumulative analysis

for i%=1 to intm1%
cuam1%(i%)=cuam1%(i%-1)+hism1%(i%)
next i%
print
print "No. of Surface Pulses =",nm1%
print
print "Max. Surface Current  =",max#
print "Min. Surface Current  =",min#
print
print "Mean Surface Current  =",meanam1#
print "Standard Deviation    =",stdam1#
print
print

'for i%=0 to 199
'print axim1#(i%),hism1%(i%),cuam1%(i%)
'next i%
print
print

REM             ****************************************

'call MaxMin (um2.buf#(),nm2%,max#,imax%,min#,imin%)
'call Histogram (um2.buf#(),nm2%,min#,max#,hism2%(),axim2#(),intm2%)
'CALL StdDev (um2.buf#(), nm2%, meanam2#, stdam2#)

'print "Max. Internal Current  =",max#
'print "Min. Internal Current  =",min#
'print
'print "Mean Internal Current  =",meanam2#
'print "Standard Deviation    =",stdam2#
'print
'print
```

```
REM ***************** Histogram  for  pulse  duration **********************

call MaxMin (td1.buf#(),nd1%,max#,imax%,min#,imin%)
call Histogram (td1.buf#(),nd1%,min#,max#,hisd1%(),axid1#(),intd1%)
CALL StdDev (td1.buf#(), nd1%, meantd1#, stdtd1#)

cudu1%(0)=hisd1%(0)                                    'Cumulative analysis

for i%=1 to intd1%
cudu1%(i%)=cudu1%(i%-1)+hisd1%(i%)
next i%

print "Max. Surface Pulse Duration  =",max#
print "Min. Surface Pulse Duration  =",min#
print
print "Mean Surface Pulse Duration  =",meantd1#
print "Standard Deviation           =",stdtd1#
print
print

'for i%=0 to 199
'print axid1#(i%),hisd1%(i%),cudu1%(i%)
'next i%
print
print

REM             ****************************************

'call MaxMin (td2.buf#(),nd2%,max#,imax%,min#,imin%)
'call Histogram (td2.buf#(),nd2%,min#,max#,hisd2%(),axid2#(),intd2%)
'CALL StdDev (td2.buf#(), nd2%, meantd2#, stdtd2#)

'print "Max. Internal Pulse Duration  =",max#
'print "Min. Internal Pulse Duration  =",min#
'print
'print "Mean Internal Pulse Duration  =",meantd2#
'print "Standard Deviation           =",stdtd2#
'print
'print

REM ***************** Histogram  for  pulse  time **********************

call MaxMin (tp1.buf#(),np1%,max#,imax%,min#,imin%)
call Histogram (tp1.buf#(),np1%,min#,max#,hisp1%(),axip1#(),intp1%)
'CALL StdDev (tp1.buf#(), np1%, meantp1#, stdtp1#)
```

```
cuti1%(0)=hisp1%(0)                                    'Cumulative analysis

for i%=1 to intp1%
cuti1%(i%)=cuti1%(i%–1)+hisp1%(i%)
next i%

print "Time–First Surface Pulse  =",min#
print "Time–Last Surface Pulse   =",max#
print
print

'for i%=0 to 199
'print axip1#(i%),hisp1%(i%),cuti1%(i%)
'next i%
print
print

REM          ****************************************

'call MaxMin (tp2.buf#(),np2%,max#,imax%,min#,imin%)
'call Histogram (tp2.buf#(),np2%,min#,max#,hisp2%(),axip2#(),intp2%)
'CALL StdDev (tp2.buf#(), np2%, meantp2#, stdtp2#)

'print "Time–First Internal Pulse  =",min#
'print "Time–Last Internal Pulse   =",max#
'print
'print

REM ********************** Plot  Histograms **************************

i..dummy% = DisplayPanel (hpa1%)
i..dummy% = PlotXY (hpa1%, HAMA.GRAPH, axim1#(), hism1%(), intm1%, 4, 1, 3, 0, 1, 6)
i..dummy% = GetKey
i..dummy% = OutputGraph (–1, "", 1, hpa1%, HAMA.GRAPH)

'i..dummy% = DisplayPanel (hpa2%)
'i..dummy% = PlotXY (hpa2%, HAMB.GRAPH, axim2#(), hism2%(),intm2% , 4, 1, 3, 0, 1, 6)
'i..dummy% = GetKey
'i..dummy% = OutputGraph (–1, "", 1, hpa2%, HAMB.GRAPH)

i..dummy% = DisplayPanel (hpa3%)
i..dummy% = PlotXY (hpa3%, HDUA.GRAPH, axid1#(), hisd1%(), intd1%, 4, 1, 3, 0, 1, 6)
i..dummy% = GetKey
i..dummy% = OutputGraph (–1, "", 1, hpa3%, HDUA.GRAPH)
```

```
'i..dummy% = DisplayPanel (hpa4%)
'i..dummy% = PlotXY (hpa4%, HDUB.GRAPH, axid2#(), hisd2%(), intd2%, 4, 1, 3, 0, 1, 6)
'i..dummy% = GetKey
'i..dummy% = OutputGraph (-1, "", 1, hpa4%, HDUB.GRAPH)

i..dummy% = DisplayPanel (hpa5%)
i..dummy% = PlotXY (hpa5%, HPTA.GRAPH, axip1#(), hisp1%(), intp1%, 4, 1, 3, 0, 1, 6)
i..dummy% = GetKey
i..dummy% = OutputGraph (-1, "", 1, hpa5%, HPTA.GRAPH)

'i..dummy% = DisplayPanel (hpa6%)
'i..dummy% = PlotXY (hpa6%, HPTB.GRAPH, axip2#(), hisp2%(), intp2%, 4, 1, 3, 0, 1, 6)
'i..dummy% = GetKey
'i..dummy% = OutputGraph (-1, "", 1, hpa6%, HPTB.GRAPH)

REM ****************** Plot  Cumulative  graphs ****************************

i..dummy% = DisplayPanel (hdle1%)
i..dummy% = PlotXY (hdle1%, HCAM.GRAPH, axim1#(),cuam1%(), intm1%, 4, 1, 0, 0, 1, 6)
i..dummy% = GetKey
i..dummy% = OutputGraph (-1, "", 1, hdle1%, HCAM.GRAPH)

i..dummy% = DisplayPanel (hdle2%)
i..dummy% = PlotXY (hdle2%, HCDU.GRAPH, axid1#(), cudu1%(),intd1% , 4, 1, 0, 0, 1, 6)
i..dummy% = GetKey
i..dummy% = OutputGraph (-1, "", 1, hdle2%, HCDU.GRAPH)

i..dummy% = DisplayPanel (hdle3%)
i..dummy% = PlotXY (hdle3%, HCTI.GRAPH, axip1#(), cuti1%(), intp1%, 4, 1, 0, 0, 1, 6)
i..dummy% = GetKey
i..dummy% = OutputGraph (-1, "", 1, hdle3%, HCTI.GRAPH)

REM ****************** Done  with  the program ****************************

i..dummy%= CloseInterfaceManager%
```

APPENDIX B

Appendix B contains the results of performed tests. Figures presenting charge in the surface current and histograms of scintillation pulse amplitude, time duration and number are attached in order like in the Table 4.23.

B.1. Solid Deposit Method – ESDD: light.

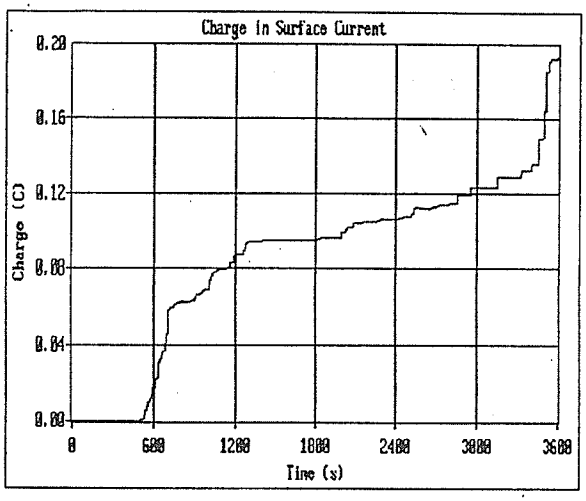

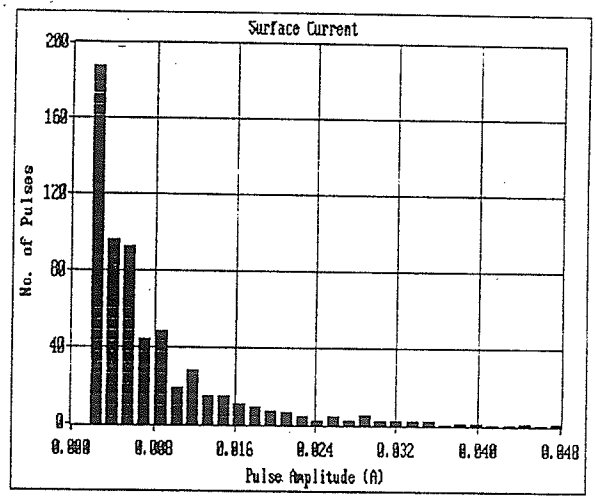

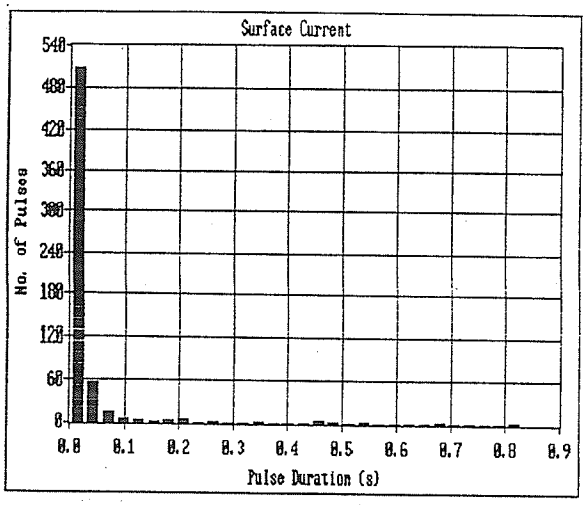

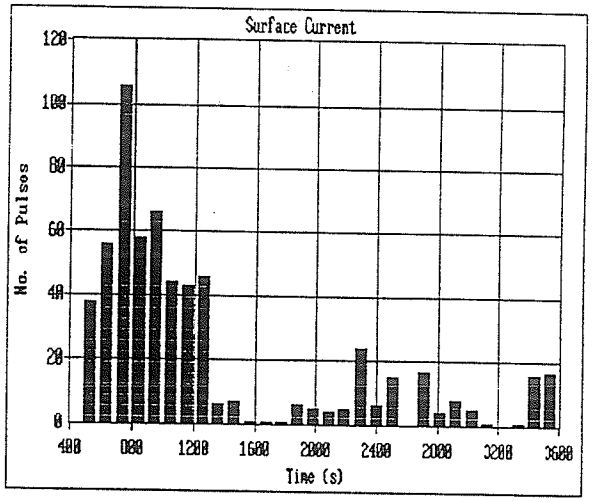

B.2. Solid Deposit Method – ESDD: moderate.

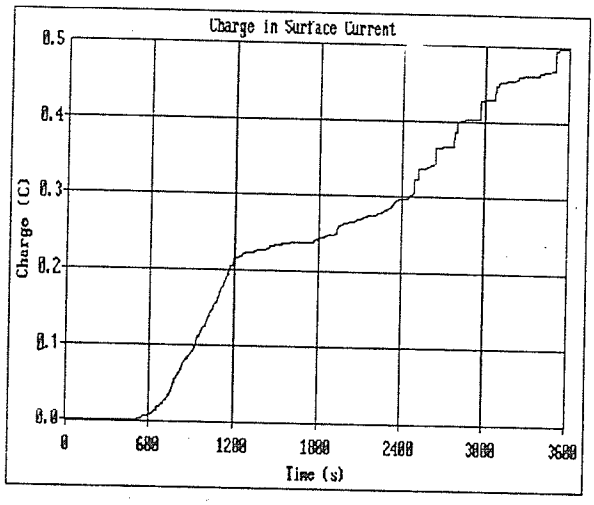

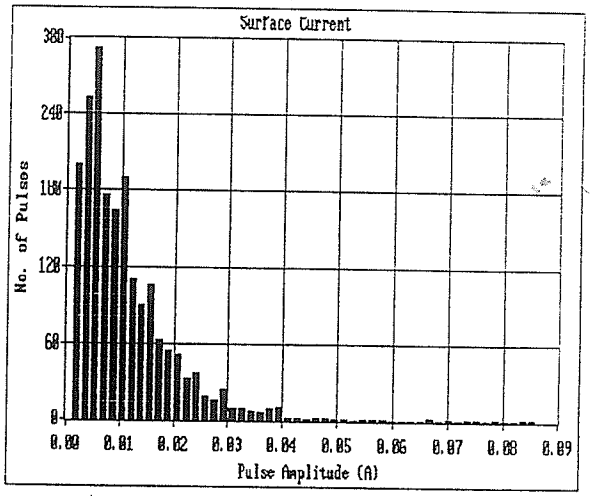

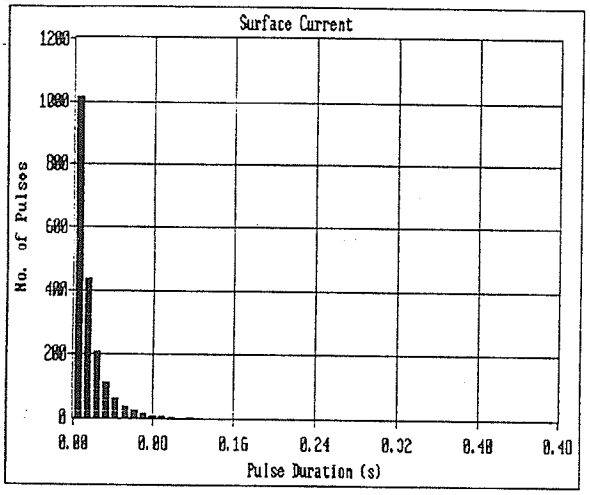

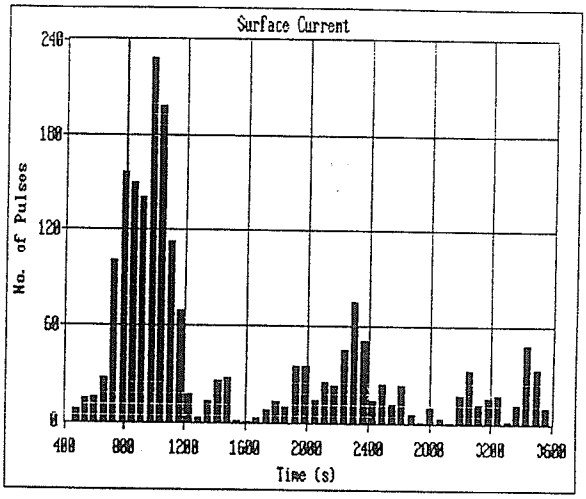

B.3. Solid Deposit Method – ESDD: heavy.

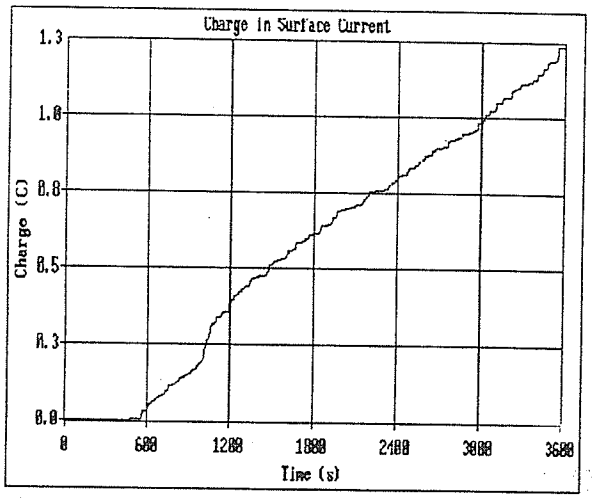

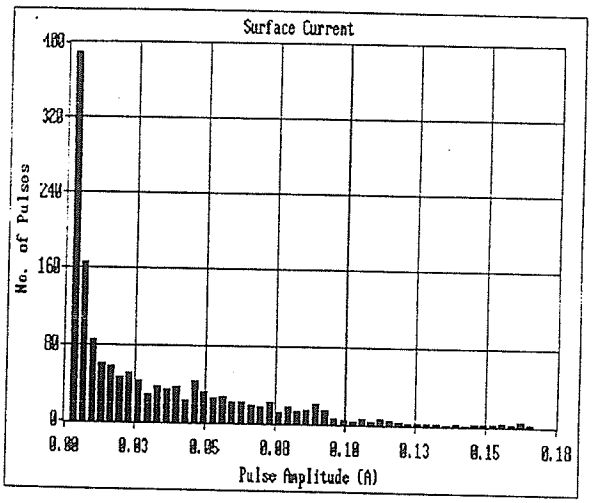

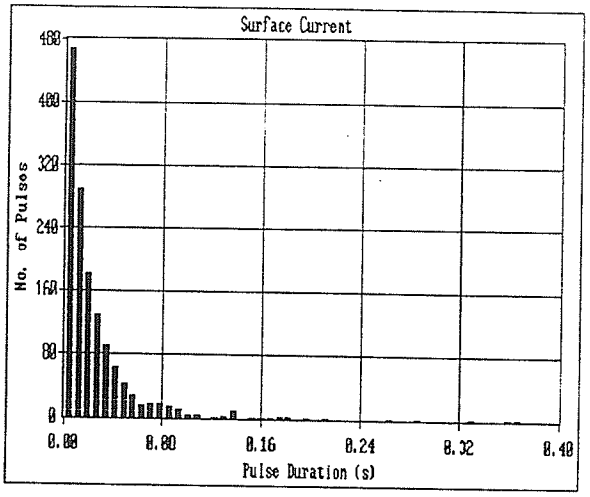

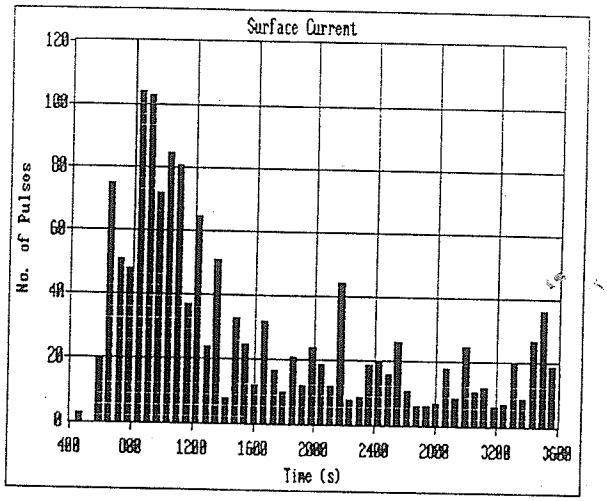

B.4. Solid Deposit Method – kaolin: heavy.

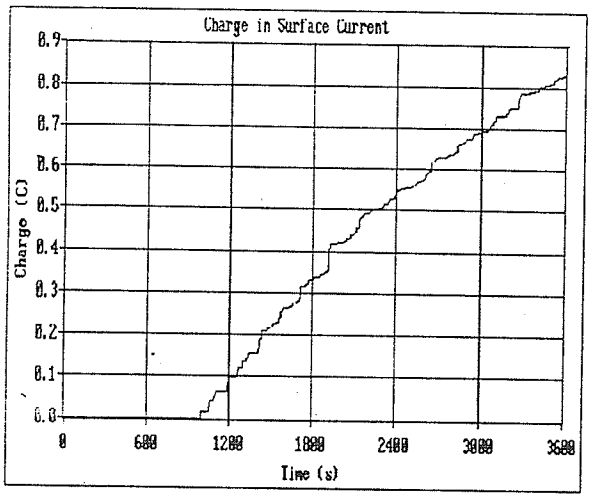

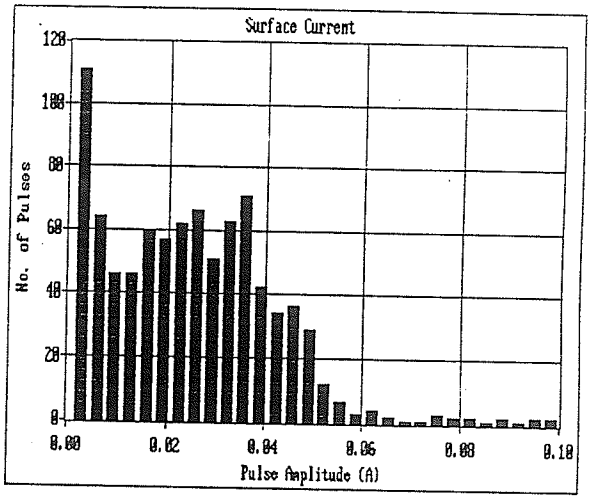

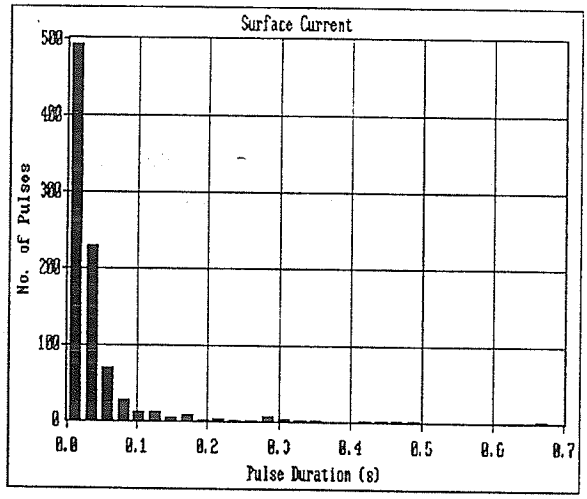

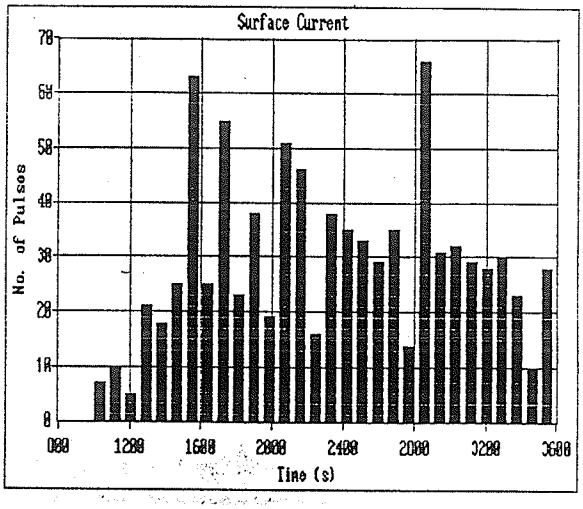

B.5. Solid Deposit Method – kaolin: light.

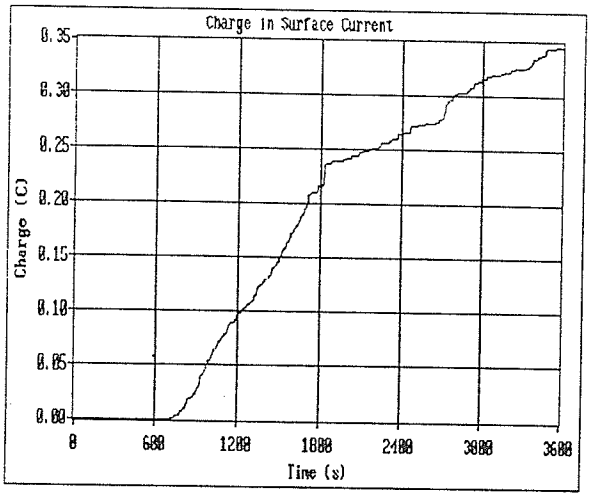

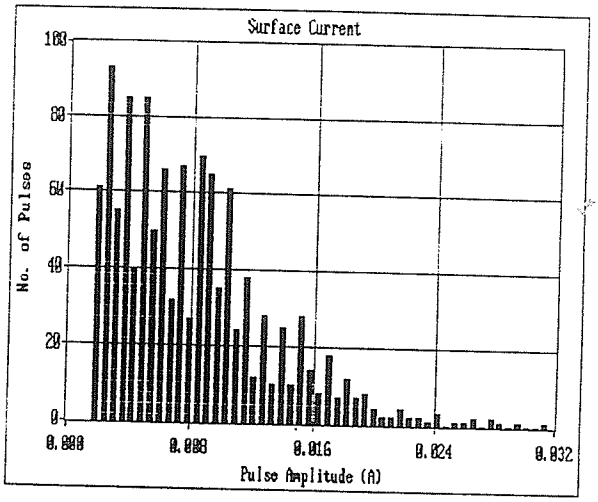

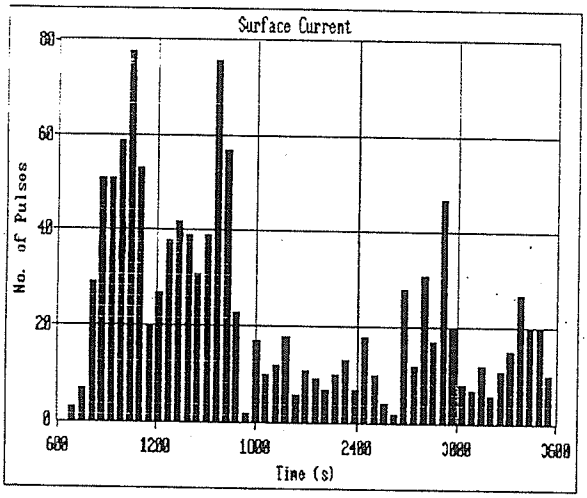

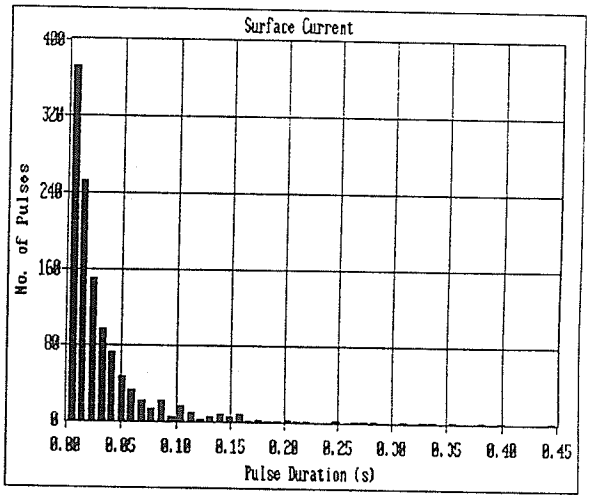

B.6. Solid Deposit Method – arrester half polluted.

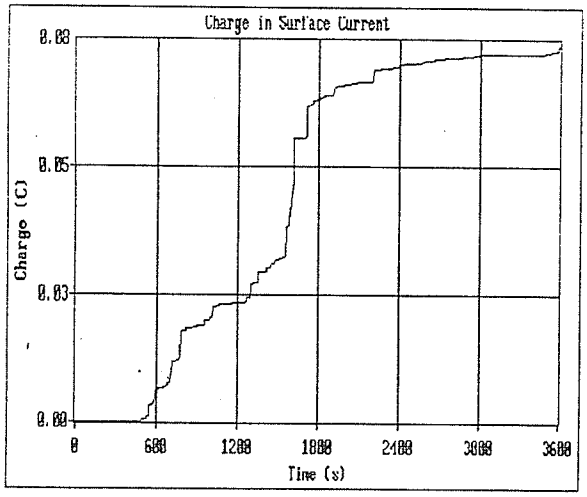

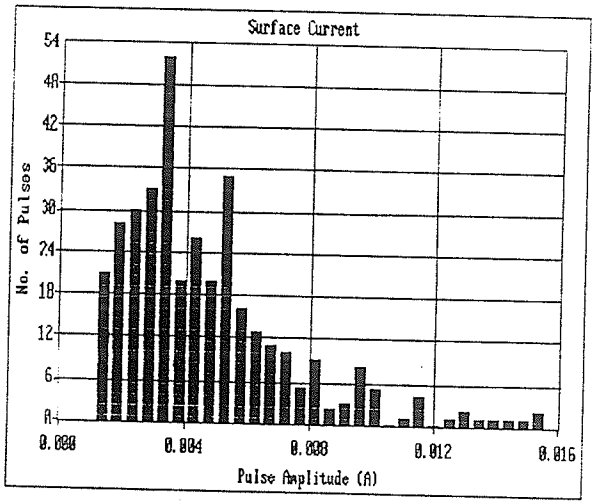

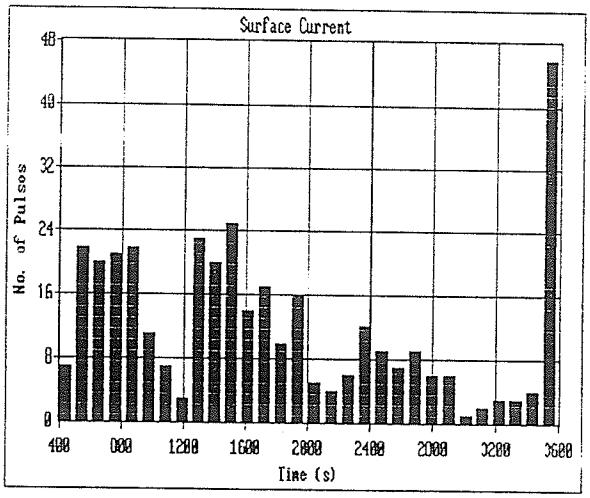

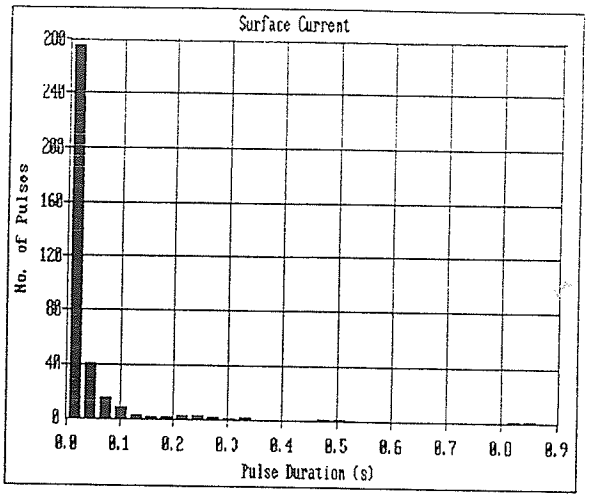

B.7. Solid Deposit Method – arrester polluted in uniform "U" shape.

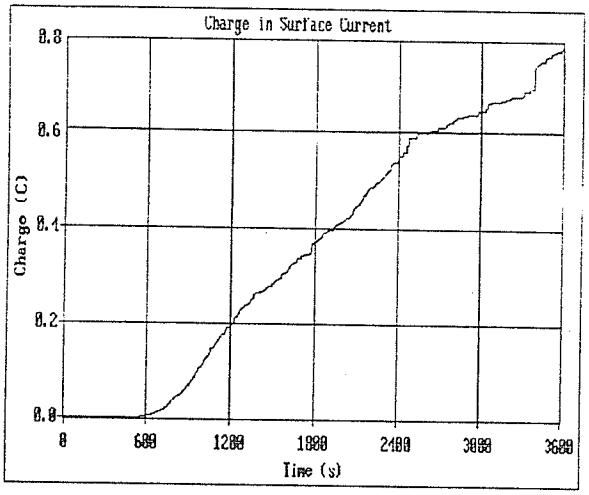

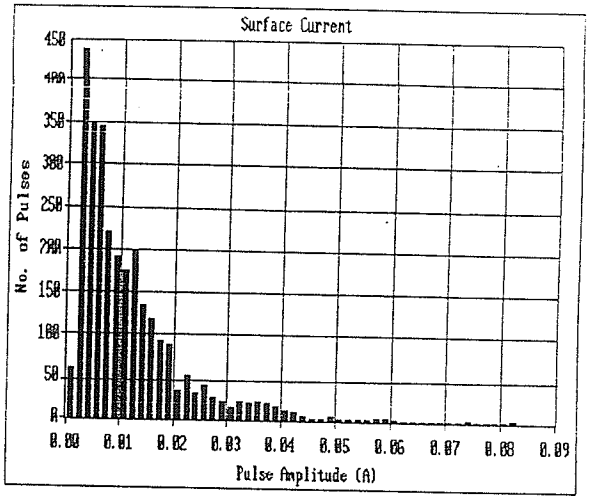

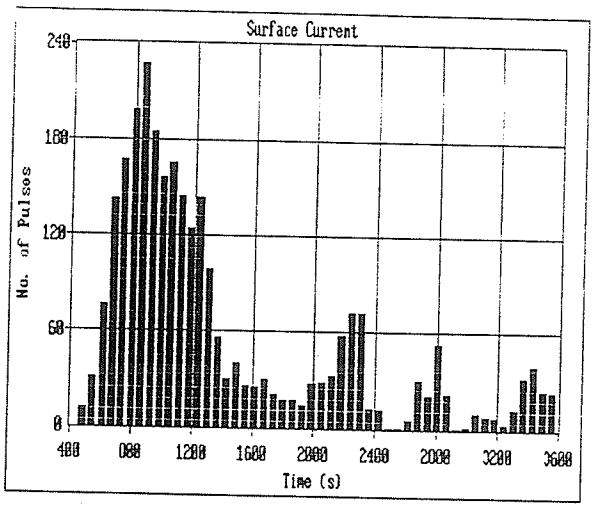

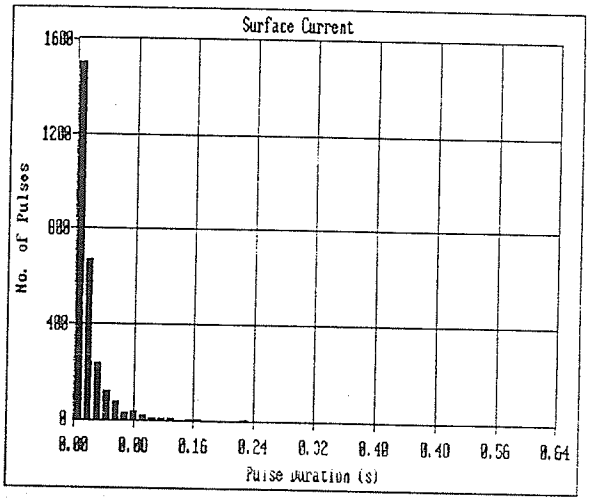

B.8. Solid Deposit Method – arrester polluted in non–uniform "U" shape.

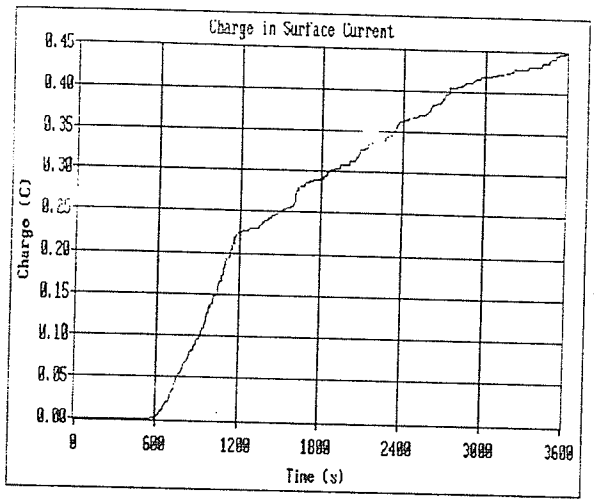

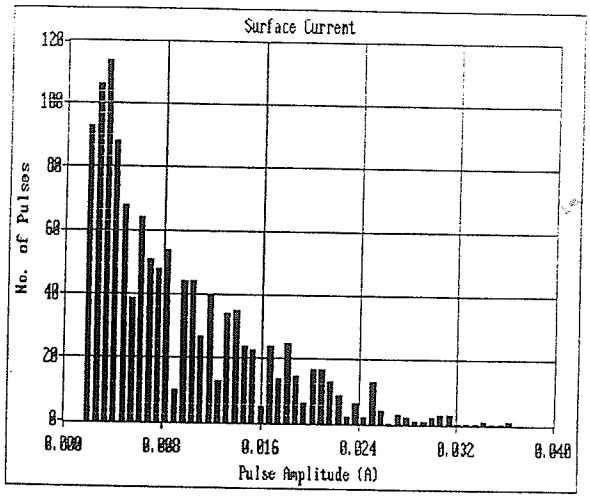

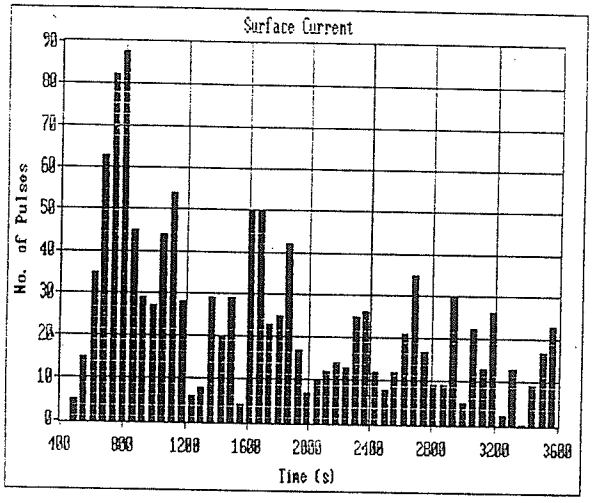

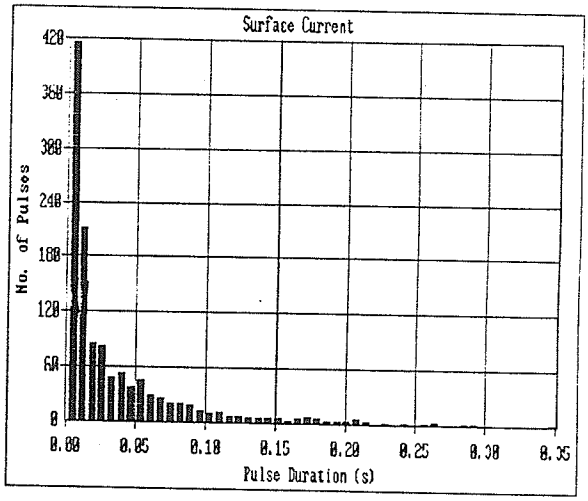

B.9. Solid Deposit Method – fog supplied with breaks.

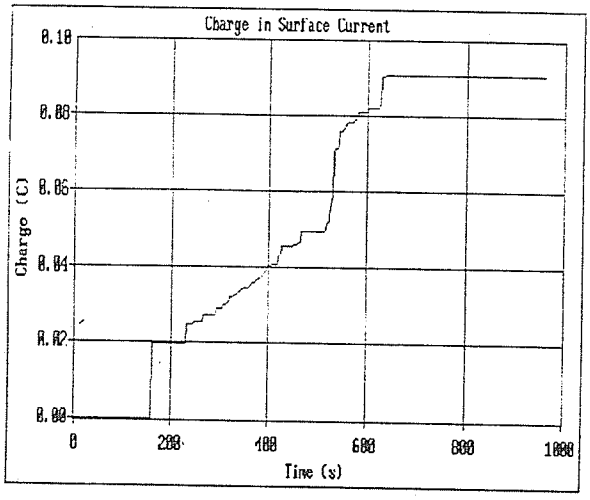

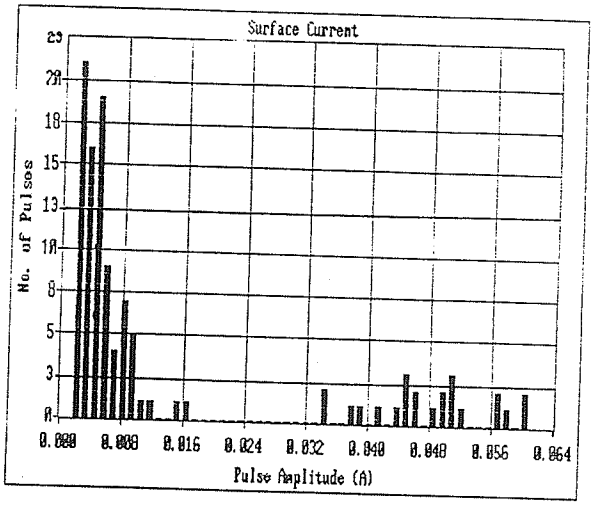

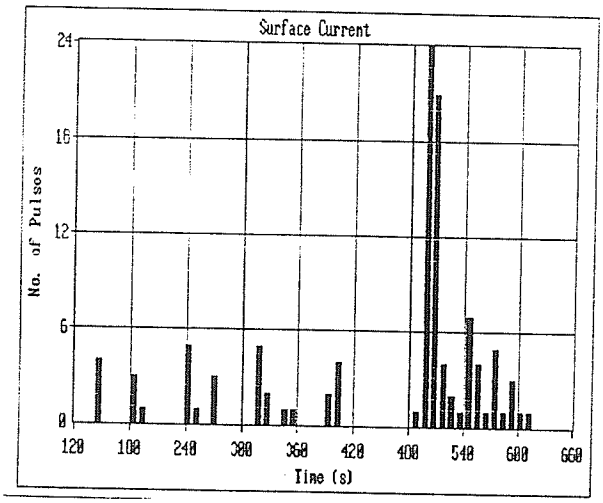

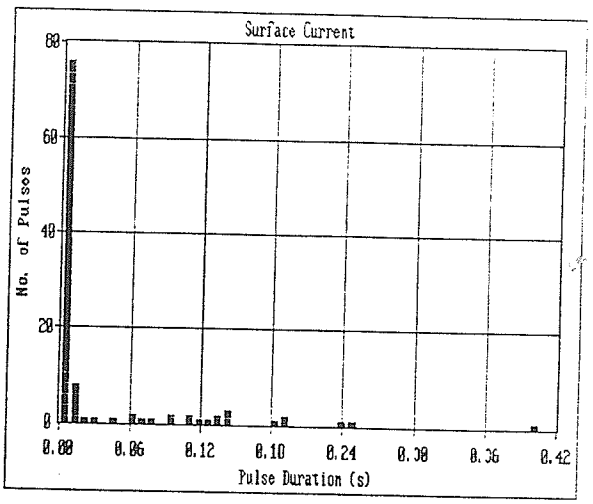

B.10. Solid Deposit Method – two arresters in series; fog supplied with breaks.

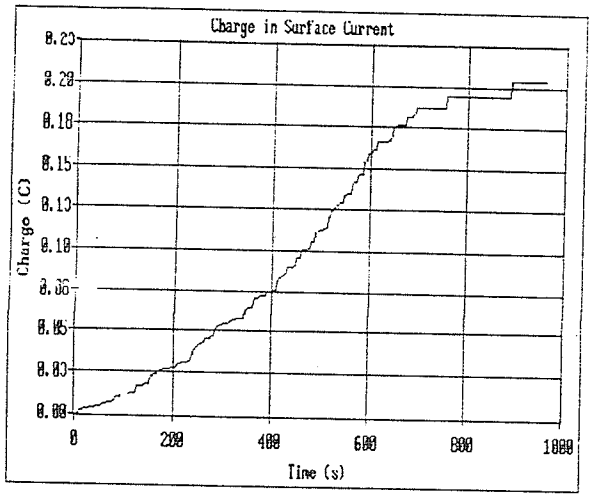

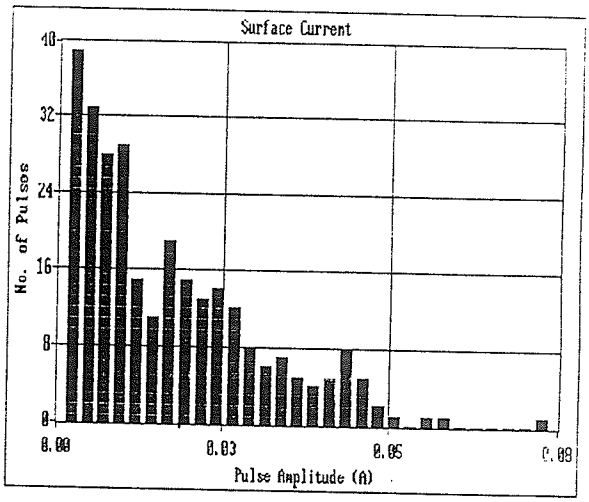

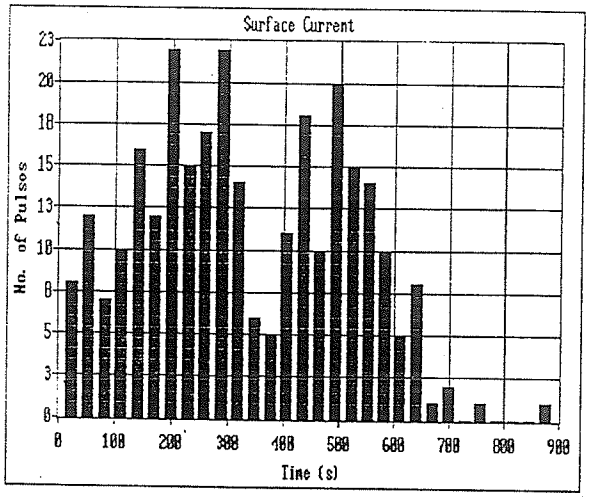

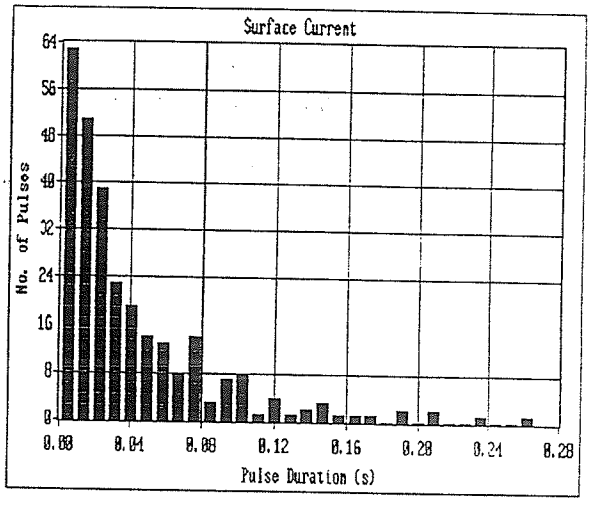

B.11. Solid Deposit Method – single arrester energized at $\sqrt{2}$ times the MCOV.

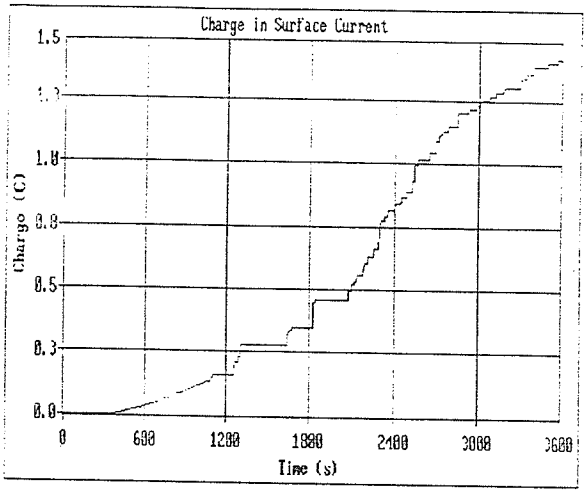

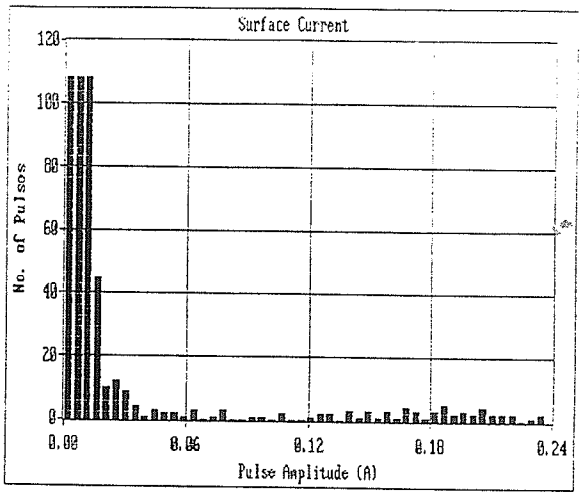

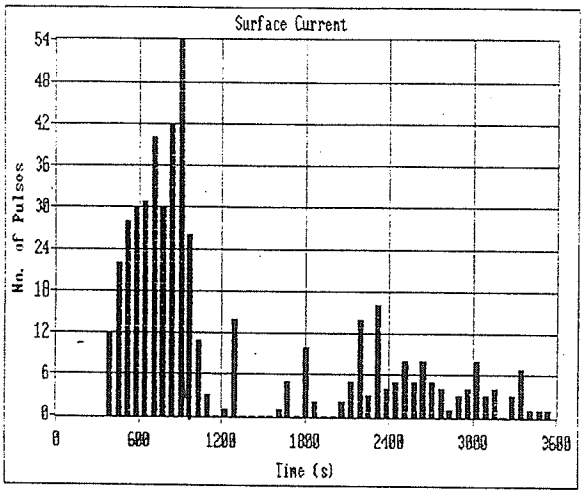

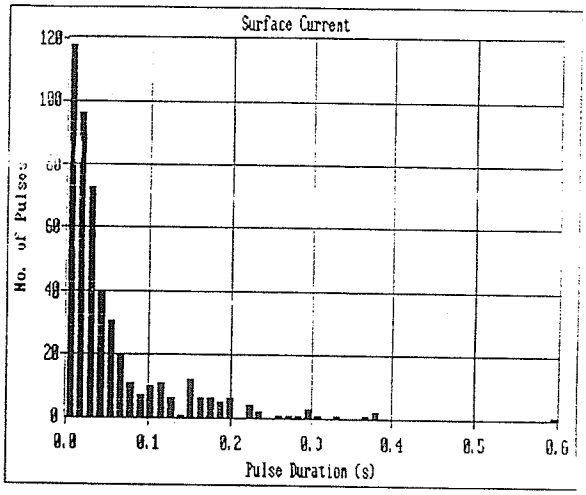

B.12. Wet Slurry Method – arrester energized at MCOV; voltage applied for 15 min.

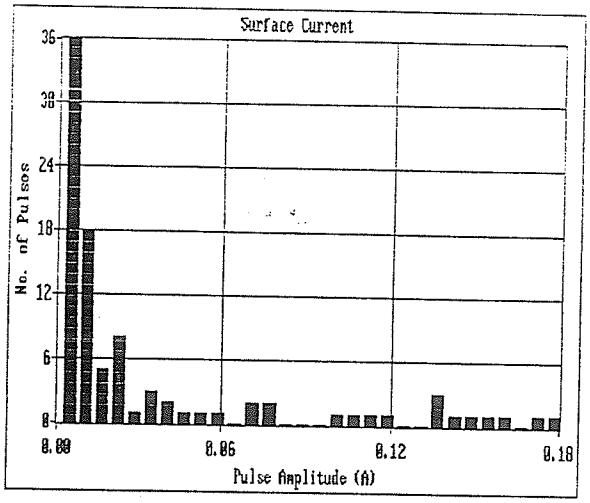

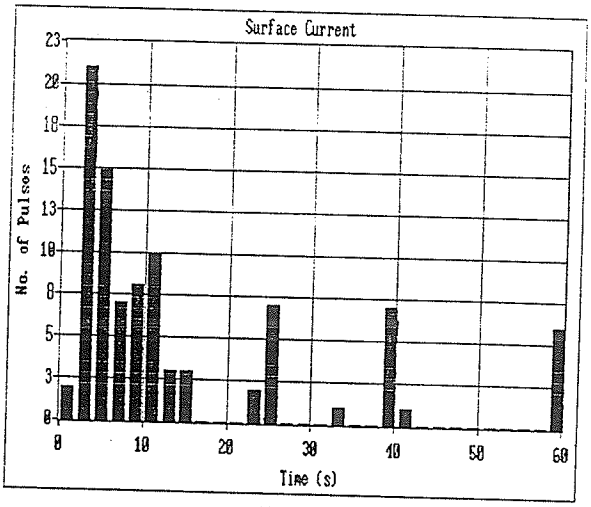

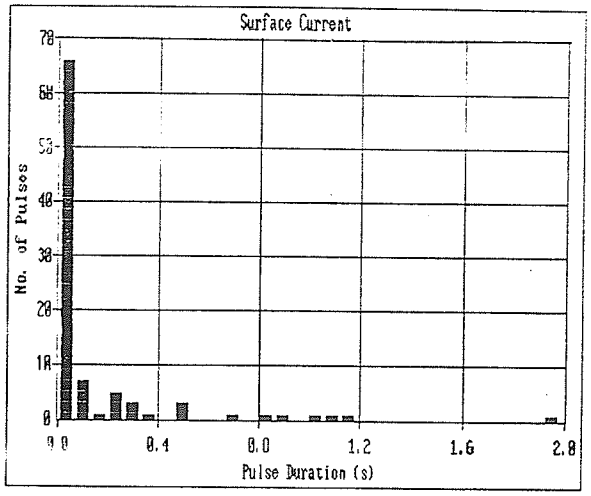

B.13. Wet Slurry Method – arrester energized at MCOV; voltage applied for 7 min.

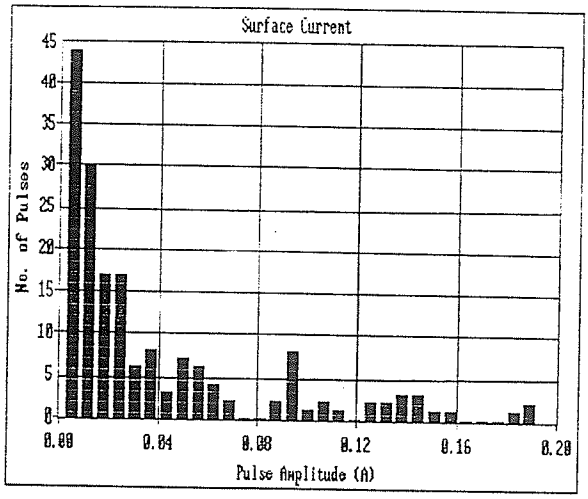

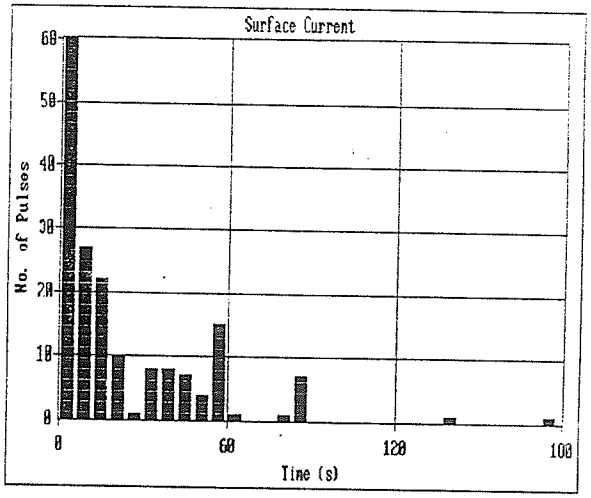

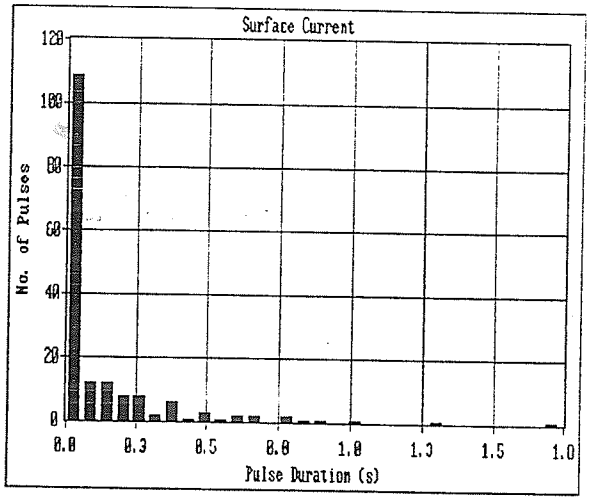

B.14. Wet Slurry Method – arrester energized at MCOV; voltage applied for 4 min.

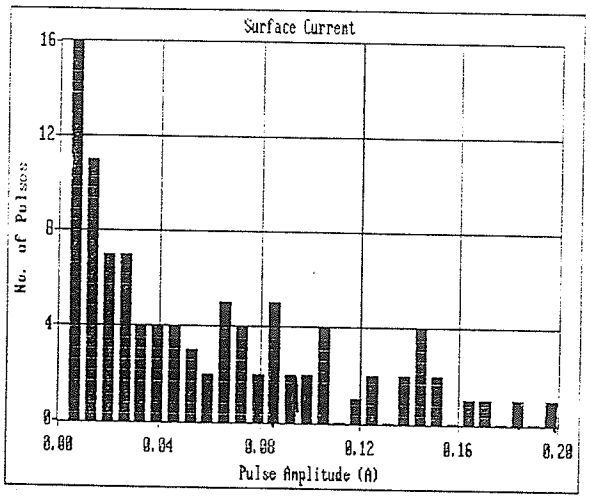

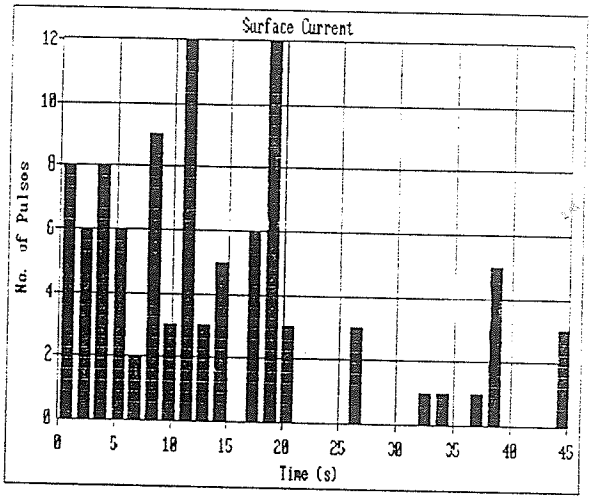

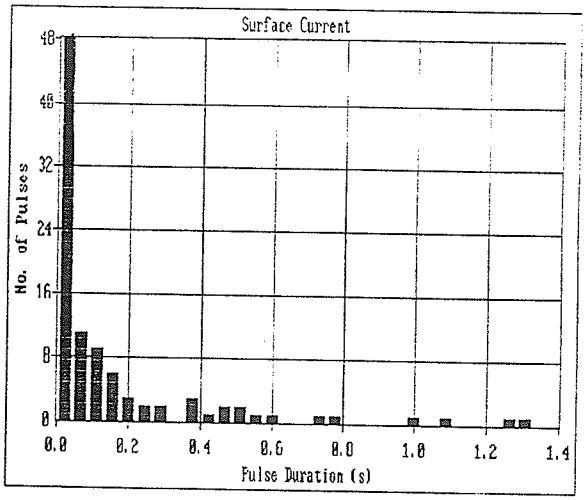

B.15. Wet Slurry Method – arrester energized at √2 MCOV; voltage applied for 4 min.

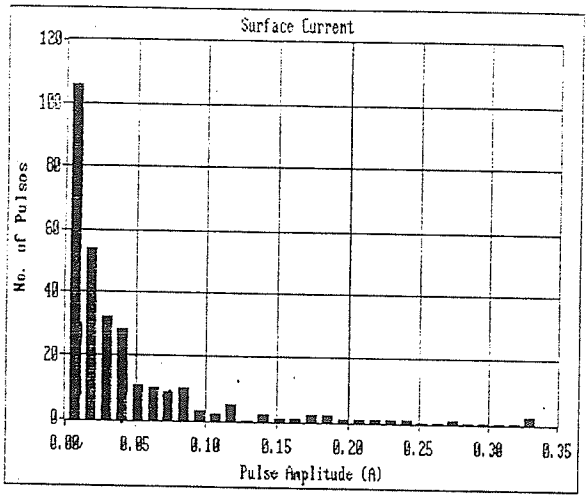

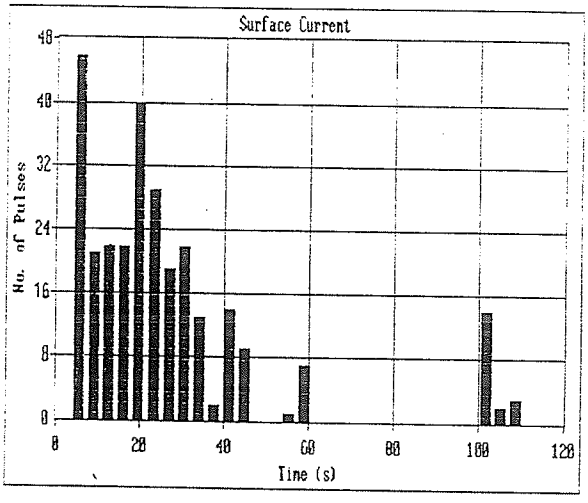

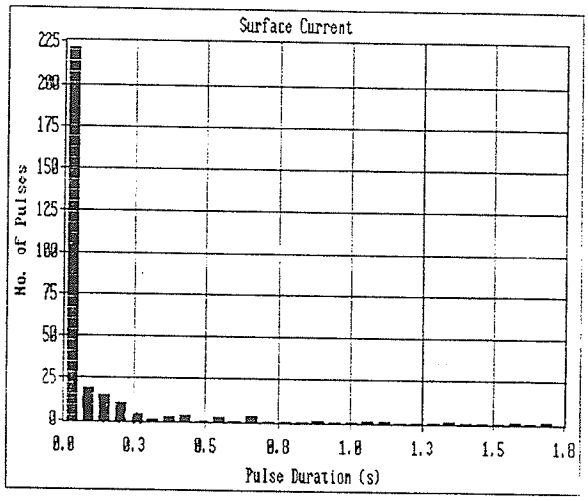

B.16. Wet Slurry Method – two arresters in series; voltage applied for 7 min.

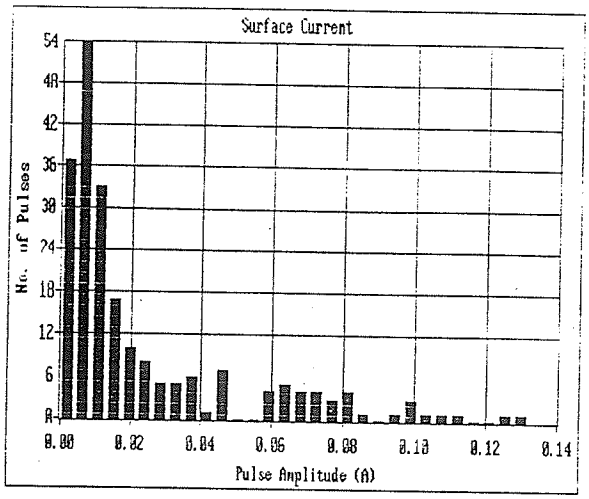

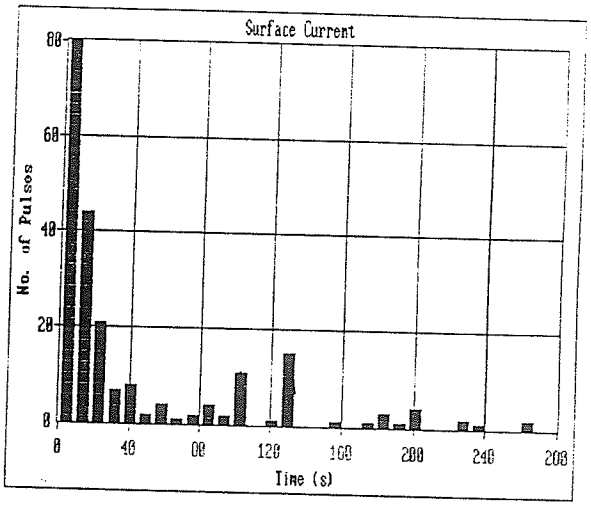

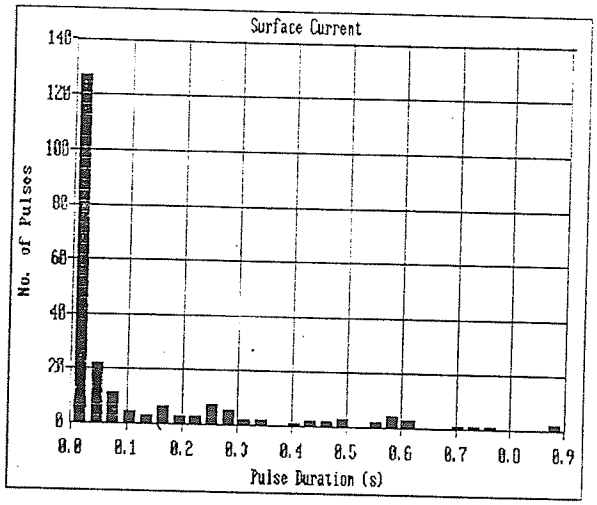

B.17. Test in accordance with Japanese Standards.

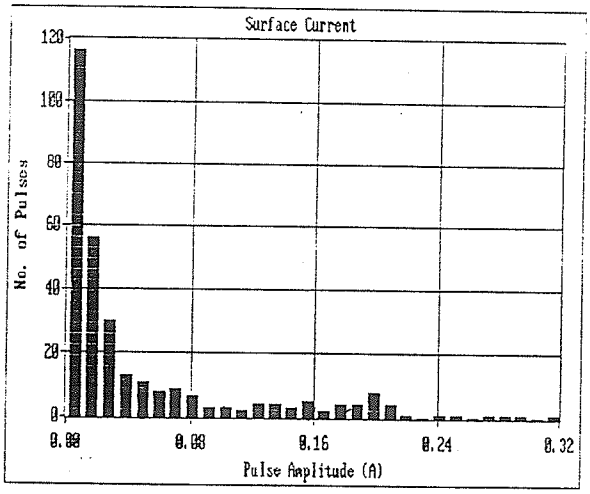

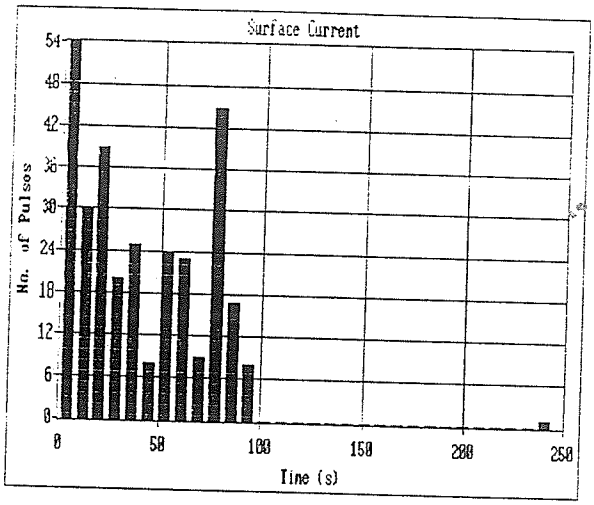

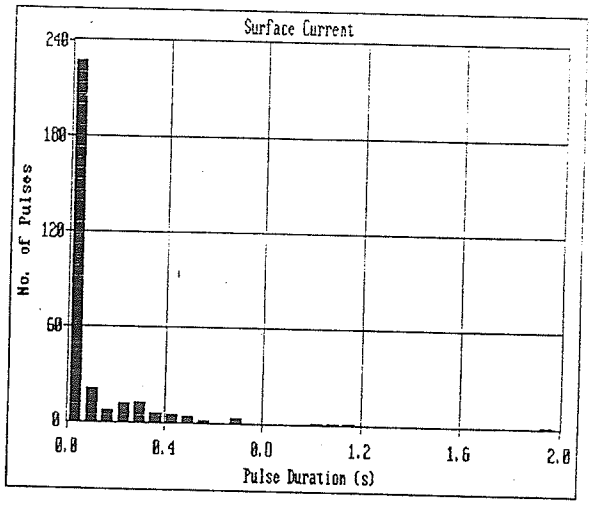

B.18. Salt Fog Test – fog conductivity: 2.9 S/m.

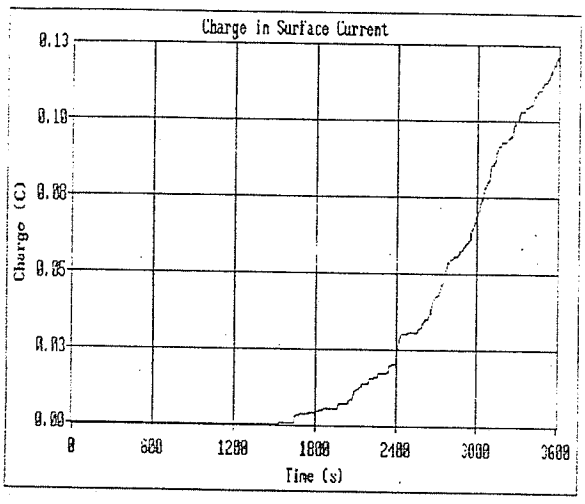

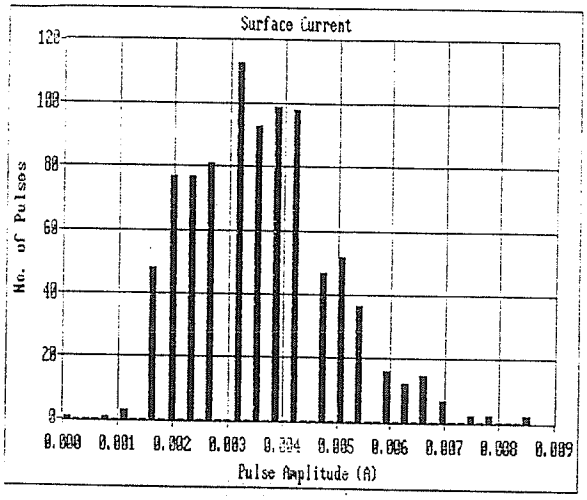

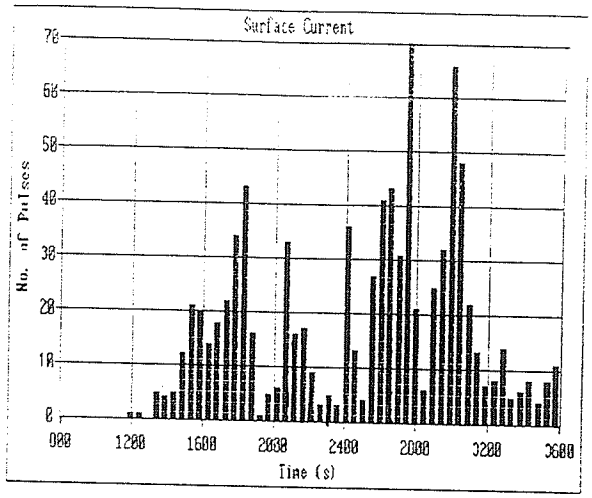

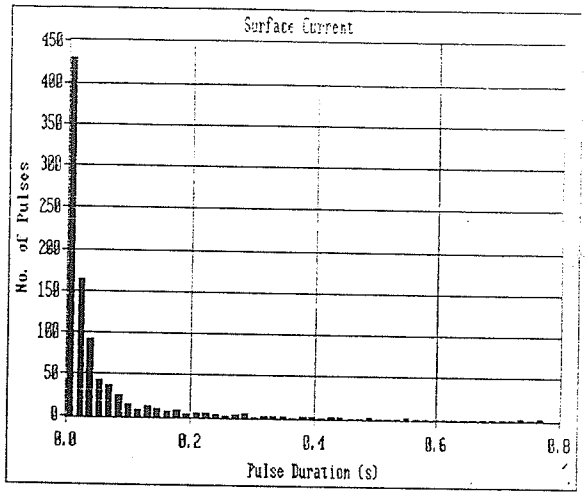

B.19. Salt Fog Test – fog conductivity: 7.4 S/m.

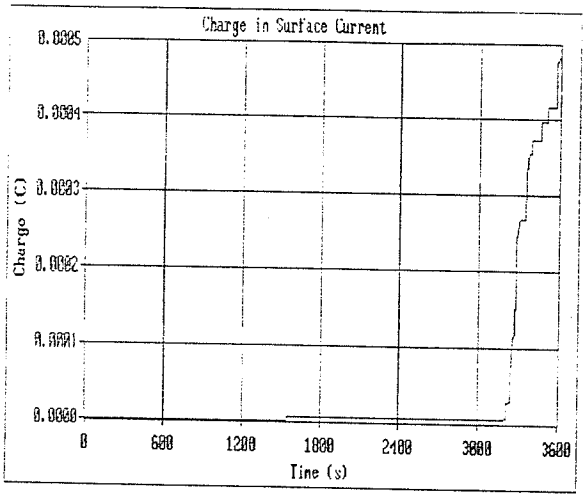

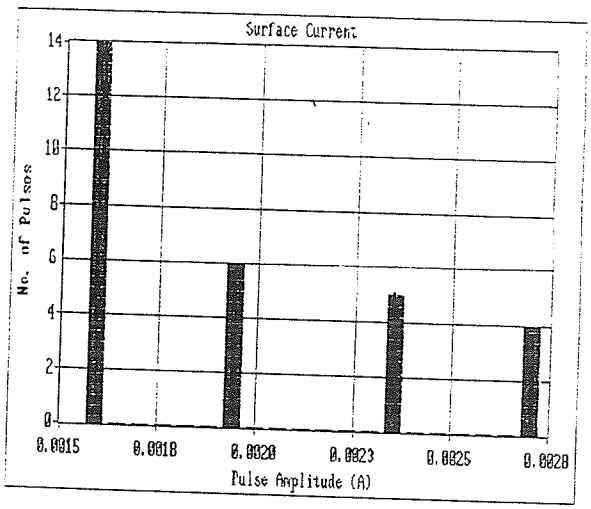

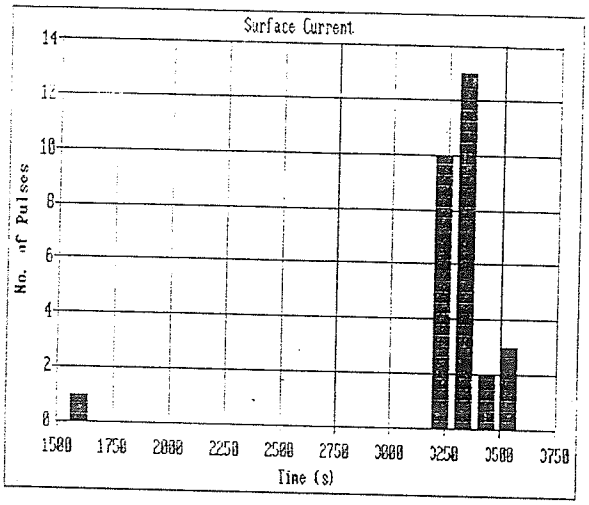

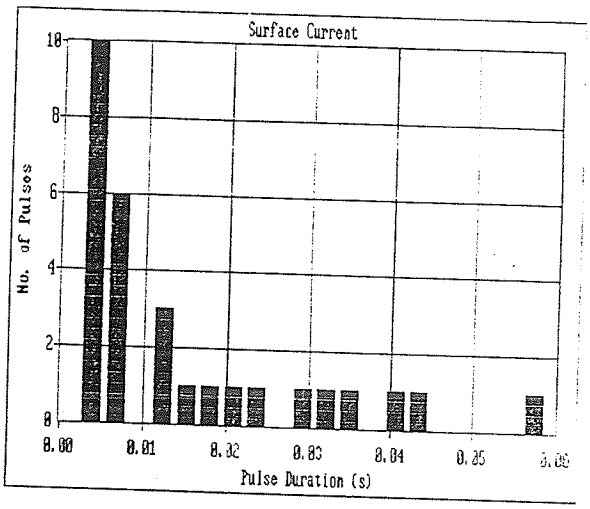

B.20. Salt Fog Test – fog conductivity: 17.8 S/m.